**Faculty of Engineering**
**Department of Mechanical Engineering**

# On the Development of a Ring Type Mechanical Force Transducer: Experimental Characterization and Finite Element Study

**Gavin Scott Manggai Van Stratan**

**This thesis is presented for the Degree of**
**Master of Philosophy (Mechanical Engineering)**
**of**
**Curtin University**

**April 2019**

**Declaration**

To the best of my knowledge and belief, this thesis contains no material previously published by any other person except where due acknowledgement has been made.

This thesis contains no material which has been accepted for the award of any other degree or diploma in any university.

Signature : ……..

Name : Gavin Scott Manggai van Stratan

Date : 8 APRIL 2019

*Specially dedicated to*

*my beloved parents who have encouraged,*

*guided and inspired me throughout my journey of education thus far*

# Acknowledgement

In preparation of this thesis, I received guidance in providing my understanding and knowledge towards the project was invaluable to completing this report. As such, I would like to thank the following individuals; First, I would like to thank my parents, John Alexander van Stratan and Siah anak Umul, partner Ruster Trida Sumbang and office mates Hong Hui, Sim Zee Ang and Martin Cho for their continued support throughout the past two years in ensuring I finished this Master degree. Secondly, to the person who saw the potential and therefore constantly encouraged me to do my Masters, I would like to thank my undergraduate final year project supervisor Dr. Mahmood Anwar for his support and teaching. Working with him during my undergrad research project provided me a significant foundation for future postgraduate studies.

During the two years of my research study, I have received much help from various Curtin University Malaysia staffs. Therefore, I would like to extend my gratitude to the following individuals; to Ms. Florence of Graduate School and Ms. Jacqueline Martin of Faculty of Engineering and Science who has provided me support to ensure administrative things are in order to ensure smooth progress for me to complete my thesis. To the technical lab assistants who has helped me during my experiments with the equipment. To the ICT department, namely Mr. Sheikh, for fast response and constantly being available for any ICT related issues and engineering software installations. And to the Faculty of Engineering and Science for providing me a scholarship to complete this thesis.

I would also like to thank the Malaysian Ministry of Education in providing me a research grant through the Fundamental Research Grant Scheme (FRGS).

To the thesis committee, namely Dr. Sumaiya Islam and Prof Lau Hieng Ho, to whom this thesis would not have been possible without their support, an immense gratitude. Dr Sumaiya has helped me greatly in preparing this thesis and other paper publications to teach and polish my writing skills. As head of my thesis committee, Prof Lau Heing Ho has been very supportive of me throughout my whole master's degree. And last but not least, to the person who has contributed significantly if not the most in completing this thesis, who's help from start to finish has been absolutely immeasurable, whose technical knowledge in the field of force measurements as well as research has been phenomenally helpful for me, and also the person responsible for providing me this opportunity to do and complete this Master study, I would like to thank my supervisor Dr. Noman Khandoker. Without his immense help, guidance, teaching and support this thesis would not have been possible.

# Publications and Awards

## Published

Scott Van Stratan, Noman Khandoker, Sumaiya Islam, Lau Hieng Ho, Sujan Debnath, M E Rahman, "**On finite element analysis of design and sensitivity of a proving ring**", Proceedings of One Curtin International Postgraduate Conference (OCPC) 2017, Malaysia.

## Submitted

Scott van Straten, Noman Khandoker, Sumaiya Islam, Hieng Ho Lau, "**Design of a proving ring with improved sensitivity and optimum stress distribution**", ICME 2018 Hong Kong (Best Paper Award).

## In Progress

Scott van Straten, Noman Khandoker, Sumaiya Islam, Hieng Ho Lau, "**Shape Optimization: Case Study on Design of a Ring Type Force Transducer**", ISME, 2019

Scott van Straten, Noman Khandoker, Sumaiya Islam, Hieng Ho Lau, "**A Review on Proving Rings and Frames for Force Measuring Equipment**" 2019.

# Abstract

This research focuses on finite element analysis of the design and sensitivity of a circular force transducer known as a proving ring. Proving ring is widely used in various engineering applications and industries for force measurement. However, the current proving ring design suffers from stress imbalance in the radial direction. Therefore, in this research study, a hypothesis was made whereby a variable cross section design idea was implemented to optimize the stress distribution in the ring and enhance the ring sensitivity. Experimental work was conducted to identify the material property and force measuring properties of an unused proving ring found in laboratory. The results of the experiment were than used as a basis for design improvements. In the preliminary work, a circular ring and octagonal ring were simulated and compared to test the hypothesis. The results were positive in that a variable cross section design, represented by the octagonal ring, results in lower stress levels. Generalized reduced gradient (GRG), bi-directional evolutionary algorithm (BESO) as well as the ABAQUS TOSCA shape optimization codes were then used to further optimize the ring with respect to stress. It was found from the optimization results that ring thickness was minimum between 45-50° where bending stress is 0 and maximum at point of load application. The varying cross section design of the optimized shape also showed reduced stress levels to varying degree based on the optimization codes used. GRG optimization saw the largest decrease in maximum stress by 98%. ABAQUS shape optimization code reduced the horizontal stress by 66.5%. BESO optimization having the most modest results of the three optimization codes with a 1% increase in maximum stress and stress decreased by 9% at the horizontal location. In terms of sensitivity, all three optimization techniques produced improved results with ABAQUS showing the largest sensitivity increase by 48.7% followed by GRG at 19.5% and BESO at 8.3%. The optimization results were then used in designing a novel modified proving ring. Comparisons to the circular and octagonal ring of similar sizes with varying thickness to mean radius ratio showed that the stress strain levels, deflection characteristics and ring sensitivity of the modified ring compared favourably. Lastly, a further enhancement was made to

the modified ring by adding a double ring design. Stress levels were seen to have significantly reduced by 48.6% with stress distribution also seen to have been more evenly distributed particularly on the inner surfaces of the ring. The outer sensitivity was found to have decreased by 48.1% however but inner ring sensitivity increased by 4.9%.

# TABLE OF CONTENT

# LIST OF FIGURES

# LIST OF TABLES

# NOMENCLATURE

| | |
|---|---|
| $\varepsilon$ | Strain |
| $\sigma$ | Stress |
| $e_A$ | Strain at location A |
| k | Ring stiffness |
| K | Correction factor for a curved beam |
| M | Moment |
| *f* | Natural frequency |
| T | Time period |
| $F_r$ | Radial force |
| $R_i$ | Inner radius |
| $R_o$ | Outer radius |
| $R_m$ | Mean radius |
| E | Modulus of elasticity or Young's Modulus |
| I | Area moment of inertia |
| $\delta$ | Ring deflection |
| w | Ring width |
| t | Ring thickness |
| U | Internal energy |

# Chapter 1

# Introduction

## 1.1 Preamble

This thesis was written with the aim of contributing significant knowledge in the field of force measurement. A common force measuring device is a force transducer. A force transducer is a mechanical device that measures applied force. Force transducers comes in many different types, shapes, capacities and form. The basic principle of a transducer is when force is applied, certain characteristics of the object will change such as height, length, electrical resistance, pressure and etc. The simplest example of this can be seen on a weighing scale with a spring acting as the force measuring member. The force acting on the spring creates a deflection which corresponds to the force acting on it and therefore the weight of the object placed on the scale.

The most common type of force transducer for high load application is the strain gauge load cell. A strain gauge is installed onto the surface of an elastic member whereby each gauge measures the local strain at each position. Force is then determined and computed from all the individual strain measurements at each location. An example would be circular force transducer or proving rings with attached strain gauges in a Wheatstone bridge configuration. Force can also be measured by means of pressure. An example of a pressure-based force transducer is the hydraulic load cell. It is a device with piston and cylinder components that contains hydraulic fluid usually in the form of oil and the loading member connected to a piston. When force is applied, the movement of the piston creates fluid pressure in the load cell. A high pressure hose or Bourdon tube with hydraulic fluid is connected to the bottom of the load cell and pressure is transmitted to

a hydraulic pressure dial gauge. A pneumatic load cell has the same basic principle as the hydraulic load cell but with air instead of hydraulic fluid. Applied force can be measured simply by moving the piston which induces pressure into a chamber sealed with a close-fitting cap. Air pressure accumulates until it is equal to the force on the cap, with any excess either bleeding out from the cap or from the nozzle. At pressure equilibrium this indicates the applied force, which can be read using a pneumatic pressure gauge. Another type of force transducer involves using a vibrating element. A tuning fork load cell can be used to measure force by measuring its resonant frequency when it is made to vibrate [1]. The load cell consist of two parallel band splines that vibrates at opposite directions in resonance. Changes in resonance due to applied force is then measured using two piezo-electric sensors located near the vibration nodes at each splines. Two other vibration-based transducers are vibrating-wire transducer and the surface-wave resonator load cell. Both these transducers have the same operating principle as the tuning fork load cell but with different vibrating element. Regardless of the type of force transducer, in order for a force transducer to work properly, calibration is required whereby increments of known force is applied over a period of time and changes in the selected parameter is recorded with respect to the force applied.

From the examples listed above, it is clear that the nature of force acting on an object to create measurable change to its physical characteristics means that there are various other types of force transducers other than the ones mentioned above. Therefore, at its most fundamental, a force transducer is basically a device that responds or reacts linearly towards applied load with high repeatability after multiple cycles of load applications. However, due to its simple design, ease of use and adaptability for various engineering uses, an elastic element-based circular force transducer or proving ring will be studied in this thesis. The term proving ring and circular force transducer will be used interchangeably from this point onwards.

## 1.2 Proving ring

Force measurement is important in numerous engineering fields and industries. The need for an accurate and highly sensitive proving ring is crucial in various agricultural practices such measuring forces at attachments or implements. In machining based industries such as in the cutting and milling process, dynamic forces are measured primarily to ensure tool life is

maintained as well as to ensure the required forces for cutting is optimal. Proving rings has also been used for other applications such as friction stir welding processes [2].

Force measurement is done on a circular force transducer by measuring the deformation of a certain parameter, usually the inner diameter of an elastic member, which corresponds to the amount of force applied. The measured force can be easily calculated based on the deflection of the elastic member if the modulus of elasticity of the material is known. Deflection caused by the applied load can be measured by using a vibrating reed and a micrometer screw or dial gauge. This method of force measurement by means of ring diametral deflection can be deemed 'mechanical'. The proving ring was first developed in 1927 by H.L Whittemore and S.N. Petrenko. Since then, the proving ring has been used in various engineering applications where for measurements plays a crucial part such as machining operations and agricultural related applications. The design and investigations on the circular force transducers or proving ring revolves around the theory of thin rings. The theory of thin rings is based on Castigliano's second theorem, which is used to derive the deflection equation of the ring. The diametral deflection in a ring is measured using digital or mechanical means and is used to calculate the force.

Various shapes based on the circular ring has been designed and studied by numerous authors to improve the proving ring. Octagonal ring shaped force transducers were studied due to their superior rigidity in machining operations and desirable natural frequency response during operation [3, 4]. Extended octagonal ring shaped force transducer has been reported by authors in the agricultural field [5, 6]. Hexagonal shaped force transducer were reported to have superior metrological performance compared to circular and octagonal shaped transducers [7]. Elliptical shaped force transducer were shown to have good metrological characteristics compared to ring shaped transducer [8]. From the numerous research reported however, a recurring theme in most of the studies conducted were the use of strain gauges to measure strain induced on the ring by the load instead of measuring its deflection. A strain gauge is a sensor that transmits electrical signals when there is a variation to its resistance due to force applied. It is usually set up in a Wheatstone bridge configuration that measures strain distribution parallel to the surface of an object. Strain measured by a strain gauge can be classified as either tensile or compressive strain depending on the location, which is usually distinguished by a positive or negative sign. When a force transducer is under load, the ring deforms. Deformation of the ring induces strain which may be more pronounced in certain regions on the ring. This regions are where strain gauges are usually placed

to accurately measure the strain distribution which can be then used to measure the force applied. Hence most studies focused on the tangential strain distribution which is parallel to the surface of the strain gauges installed.

This research attempted to improve the design of the proving ring with respect to stress and its sensitivity with or without the use of strain gauges. This ensures the sensitivity of the ring is essentially optimal regardless of the force measuring method used. To achieve both goals of optimal stress and increased sensitivity, radial strain distribution studies were conducted to improve the sensitivity of the ring with increased deflection and strain the desirable outcome. Stress distribution studies in the radial direction were conducted to determine the stress induced on the conventional ring during a particular loading cycle. Cross sectional parameters were varied to study the effect of the dimensions on the stress distribution and sensitivity of the proving ring. The results of this were used and compared in the next section which involves optimization work by means of various algorithms conducted to further optimize the ring shape with respect to stress without compromising the ring sensitivity. The results of the optimization work saw a common shape with ring material redistributed at various locations around the ring. This creates a varying cross section ring design. Sensitivity of the proving is essential for proper usage and accuracy in measuring the applied force. This research study on the improved proving ring design will see a reduction in cost which would benefit small to medium sized industries.

## 1.3 Thesis Structure

This thesis is broken down into five chapters. The first chapter establishes main ideas and motivations behind the selection of the topic. The background and introduction to force measurements, force transducers and the proving ring has been done in the previous section.

In the second chapter, a thorough literature review was be presented. The first half of the chapter covered various aspects of the proving ring including ring shapes, design stresses, factors affecting the proving ring and its various applications. The second half covered the research gap and questions derived from the literature review and finally the problem statements and research objectives.

In the third chapter, all methodology pertaining to the work in this thesis will be presented. Experimental technique employed in measuring the deflection of the ring with respect to the load will be shown. Various finite element analysis parameters for simulation and optimization work will be discussed. Shape optimization techniques used in this study will also be presented. Shape optimization techniques include bi-directional evolutionary structural optimization or BESO technique, nonlinear optimization generalized reduced gradient technique using visual basic code and shape optimization through finite element simulation using the TOSCA optimization suite found in ABAQUS.

The fourth chapter presents the results and discussion of the work done in the methodology section. Experimental results used to obtain and calculate the modulus of elasticity of the proving ring will be presented. Next, preliminary results with respect to conventional proving rings such as the circular and octagonal ring shape transducers will be discussed. Results from the three optimization techniques will be scrutinized as well as further design suggestions with respect to the shape optimization results obtained from the optimization work.

The fifth and final chapter will summarize the thesis as a whole as well as including the main findings and outcome of this research study. Any shortcomings or limitations encountered throughout this research will be discussed and therefore future recommendations related to this will be presented as well.

# Chapter 2

# Literature Review

## 2.1 Introduction[1]

A proving ring, also known as a force transducer, is a mechanical device that measures applied force. The word transducer means a device which converts one form of energy into another. In a proving ring, this is done by measuring the deformation of an elastic member, which corresponds to the amount of force applied. The force can be easily measured based on the deflection of the elastic member if the modulus of elasticity of the material is known. Deflection caused by the applied load can be measured by using digital sensors that uses strain gauges or by using a vibrating reed and a micrometer screw. A dial gauge or micrometer screw and a vibrating reed is a typical 'mechanical' approach to measuring force. The deflection of the ring is then measured which corresponds to a specific load value. Strain gauge on the other hand, which is a resistance foil type sensor, measures the strain induced onto the ring by the load. This is done by measuring the change in resistance in the strain gauges as the ring deflects. Hence by knowing the

[1] *The first five sections are currently being prepared for future submission as a review paper for journal publications. These sections are from Introduction up to Applications of Proving Rings.*

strain load values can be easily calculated. A comparative study was conducted by Kumar [9] which showed the strength and weaknesses of both these types of force measuring system. The study found that the dial gauge, in dial and digital form, suffer from multiple errors. The strain gauge however has optimum metrological properties with minimal errors.

Sensitivity is a major factor when using a proving ring to measure force as this will affect the accuracy of the force measuring device. Sensitivity is defined as the amount of strain per unit force acting on the ring [10]. To maximize sensitivity, one must maximize strain. This means the deflection of the proving ring must be increased or maximized which in turn maximizes the strain induced on the ring. However, this would negatively affect the rigidity and the life span of the ring. Driven by the need to improve the sensitivity, rigidity and therefore accuracy of the proving ring in measuring applied force, multiple authors have published their research on the design of the proving ring for various engineering applications. At the heart of their research the authors have tried to improve the proving ring by implementing various shapes which are mainly transformed from the circular ring. Some of the more common examples found from literature besides the circular shape are octagonal ring and its extended form.

In order to provide a meaningful review on the design of the proving ring, the scope and boundaries of this review must first be established. This review study will not address the effects of material selection on the proving ring performance. Although material selection is an important criterion on the design of the proving ring, it is logical to think that it would have a considerable effect on the analysis of the proving ring design and will therefore require a whole different research altogether. Although most papers presented here have other components or topics related to the study of force transducers, this review will only focus on the design of the elastic element of the study. Lastly, this review will only cover force transducers with an elastic element.

Figure 2.1 A proving ring under axial load

## 2.2 Definition of a Proving Ring

The most common shape in proving ring design is the circular shape. Many design procedures have been reported over the years from various journal articles. The earliest report on the proving ring theory was developed by Timoshenko [11] and Filon [12] in which they described the theory behind stress induced on a ring due to bending. Other studies has also been aimed at understanding stress distribution due to loading [13]. Similarly, displacement or deflection of a ring under compressive load has also been extensively studied [14]. These studies were used as the basis for proving ring designs in the coming years.

As was mentioned before, when force is applied on a proving ring, this causes diametrical deformation of the ring shape. This deformation, also called deflection, is similar to how a simple bar would bend or deflect when force is applied at one end while the other end is fixed. Using that analogy, the deflection equation for the circular ring can be derived. Therefore, utilizing strain energy theory and Castigliano's Second Theorem, the following equation which governs the deflection characteristics of the proving ring is derived [15]:

$$\delta = 0.1485\left(\frac{FR^3}{EI}\right) \quad (2.1)$$

Where,

F = Force,

R = Outer Radius

E = Modulus of Elasticity

I = Area moment of inertia

## 2.3 Design of a Proving Ring

The proving ring has been used since the 1920s. The proving ring design generally revolves around the use of an elastic member with a circular or elliptical inner shape. Many proving ring shapes exist depending on its capacity and use. The more common ones are the circular shape, octagonal shape and double extended octagonal rings.

### *2.3.1 Shapes*

*Circular shape*

The earliest known study on proving ring design was published by Ito et al. [16-17]. They found that increment of thickness to mean radius ratio results in increase in sensitivity and rigidity of the ring. The role of stress analysis in the design study of a force transducer has also been published in which they discussed stress analysis on the design of circular ring with end bosses [18]. A simple design procedure using analytical means was discussed by Libii [15]. The author presented multiple equations in designing a simple proving ring with attached dial gauge. The equations derived were fundamental in calculating the stress, strain and deflection of a ring under

compressive load. Finite element analysis approach has also been used in designing the proving ring by Chen [19]. This method was used to identify the maximum stress and strain locations on the ring for optimal strain gauge placement. Figure 2.1 shows the stress distribution along a half ring. The maximum stress was found at the inner and outer portion on the top side the ring. Second larger stress was located at the inner and outer surface on the rings horizontal side indicated by the middle peak in Figure 2.1. The strain distribution also showed a similar pattern. With this knowledge the authors found the ideal location of strain gauge placements to be at the horizontal sides where the second larger strains were located. Although this study did not present any significant improvement or modifications to maximize the sensitivity of the ring, it does indicate critical locations of where sensitivity can be maximized, and the maximum stress reduced. The use of strain gauges does have its disadvantage however. Patrick et al. [20-21] presented an application of proving-ring technology to measure thermally induced displacements in large boreholes in rock. Their study involves the use of strain gauges attached to proving rings to measure displacements in micrometers of cooled rock. They found that most of the force transducers failed due to electrical shorts in the wiring circuit connecting the strain gauges. The electrical shorts were due to contamination caused by moisture. This study proved that strain gauges, although accurate, is susceptible to damage in its electrical circuit.

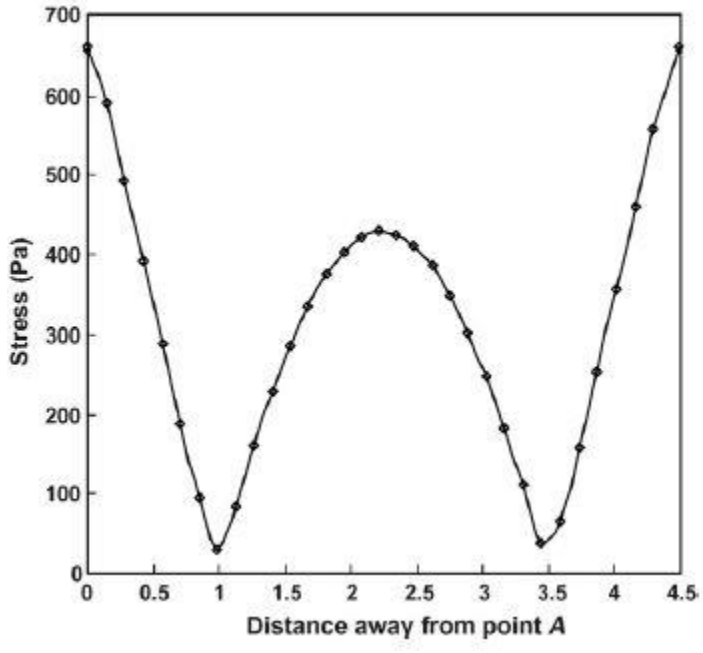


Figure 2.2 Stress distribution along a half ring [19]

Multiple design studies have been presented by Kumar et al. [22-27] in regard to the circular proving design for general force measuring applications. The basis of their studies were the fundamental equations governing the deflection, stress and strain due to loading. The equation showed that the deflection of a circular ring is inversely proportional to the width of the ring and proportional to the cube of the ratio between radius and thickness of the ring. The highest axial deflection for a simple ring was achieved with t/R ratio of 0.10 and t/b ratio of 0.175 [22]. The stress distribution was found to decrease along the ring up to an angle of 40° where the minimum stress was located, and then increases along the ring quadrant. This observation was also seen with deflection, which is highest at the point where axial force is applied, and decreases up to the other end of the quadrant, where deflection is considered negligible [24]. A low capacity ring shaped was also discussed [27]. The authors claimed that most high capacity thin rings have thickness to mean radius ratio t/R between 0.1 to 0.5 but for this study the ratio chosen was <0.05 since it is for low capacity. These studies however were mostly concentrated on the performance aspects of the transducer and its design procedures that were based on developed equations. Stress distribution in the radial direction were not studied.

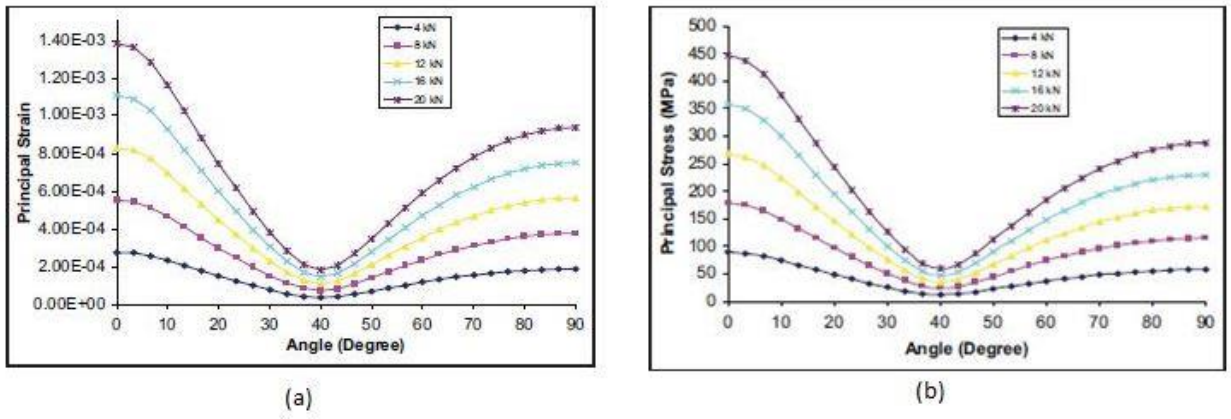


Figure 2.3 (a) Stress and (b) strain distribution in a quarter ring [26]

Other ring shape force transducers were also studied based on their intended applications. Jain et al. [28] presented a dynamometer design utilizing a short hollow cylindrical bar using resistance strain gauges. The length of the cylindrical bar is 35mm with an outer diameter of 15mm. Strain gauges were attached in a Wheatstone configuration at various locations along the cylindrical bar. From the calibration test, the output voltage had a linear relationship with all three

component forces. However, the developed dynamometer was quite small in design and therefore used in smaller load applications up to 3500N.

*Octagonal Shape*

Octagonal or octal ring is a type of proving ring with eight straight edges with a circular inner radius. The ring is derived from the circular shape with various enhancements based on its intended purpose. From literature, the most common desirable property of an octagonal ring shape design is its superior rigidity compared to the circular ring [29]. Its metrological performance has also been established to be better than the conventional circular ring [30]. Octagonal rings are also chosen in certain force measuring equipment due to having less deflection requirement to measure an equivalent strain [31]. Octagonal rings have been extensively used in machining operations due to their superior performance in force measurements. During machining operations such as cutting or milling, the three force components measured are primary or main cutting force, feed force and thrust force. In this type of application, multiple reports have been made of a four octagonal ring configuration for the developed dynamometer [2, 32, 33]. The rings are usually dimensionally small to fit the whole dynamometer design.

As was mentioned earlier, octagonal rings have been utilized mostly in machining operations. One of the earlier design studies was done by Saglam [34]. Through analytical solutions and theory of thin rings, they found the optimal strain gauge location to be 45° from the vertical axes as opposed to 39.5° for a circular ring. They identified these locations as where strain gauges are ideally placed on the inner and outer ring surface. Further calibration results showed the cutting forces exhibit excellent linearity with the output voltage. Cross sensitivity between outputs were small enough to be deemed negligible. From the face milling test conducted, they found that the dynamometer recorded cutting forces similar to calculated values and therefore showed positive results in real world application. Korkut [35] developed a dynamometer design and its construction for milling operation. The dynamometer had a four-octagonal ring configuration, each attached to a strain gauge, to form a measuring bridge. Dynamic characteristics of the ring such as frequency were analyzed and found to fulfill the criteria of having a natural

frequency at least four times than the operational frequency during milling. The effect of strain gauge locations was also studied. The dynamometer was found to have sensitivity of ±5N. Cross sensitivity of the dynamometer was at 0.05%. The author however did not perform any strain analysis on the designed ring.

Yaldiz et al. [29, 36, 37] published a series of studies on the design of an octagonal ring mainly used for force measurement in cutting and machining processes. They studied the design on a turning dynamometer with octagonal rings as its sensing element to measure the static and dynamic cutting forces using strain gauges and piezoelectric accelerometer. Due to the nature of the application, the ring material selected was based on a set of criteria namely rigidity, heat conductivity, corrosion resistance and high natural frequency. From the calibration test, it was found that for cross sensitivity test, the errors found were less than 1% for all axes, with Y axes being the smallest at 0.17% for main cutting force. The eccentricity test showed that the output errors for all three force components were also less than 1%, with feed force measuring the highest at -0.8%. In the second study, strain locations were studied to maximize sensitivity of strain gauges. Optimal location was found to be at 45° from the vertical axes instead of 39.6° for a conventional circular ring. In the third case, they studied the design and development of a milling dynamometer measuring the three component forces during milling operations using strain gauges fixed onto octagonal rings and piezo-electric accelerometer. This study focuses on sensitivity and rigidity. Linearity test was conducted and was found to be within the range of 1.2-1.5% for all three force components. Cross sensitivity test revealed that the errors obtained were within 0.6% to 1.7% for all three axes. Eccentricity test conducted showed error obtained by applying a force of 1000N at center and 50mm from the calibration point was 0.13% for the thrust force and 0.18% for the remaining two forces. Performance test showed that the error obtained was 0.15%. The resulting dynamometer was constructed and was found to measure torque, static and dynamic cutting forces reliably.

Karabay et al. [3, 38, 39] recommended some dynamometer designs incorporating the octagonal ring shape for use in machining applications. The author mentioned the need for dynamometers to be stiff with minimal deflection required in the range of $2.5 \times 10^{-4}$ to $2.5 \times 10^{-2}$ mm. Octagonal ring shape was selected that fits these required criteria. The author emphasized the advantages of using an octagonal ring which critically was much more stable in the horizontal

force direction than a circular ring. The rings were arranged in a circular pattern with strain gauges attached at 45° which is similar to previous studies concerning gauge location. Two of the octagonal rings were mounted with eight strain gauges each; four gauges to measure tensile and compressive strains when thrust is applied and the other four to measure tensile and compressive strains when torque is applied. The designed dynamometer can be used safely for measurements of cutting forces for drills with diameters from 5-16mm and feeds from 0.152 to 0.356mm/rev with material hardness up to 250HB. The sensitivity of the dynamometer was ±5N with cross sensitivity determined at 0.05%.

Sun et al. [40] published an alternative method to optimize octagonal-ring transducer. The authors investigated the optimization of the design of an octagonal ring transducer through stress design criterion concept and finite element stress predicting method on three different designs of the ring with different thickness. The octagonal ring was determined to measure a two component forces (vertical force P and horizontal force F) and a single torque component M. In the design analysis, three rings with varying dimensions were compared: model 1 had a thickness of t = 4 mm, model 2 with thickness t = 5mm and model 3 with thickness 6mm. Models 1 and 2 were of equal size however Model 3 was larger than the other two. From the calibration results, they found that all three models showed excellent linearity, with model 1 having the highest output voltage. Also, they found that model 1 had the lowest maximum force for both force components with model 3 having the highest. From the FEA, the authors found that the maximum predicted stress in both P and F direction were smaller than the set stress design criterion. From the FEA stress prediction results, maximum stress in the P direction were almost similar across all three models, with model 2 being the lowest. The maximum stress in the F direction differed between model 1 and the other two models, with model 2 having the highest maximum stress value by a slight margin and model 1 having the least. Lastly the authors revealed that the average stress error in the P direction was higher than average error in the F direction, which were 18.8% and 5.2% respectively. However, stress strain characteristics of the ring design was not studied.

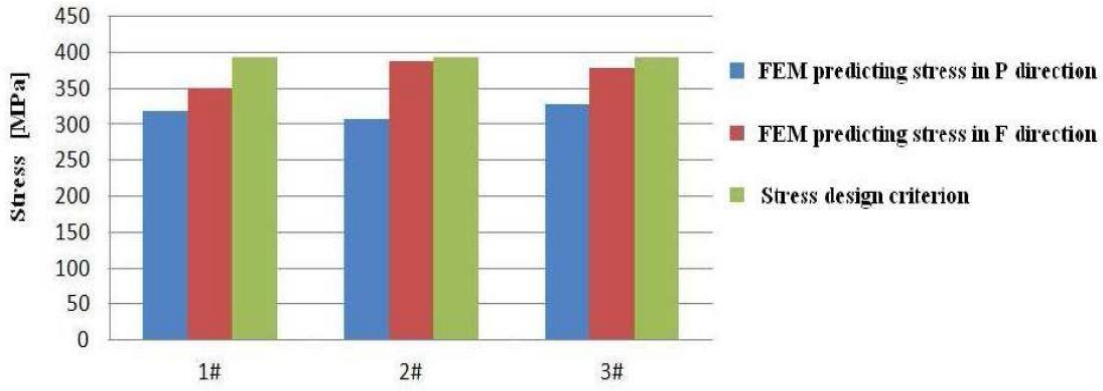


Figure 2.4 Comparisons between stress levels in all three ring designs [40]

Abuhasel and Soliman [41, 42] presented a performance analysis of octal rings as mechanical force transducers. They studied various parameters of an octal ring design as a sensing element and its influence on the stiffness and sensitivity of the ring. Design parameters such as height, thickness, width and edge radius were varied to determine face length and inner diameters. From the simulation results, they found notable strain variation between compressive strain and tensile strain along the ring face. The authors also found regions where strain is maximum and minimum. From the results, the maximum values for tensile and compressive strains were higher than tensile strains and therefore ideal locations for strain gauge placements. The authors also studied ideal strain gauge length and its relationship with the average strain. They found that generally increasing gauge length results in lower average strain values for all three strain components. At a certain length, values of strains such as compressive and tensile strain are equal and therefore such lengths are deemed optimal.

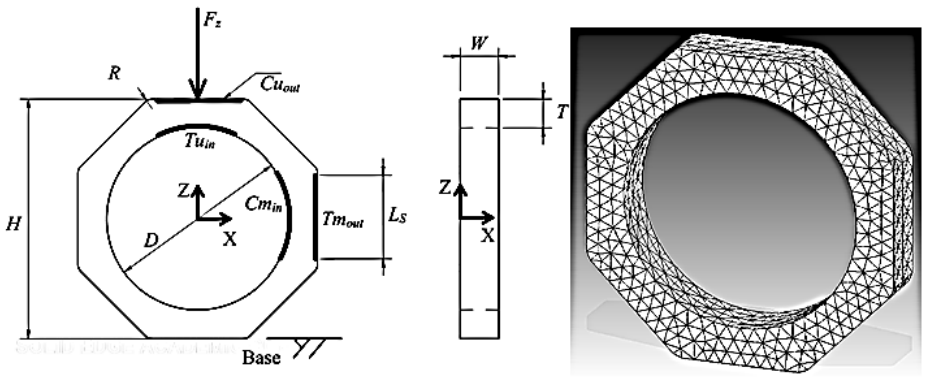


(a) (b)

Figure 2.5 (a) Schematic design of the octal ring (b) FEA analysis conducted on the designed octal ring [41, 42].

Dhanal [43] presented an octagonal design with boss extensions on the top and bottom side of the ring. From the calibration results, all three component forces showed excellent linearity. The FEA study was conducted simulating loads of 130, 190 and 300kg. From this study, they found the stresses and strain regions were more pronounced in the X direction compared to the other two directions. The authors also compared micro strain measurements in all three directions with values obtained from the FEA study. It was found that the measured micro strains values differed varyingly with values obtained from FEA analysis which were lower, with only measured strain values in the X direction at 130kg being higher than the FEA value. Deviation between measured micro strain values in X direction were 4.5% and 3.5% for 130 and 300kg respectively. Micro strain value in the Z direction produced the largest deviation at 43% and 18% for loads 130 and 300kg respectively.

Uddin et al. [4] presented a novel design approach of an octagonal ring with a modified ellipse geometry for cutting force measurement. The objective was to increase strain to displacement ratio to maximize sensitivity. It was found that maximum strain for the ring occurs at 90° and 47.5° under axial and tangential forces respectively. The designed transducer was found to have maximized sensitivity at 15% axial and 25% tangential loading. They also found that highest sensitivity was achieved when the ratio of equivalent radius and effective thickness was 0.256. Calibration was done on the transducer and was found to have less than 2% error in force measurement. The average error for cross sensitivity was found to be 5% whereas overall

uncertainty in measurements was up to 1.78%. The authors found that by introducing an elliptical shape into the ring, the sensitivity of the octagonal ring has been increased by 15% and 25% in the axial and tangential directions respectively. This design approach shows a variable cross section design can increase the sensitivity of the ring without compromising the stress induced on the ring.

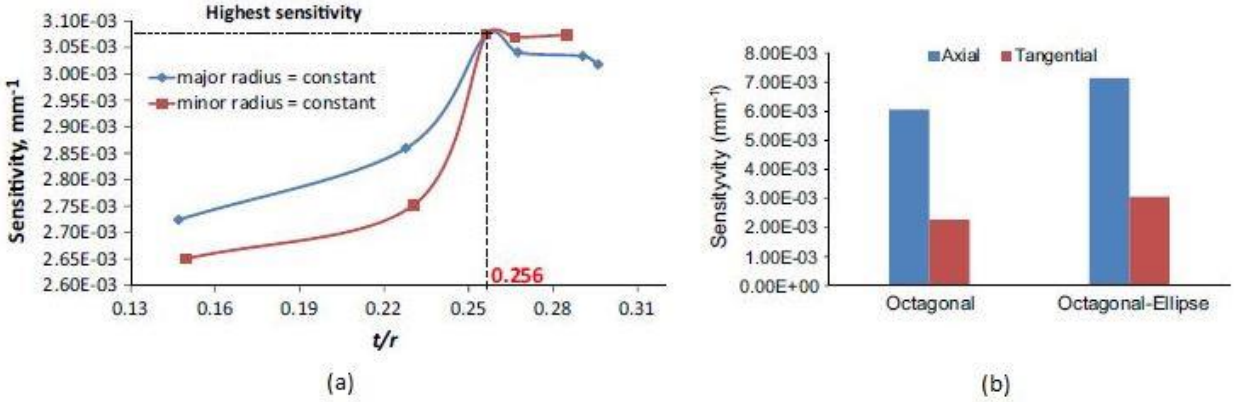


Figure 2.6 Uddin et al. showing (a) ring sensitivity with respect to t/r and (b) sensitivity comparison between octagonal and octagonal-ellipse ring shape [4]

*Double Extended Octagonal Shape*

Although research into other shapes has been presented, the more popular shape that has been reported by numerous authors was the double extended octagonal ring. The double extended octagonal shape is an octagonal based proving ring with a horizontally extended design. Various reports has been presented on its practicality and its advantages in various engineering fields as an important force measuring component in dynamometer designs [44]. The double extended octagonal rings have been used in agricultural field [5, 45-51].

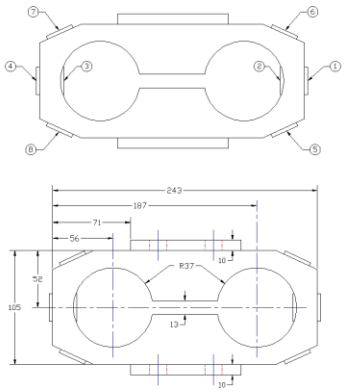


Figure 2.7 A typical double extended octagonal ring showing two inner circular radii connected by a narrow slit [51]

One of the earliest reports on the extended octagonal rings established practical design constrains limits width to mean radius ratio (b/r) between 1 to 3 [52]. Therefore, most ring designs usually follows this ratio on top of other design requirements. An early dynamometer design incorporating an extended octagonal ring was presented by O'Dogherty [53]. The dimensions of the ring were length L = 121mm, side thickness t = 3.5mm and width w = 38.1mm. These dimensions were justified based on design practicality when mounting the ring to the knife. The thickness of the ring however was calculated by approximation based on a developed equation concerning the tangential force. The bridge sensitivity from the calibration test was found to be 2.29 and 1.34 times higher than the calculated for vertical and horizontal forces respectively.

McLaughlin et al. [54-56] published several reports on the design of double extended octagonal ring transducer for force measurement. The extended octagonal rings were placed at opposite sides of the drawbar attached with 4 semi rigid bolt joints on the top and bottom portion of the rings. Dimensions of the rings were 12.7, 50.8 and 76.2mm for thickness, width and inner circular diameter respectively. These dimensions were obtained through trial and error. The calibration results showed that the octagonal rings have excellent linearity and sensitivities. Cross sensitivities obtained were compensated by the derived predictive force equations. The dynamometer was also used in a field test involving a spring tine cultivator and a one-way discer with acceptable results. The second study was on the effect of strain gauge misalignment on cross sensitivity of extended ring (ER) transducer [56]. They presented an investigation on the theoretical analysis using analytical equations to resolve the effect of strain gauge misalignment

on the cross sensitivity of an extended ring transducer. For strain gauge misalignment, the authors studied the effect of tangential and angular strain gauge misalignment and effect of mismatched strain gauges. Tangential misalignment was defined as a misalignment in the x-y plane. Angular misalignment is when the strain gauge is located at the desired angle and location of the extended ring, but its gauge grid is not parallel to the x-y plane. On the effect of tangential misalignment, the authors found cross sensitivities of horizontal bridge to vertical loading was 4.48 $x10^{-3}$ N $N^{-1}$ and vertical bridge to horizontal loading 1.20 $x10^{-2}$ N $N^{-1}$. The author noted that sensitivity to vertical loading was much lower compared to horizontal loading which results in higher cross sensitivity for the vertical bridge. From the combined angular and tangential misalignment analysis, the results showed that angular misalignment had no effect on the cross sensitivity when tangential alignment was perfect. Strain gauges measuring moment against either vertical or horizontal loading however were considerably affected, with cross sensitivity increasing as the angular displacement increase. They noted that all these effects may be due to various factors such as locations of strain gauges at the secondary strain nodes and the effect of secondary loading. It was found that angular misalignment had minimal effect when strain gauges were located at the secondary strain node where tangential misalignment predominates but had large effect when located in regions of high strain due to secondary loading. On the effect of nominal gauge location with, the analysis found that tangential misalignment results in cross sensitivity of 0.004 N $N^{-1}$ and 0.012 N $N^{-1}$ for horizontal bridge to vertical loading and vertical bridge to horizontal loading respectively. This was consistent with earlier reported findings which the author suggest might be because of tangential misalignment being the cause of the observed cross sensitivity. A third study was on the effect of load fixture design on sensitivity of an extended octagonal ring (EOR) transducer [55]. Identical loading and support fixtures were constructed for vertical loading with varying spaces on the faces of an extended octagonal ring (EOR). Calibration test was conducted by varying the space between the contact points on the loading and the support fixtures. The second calibration test studied the effect of varying the bolt torque from 0 to 135 Nm on the sensitivity of the EOR at different load spacing length. From the first calibration test of varying load point spacing, they found that initially sensitivity decreased slightly but dropped rapidly beyond 100mm with sensitivity of about 60% of the nearest point when load point spacing was 190mm. From the second calibration test, for 70mm and 150mm, there was no observable change to the sensitivity across the range of mounting bolt torque. However, the further the loading point distance the more

change was observed, with loading point spacing of 190mm having a 7.3% decrease in sensitivity as the mounting torque was increased. Further observations revealed that maximum sensitivity was achieved when loading point spacing distance was 70mm or lower. From the results obtained on the mounting bolt torque, they claimed that the change in sensitivity was due to the additional torque on to the bolt tension introducing a bending moment that interacts with the loading plate. This creates distortion on the loading plate and the EOR from two different sources of tension, the other being the air cylinder applying a compressive load on the loading plate. The authors noted that the effects of these interactions were more pronounced the further away the loading point is from the bolt tension due to opposite bending moments from both instances. Consequently, due to the nature of the studies stated above, the authors did not present any stress or strain analysis on the extended octagonal ring. The study was purely on the effects of various measuring conditions and its interactions of different sources of loading and tensions at different locations on the sensitivity of the EOR.

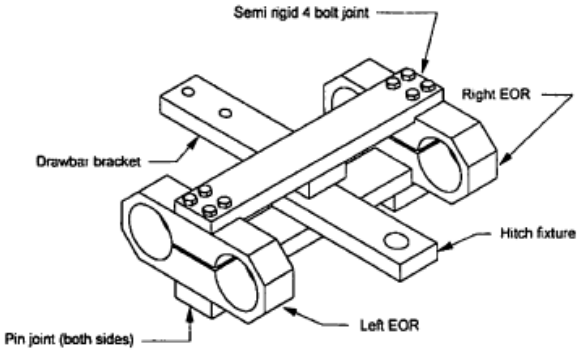


Figure 2.8 Dynamometer diagram showing the locations of the extended octagonal rings [54].

Kheiralla et al. [47] presented a design of an extended octagonal ring dynamometer to measure horizontal and vertical forces acting on a three point hitch on a tractor. Three extended octagonal rings were used in total as shown in the Figure 6. The sensing elements were placed between an inverted U frame and hook brackets where the forces were to be measured. Strain gauges connected in a Wheatstone bridge configuration were used to measure the strains on each of the extended rings. Strain gauge locations based on strain energy theory were found to be 90° and 39.6° for draft and vertical force respectively. These locations give the best measurement with

negligible cross sensitivities. Horizontal and vertical displacements for the top and bottom rings were also calculated. For horizontal displacements, the top ring measured $2.24 \times 10^{-3}$ mm/kN and $2.76 \times 10^{-3}$ mm/kN for the bottom side. For vertical displacements, the top side and bottom side were both measured at $16.9 \times 10^{-3}$ mm/kN. The maximum rated capacity for each transducer were set at 25 kN and 10 kN for draft and vertical forces respectively but the whole dynamometer was designed for 50 kN and 20 kN. From the static calibration results, the strain output bridge showed excellent linearity with the applied load with obtained R-squared value of 0.99. The measured mean sensitivities obtained were 25.19 μStrain/kN and 25.60 μStrain/kN which indicates highly accurate measurements. However, predicted values based on computation for the sensitivities were slightly higher than the obtained sensitivities. The stiffness of the combined dynamometer was found to be acceptable based on the natural frequency found.

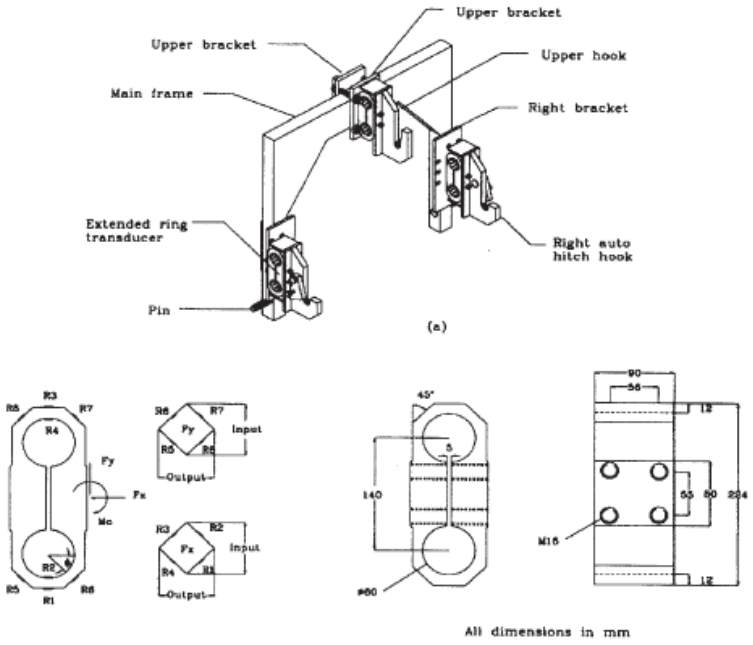


Figure 2.9 Arrangements and schematic diagram showing the extended octagonal rings [47]

Ortiz-Laurel [57] suggested a dynamometer design for traction forces measurement on draught horses involving an extended octagonal ring transducer. The authors designed four transducers connected with strain gauges whereby each was assembled individually to measure horizontal and support forces acting on each foot of a draught horse which the transducers were

attached to. They stated that the use of octagonal rings was due to the ease of usage along with its rigidity and stability. The maximum vertical force measurement was deemed to be 10 kN whereas the horizontal force was 5 kN. From the calibration results, the transducers showed excellent linearity with negligible hysteresis. Cross sensitivity obtained was also low. Raheman et al. [58] presented a novel study on a computer-aided design of an extended octagonal ring transducer for agricultural implements. They developed a program code that decides the best possible combination of dimensions for a transducer based on the user inputs. This was done by varying length to mean radius ratio (L/r) and width to mean radius ratio (b/r). For their study, dimensions were selected based on space availability. Thin ring theory was used to derive equations for the program to aid the design of the transducer. Based on the derived equations for bending moment, the authors found that the optimum strain gauge locations to be at angles 39.5° and 90°. In the design procedure, the authors placed emphasis on the value of mean radius to thickness ratio to conform to thin ring theory. This ratio was set at $r/t \geq 3$. However, they also noted that the ratio of width to mean radius b/r has a greater effect on the values of mean radius to thickness ratio r/t by 72% increase over the range of values 1 to 3 compared to the ratio of length to mean radius (L/r) with increase of 35%. The program was designed for the user to input specifications such as material and strain gauge to design the transducer to measure both component forces up to 1kN with moment arms of 500mm and 250mm. The program then initiates a simulation of values of L/r and b/r for different r values with safety factor set at 1.35 and outputs a set of desired dimensions based on the input requirements. Initial analysis using the developed equations predicted that sensitivity values of 0.114 mV/kg and 0.094 mV/kg for horizontal and vertical forces respectively. The actual sensitivities obtained were 0.120 mV/kg and 0.092 mV/kg for horizontal and vertical forces respectively. The authors claimed that the low difference between actual and predicted value proved the competence of the program.

Afzalinia et al. [6] presented an extended octagonal ring transducer design for the compression chamber of a large square baler. The transducer consists of two extended octagonal rings situated parallel to each other connected by four brackets. Through theoretical means, they identified the optimum strain locations to be 39.5° and 140.5° for axial force and 90° for vertical force measurement. The dimensions of the rings were determined by adhering to various design requirements based on the ring such as strain gauge and housing size. The authors then calibrated

the transducer by applying forces in all three directions simultaneously and independently which produced excellent linearity. Based on the analytical equations used to predict the sensitivities of the sensor, the calibration test showed the theoretical values calculated were well below the obtained sensitivity values.

Another octagonal based design approach was provided by Shishvan et al. [59] who studied the evaluation and comparison of stress node on extended octagonal ring transducers by strain energy theory and finite element method. The designed ring had a total length of 184.8mm and width of 76mm with inner circular diameter of 30mm. They utilized strain energy theory and finite element method to investigate the stress nodes location and calculate strain distribution on the octagonal ring transducer due to horizontal and vertical forces to identify ideal locations for strain gauge placement and to minimize cross sensitivity. They found that at specific inner and outer locations on the ring, unique strain characteristics at these locations enables horizontal and vertical forces to be measured independently of each other. From the finite element method, the optimum strain gauge locations were determined to be 79.5° and 75° outer and inner side of the circumference respectively for horizontal force measurement. For vertical force measurement, the optimum strain gauge locations were 18.5° and 161° on the outer side of the circumference.

Dynamometer designs has also incorporated unique ring arrangements involving the extended octagonal ring to produce better transducer performance. One such example was provided by Nalavade et al. [60, 61]. The design of the transducer utilized a double DEOR configured back to back along at right angles along the longitudinal axis forming a cross. Dimensions of the ring were based on assumptions due to design requirements during usage of the transducer. Finite element analysis was used to study the performance of the DEOR under various loading conditions which leads to the ideal locations for strain gauges. The FEA study was conducted based on a linear elastic model using a uniformly distributed force of 5kN on both X and Y direction on the central area of opposite faces. From the FEA study, the authors found the optimum strain gauge locations to be at angles 34° for force measurement in X direction and 90° for force measurement in Y direction. Calibration was conducted on the fabricated DEOR in two phases. The first phase was conducted on a calibration desk and the second phase calibration was done on an actual mounted position. The first phase was done as a confirmation of the workability of the DEOR. The second phase was conducted to improve the accuracy of the DEOR and to

minimize the cross-sensitivity effects on the transducer. From the static calibration desk test, the authors found that cross sensitivity effects were less than 2%. From the actual mounted position, initially the authors found that cross sensitivity varied significantly ranging from 5% to 123% with X,Y direction having the highest cross effects value of 123% and 95%. The authors noted that this may be due to the longer moment between the DEOR transducer and the point of force application. The position of the DEOR transducer was brought closer to the disc and this resulted in cross effects values dropping significantly to ranges of 2.47% to 33.3%.

Abbaspour-Gilandeh et al. published two separate studies on the extended rings [62, 63]. The first was an extended octagonal ring transducer for measurement of tractor-implement forces. To find the optimum strain gauge placement, analytical and finite element analysis were used. In both cases, horizontal force of 25kN and vertical force of 15kN were applied independently onto the transducer. The result from both approaches generated a strain gauge location at 39.54° and 90° for the independent measurement of vertical and horizontal forces respectively. All three transducers had cross sensitivity values ranging from 0.97 to 0.99% for horizontal force measurement and 0.92 to 0.96% for vertical force measurement. Following up from their first study, they designed a dynamometer using extended octagonal rings in a novel configuration [63]. Two extended octagonal ring transducers rated at 20 kN were arranged back-to-back at right angles to each other with a tubular torque meter separating the transducers as shown in Figure 7. The transducers were placed in a dynamometer frame that was designed and analyzed using finite element method. Strain gauge locations were obtained using strain energy theory and data collected from the node points. From the static calibration test, dynamometer showed desirable precision, sensitivity and repeatability. Calibration curves obtained showed excellent linearity between the bridge output voltage with the measured forces and moments in all directions during calibration. Unlike the previous study however, they did not report any improvements made to the sensitivity or stress distribution of the ring.

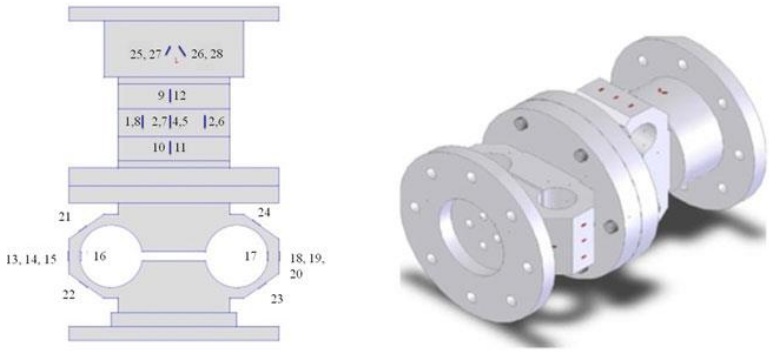


Figure 2.10 Arrangement of the extended octagonal ring force transducers [63]

Godwin [64, 65] presented an extended octagonal rings dynamometer design for use in tillage studies. Each ring is an octagonal shaped transducer designed with two circular rings on opposite ends connected by a narrow slit. The ring had a length of 173.7mm, thickness 51mm, and inner circular ring diameter 63.5mm with thickness of 4.39mm. Strain nodes were found based on previous research where the proposed strain gauge locations for optimum performance. For simple ring dynamometers, the locations were 39.6° and 90° based on strain energy theory and 50° and 90° for octagonal ring dynamometers based on photo elastic methods. The author utilized the second set of angles initially. However, calibration test found that the output from the force bridge measuring force in the horizontal direction was not independent of the position of the force. The author claims this is due to point loading on the half ring in compression causing force output to be sensitive to the position of the force. This was rectified by inserting two plates; the first between the mounting and the transducer and the second between transducer and tine. Calibration test found that cross sensitivity was negligible when the horizontal force measurement gauge was at 34°. Sensitivity obtained was 1.35 times larger than the predicted value.

*Miscellaneous Shapes*

Despite the numerous octagonal based designs, other shapes have also been reported as well. One such example was reported by Prasad et al. [66] on the design of a square ring-shaped force sensor. The square ring was rated at 20 kN. From the stress distribution analysis, it was found that maximum stress occurs at the top surface at the point where force is applied. Stress and strain distribution were shown to have similar characteristics whereby propagation decreases along the

surface towards the edge of the ring. The maximum stress and strain values found along the surface of the square ring was also almost four times lower than on a circular ring. From the deflection characteristics analysis, the maximum deflection found was 0.927mm compared to 1.749mm for circular ring shape. The authors summarized that from the finite element analysis, the stress-strain characteristics of the square ring were about a quarter of the stress-strain characteristics of a circular ring-shaped force sensor with deflection found to be almost half of similar capacity.

Examples of elliptical shaped proving ring designs were also presented. Kaushik et al. [67] published a research on preliminary investigation on metrological characterization of elliptical shaped force transducer. The authors designed an elliptical force transducer rated at 20kN based on the theories of thin rings. The authors found that based on the stress, strain and deflection analysis, the optimum location for the strain gauges are at an angle of 90° from the vertical axis on the outer side of the curved surface. It was also shown that the elliptical ring exhibited excellent metrological characteristics compared to other ring shaped for transducers with minimal cross sensitivity due to optimal strain gauge locations. Relative deviations based on multiple sources of error was found to be less than 0.1% with reversibility error within the range of 0-0.03%. A second example was provided by Kumar et al. [8] who published a paper on the investigations on metrological characterization of an elliptical shaped force transducers for precision force measurement. Computational deflection measurement was found to be 2.461mm at 20kN. The ring was fabricated, and experimental deflection was found to be 2.488mm. The elliptical shaped transducer was found to have a better uncertainty of measurement compared to both ring and hexagonal shaped transducers especially at lower applied force but the ring shaped was better when applied force was 20kN, with uncertainties measured at 0.01 for ring shaped as opposed to 0.02 for elliptical shaped.

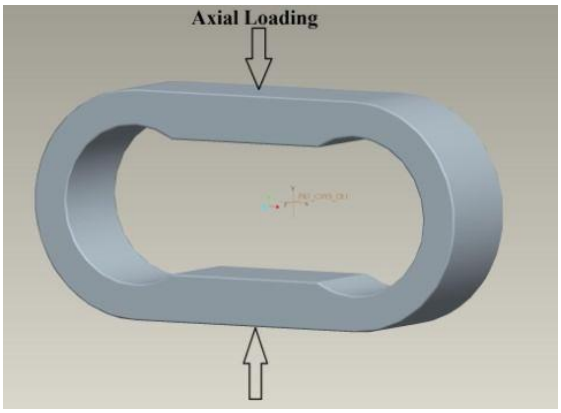


Figure 2.11 Elliptical ring design [67]

A study on a six sided hexagonal ring design was presented by Kumar et al. [7]. The authors discussed the development of a hexagonal-shaped forced transducer with modifications to improve its performance. It was found that in terms of deflection calculations, computational and experimental values had negligible deviations (1-3%). However, both values had slight deviations (7-10%) compared to analytical. The uncertainty of the modified ring was found to be ± 0.10%. The authors found that the metrological performance of the hexagonal shape was superior compared to ring-shaped or octagonal-shaped force transducers, but uncertainty of measurement was slightly higher.

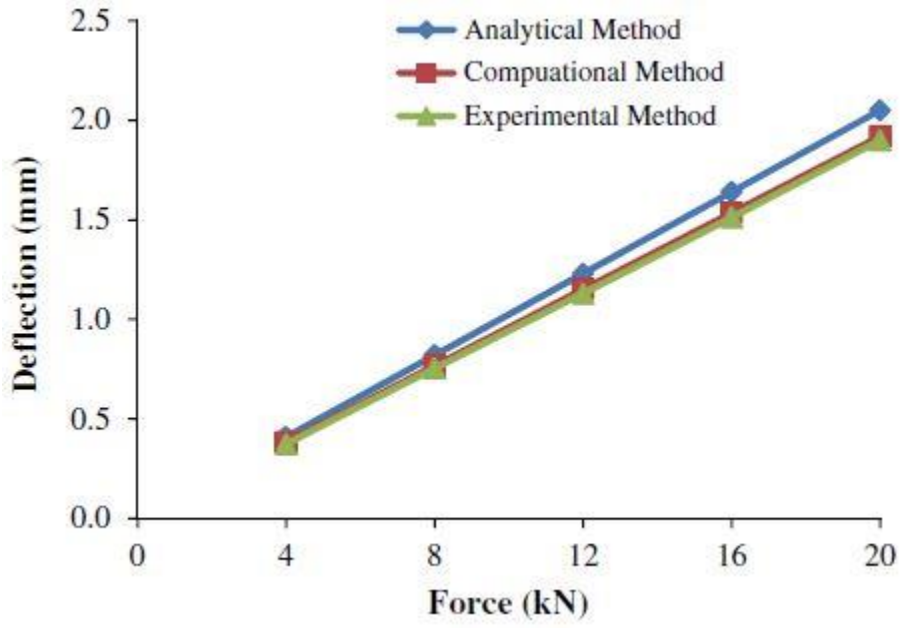


Figure 2.12 Deflection of the modified ring based on different methods [7].

A study incorporating a varying ring thickness at different locations throughout the ring cross section was observed by Rahman et al. [68, 69]. They studied an optimum design of a circular proving incorporating a variable cross section approach. The premise of the idea was based on the deflection equation, in which, keeping all other parameters constant, the moment of area I from the equation can be controlled to affect the deflection of the ring. The ring was designed with variable cross section with mean diameter R = 127mm. The proving ring had 24 variable cross sections or 6 sections per quadrant. The manufactured ring was then tested with top attachment and without. The results showed that the ring had more deflection without the attachment then with. Also, it was found that for a conventional ring the deflection calculated was much lower than the modified ring. The total stress on the variable cross section ring was also found to be much lower than the conventional ring. The authors presented a modification that could enhance the deflection of the ring by varying its cross section and hence controlling the moment of area of the ring. However, it was noted that the mean radius and therefore thickness was the varying parameter. Effects of varying the width of the ring was not studied.

Rodriguez-Fuentes [70] presented a design, manufacturing and calibration of a circular ring type monolithic load cell addressed to drawbar pull testing of the farm tractor. Design procedures and material selection were done by referring to standards set by agricultural bodies. The capacity of the load cell was determined through consultations with agricultural tractor manufacturers. The load cell was then designed and manufactured with strain gauges located at 90° in a Wheatstone bridge configuration. Calibration test was conducted, and the results showed that the output voltage and force showed excellent linearity. They then calculated the maximum stresses and moment. From the calculations the factor of safety was determined to be 4.06 and 1.83 for the load cell and strain gauge respectively. They concluded by claiming that the designed load cell could measure forces with 99% certainty. However, the study also did not include stress or strain analysis on their designed load cell.

Zhao et al. [71-73] presented a study on design and development of a cutting force sensor using octagonal rings based on semi-conductive strain gauge. In this study, the authors study the use of semi conductive strain gauges fabricated by microelectromechanical systems (MEMS) technique for cutting force measurements. Strain gauge were placed at 50° and 90° which the authors referenced from previous research. From the initial analysis, they found that the simple

octagonal ring design was not sufficient due to higher requirements of 666Hz for natural frequency in the tangential force direction with the calculated octagonal ring value only at 499Hz. Ergo, a biaxial cutting force sensor utilizing two octagonal rings connected perpendicularly to each other from the horizontal axis was devised. The new design was termed two mutual-perpendicular octagonal rings (TMPOR). From the FEA conducted, they found that the proposed design has a natural frequency of 928Hz. Semi-conductive strain gauges were chosen due to improved sensitivity and gauge factor having one or two orders of magnitude over the conventional metal foil strain gauge. From the static calibration test, the authors found excellent linearity between the output voltage and force applied, with the sensitivity of the semi-conductive strain gauge about 16 times of the metal foil strain gauge. The authors however noted that the theoretical value of semi-conductive sensor to metal foil sensor was 19.2 times against the experimental value of 16. They claimed that this may be due to various reasons such as positional error of the strain gauge or inconsistent adhesive thickness affecting the results. Cross interference in the thrust force direction was higher and was attributed to the fixing method between the cutting tool and the sensor. The modal impact test conducted showed that force sensor can be used at high speeds at spindle speed not more than 17,205 rev/min. They also found that the natural frequency obtained was lower than the simulated natural frequency. This was attributed to issues during assembly of the transducer.

Liu et al. [74] reported a three-component strain gauge dynamometer for grinding and polishing force measurement. The authors published a report on the design of a dynamometer for an automatic grinding system with a heavily modified elastic element they termed an octagonal measuring block. The measuring block design incorporates a square shape outer side with an octagonal shape inner cut out as presented in the figure below. Strain gauge locations were selected based on maximum axial strain due to various forces. These were placed at the inner and outer locations at the horizontal sides of the measuring block for maximum axial strain due to force in the horizontal direction. For forces in the x and z direction, the strain gauges were placed on the inner and outer portion of the horizontal sides of the octagonal inner shape. For force in the y direction, strain gauges were placed at the middle of the bottom portion of the measuring block. From the static calibration test, the output voltage from the bridge circuit showed linear correlation with each component forces. The results also showed minimal interactions between measurements

of individual force components. The dynamometer was then used in a surface-finishing operation and the output results indicate the dynamometer performed as expected.

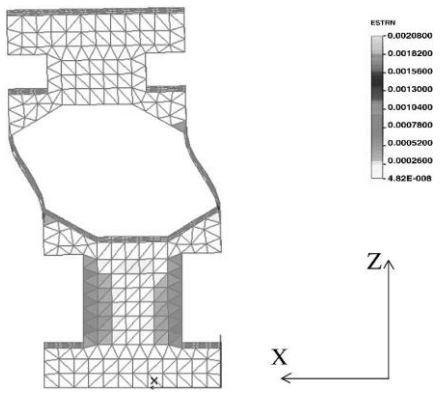


Figure 2.13 FEA model of the force transducer developed by Liu et al. [74].

Rao et al. [75] published a design and fabrication of a new type of dynamometer to measure radial component of cutting force and experimental investigation of optimum burnishing force in roller process. The authors presented a design approach to fabricating a modified circular ring transducer to measure radial force in cutting and roller burnishing process. Strain gauges were fitted in a Wheatstone configuration at inner and outer side of the straight edges of the ring to measure the strain induced by the radial force. From the static calibration process, the outputs were shown to have a linear relationship with the force induced. However, no stress analysis was included in the study. Also, from the dynamometer fixture the ring was attached to it was not obvious how or in which direction the force is applied.

A dynamometer designed with an elastic element taking the shape of a circular hollow bar was presented by Panzera et al. [76] to measure turning force. Strain gauges are placed at the outer surface of the elastic element. From the calibration test, the results showed that the three component forces decrease slightly at 5% as the cutting speed increases. Feed rate and depth of cut showed a linear relationship with the three force components. The authors found that this shows the feed rate and depth of cut has a more significant effect on the forces than the cutting speed. They concluded that the developed dynamometer was reasonably designed and compared favourably with a piezoelectric dynamometer.

Qin et al. [77, 78] published a report on a milling torque sensor implementing a modified thin-walled cylinder as the sensing element. They determined the crucial design parameters for the sensor were the radius, thickness and length of the thin-walled cylinder. Length and radius of the cylinder was to be minimized so as to increase the stiffness of the sensing element without compromising the sensitivity. Thickness of the cylinder should also be reduced to obtain a maximized sensitivity. Finite element simulation was used to locate the surface strain on the cylinder with straight outer sides machined onto the cylinder to facilitate easy strain gauge placement. Piezoresistive MEMS strain gauges in a Wheatstone bridge configuration was used to measure the strain induced by the torque during milling. Static calibration results showed that the sensitivity was improved to 0.13 mv/Nm with a linearity error of less than 1.6%, indicating that the sensor is highly accurate. Modal impact test was also conducted to ensure its natural frequency was suitable for machining process. The natural frequency was found to reach 1216 Hz which indicates that it can be used for machining process up to 8445 rpm. They then conducted cutting test on the developed torque sensor between 500 rpm to 2000 rpm. At 800 rpm, irregularities were found due to one of the tool teeth breaking during the milling process. This indicates that the torque sensor could pick up milling tool breakage or other signs of wear and tear through anomalous signals.

Chen et al. [79] reported on nonlinear mechanics of a ring structure subjected to multi-pairs of evenly distributed equal radial forces. They used multiple existing ring theories combined with finite element analysis to develop a theoretical approach to studying a ring in tension or compression. The authors found that under both stress modes the ring always forms a regular polygon with 2N sides under N-pairs of equal radial forces. However, in compressive mode the ring was found to have a flower like pattern. They found that the ring experiences multiple states depending on the type of stress. Theoretical approach was found to be in accordance with the finite element results which validates the findings. The topological experiment conducted also matched with the previous two results. However, the study was done for ring structures within the nano to micro range systems.

A dynamometer design incorporating a monolithic design of straight plates and octagonal strain rings was presented by Brewer and Hull [80]. Initial calibration results showed that the developed dynamometer produced non-linearity between load-strain relations and inaccuracies

with respect to loads that occur during bending. From the finite element simulation, the authors found that this was due to excessive interface plate bending. This was solved by having interface plates that are stiffer than the octagonal strain rings and to connect the plates to the environment to have similar boundary conditions for both plates. The authors claimed both these suggestions would solve the problem of non-linearity between the load-strain relationships experienced by the dynamometer.

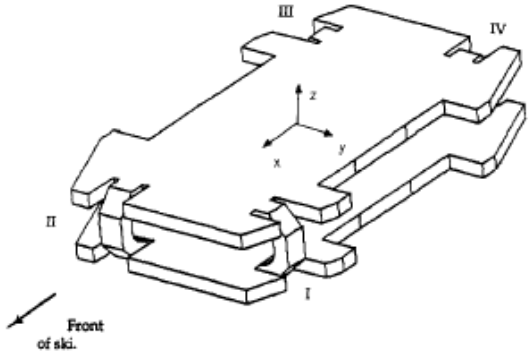


Figure 2.14 Interface plate design approach involving octagonal strain rings suggested by Brewer and Hull [80].

### *2.3.2 Capacity*

Generally, the capacity of the rings is directly affected by the geometry of the ring. Engineering applications that require smaller rings due to space constraints tends to favour the octagonal shape [3, 38, 39]. Agricultural applications with no space constraints and with higher load requirements tends to favour the sturdier double extended octagonal rings [6, 60, 61]. The following table shows some capacity examples from recent literature.

Table 1. Comparison of ring capacity reported from literature

| Ring | Capacity | Application | Author |
|---|---|---|---|
| **Circular** | 50 kN | General force measurement | Kumar et al.[22] |
| **Circular** | 5 kN | General force measurement | Kumar et al.[27] |
| **Octagonal** | 1 kN | Cutting force measurement | Uddin and Songyi [4] |
| **Octagonal** | 5 kN | Machining Operations | Yaldiz and Uncasar [36] |
| **Double Extended Octagonal** | | | Chen, McLaughlin and Tessier [5] |
| **Double Extended Octagonal** | 1.09kN vertical and 1.24kN horizontal | Sugar beet topping knife | O'Dogherty [52] |
| **Cylindrical Bar** | 3.5 kN | Lathe tool dynamometer | Jain et al. [28] |
| **Square** | 20kN | General | Prasad et al. [66] |

Capacity of the proving ring is determined based on its intended use and shape. Usually, octagonal rings have the lowest rated capacity. Double extended octagonal rings can have varied capacities based on the force direction or application. Circular rings however can measure forces from as low as 5N to as high as 1MN [18]. Load rings for general force measurements based on the circular shape has been manufactured to measure loads from 5kN to 50kN. One report of a cylindrical bar used as a component in a lathe tool dynamometer measured forces up to 3.5 kN [28].

Force measurement in machining is usually much lower than in agriculture. Multiple reports have been made of cutting tool dynamometer used in machining operations measuring forces up to 5kN but generally most octagonal ring-based dynamometers are rated between 3 kN to 3.5kN [29, 33, 36, 37]. In agricultural processes, the maximum force measured can vary quite significantly and depending on the direction of force measurement with the horizontal or draft

component much higher than vertical. Chen et al. [23] reported an extended octagonal ring design with capacity of 90kN draft force and 17.5kN vertical force. 20kN and 50kN. Kheiralla et al [47] reported a lower combination of maximum capacity values with horizontal and vertical forces of 25 kN and 10 kN respectively. A summary of the different combinations of horizontal and vertical forces reported by various authors is presented in the table below.

Table 2. Maximum rated horizontal and vertical capacity reported by various authors

| Author | Horizontal Capacity | Vertical Capacity |
|---|---|---|
| **Chen et al [5]** | 90.0 | 17.5 |
| **McLaughlin et al [54]** | 45.0 | 13.0 |
| **Kheiralla et al [47]** | 25.0 | 10.0 |
| **Ortiz-Laurel [57]** | 5.0 | 10.0 |
| **Abbaspour-Gilandeh [62]** | 25.0 | 15.0 |
| **Onwualu [46]** | 4.4 | 4.0 |

### *2.3.3 Design Stresses and Strains*

Multiple reports found the maximum stress and strain to be at the top outer part where force is applied and the bottom fixed portion of the ring. The distribution of maximum stress and strain in this location tends to be smaller and identical. The stress and strain distribution then tends to decrease up to 39.6° from the point of axial force which then increases along the periphery of the ring [22]. This location is also known as strain nodes and is considered the precise location of strain gauge placement for strain measurements. A second larger stress location is found more evenly distributed along a larger portion of the ring at the horizontal side [19]. The following figure illustrates the typical stress distribution on a circular proving ring. It can be observed that the point of force application at the top portion of the ring contains the highest stress values. Along the periphery of the ring the stress can be seen to be distributed along a larger surface area.

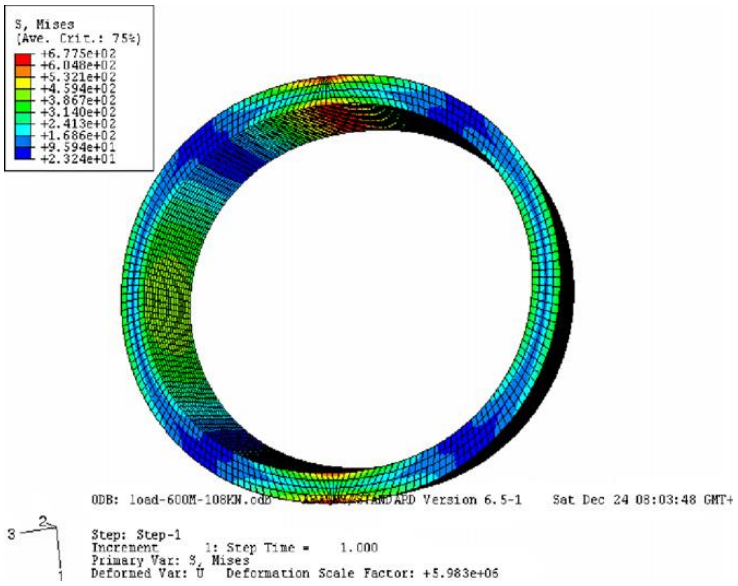


Figure 2.15 Finite element analysis of a circular ring presented by Chen et al. [19]

Studies were also conducted on multiple other ring shapes that illustrates different stress and strain distributions for each type of ring. Similar to the circular ring design, the maximum stress value tends to center at the point of force application. Kumar et al. [7] through their study of a hexagonal design found the stress to minimize up to and angle of 50° from the point of load application and increase up to 90° of the horizontal axes of the ring. A study on a square ring designed found stress and strain to be irregular due to the shape of the ring. Higher stress values were found to be concentrated on the inner circular surface of the ring as opposed to the sharp edges. They also found that stress and strain values to be significantly lower compared to a circular ring of similar capacity. Stress and strain distribution in an extended octagonal ring can differ significantly depending on the direction of force application. From Figure 2.17, Chen et al. [5] illustrates their extended octagonal ring design showing significantly different strain distribution when subjected to different types of load. It can be observed that strain values are higher at locations around the inner circular section. Due to this variation, optimal strain gauge placements were determined to be at 80° outer and 75° inner circumference for horizontal force measurement. For vertical force measurements, strain gauges were placed at 18° and 162° inner circumference.

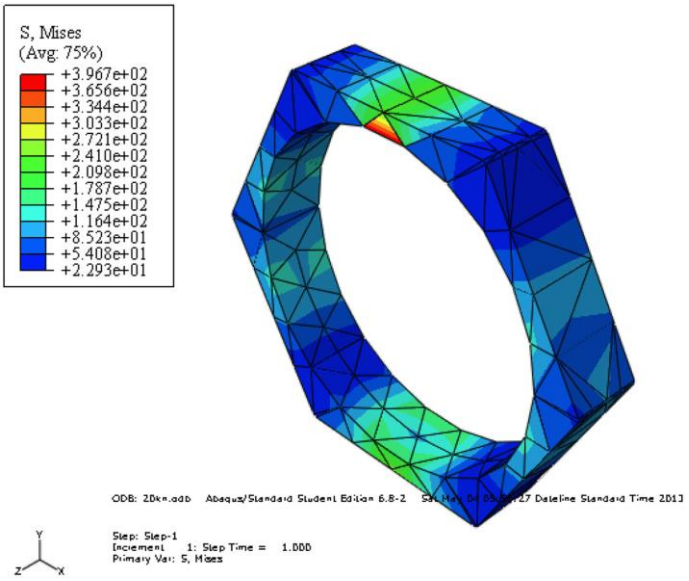


Figure 2.16 Von Mises stress distribution presented by Kumar et al. [7]

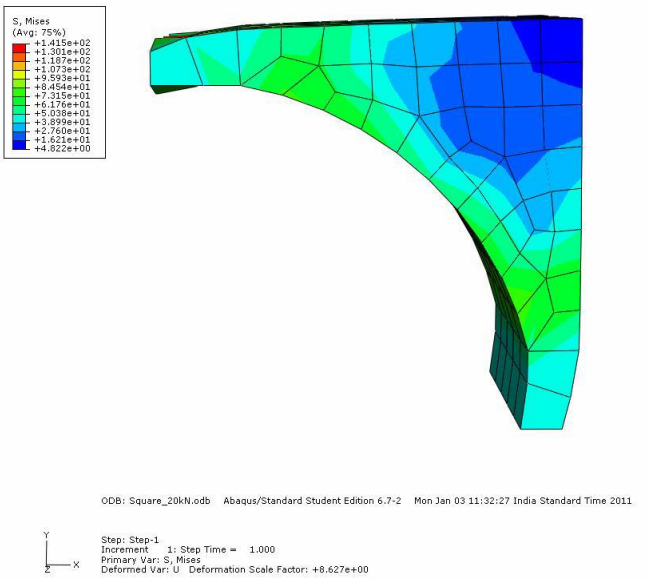


Figure 2.17 Von Mises stress distribution on a square ring presented by Prasad et al. [66]

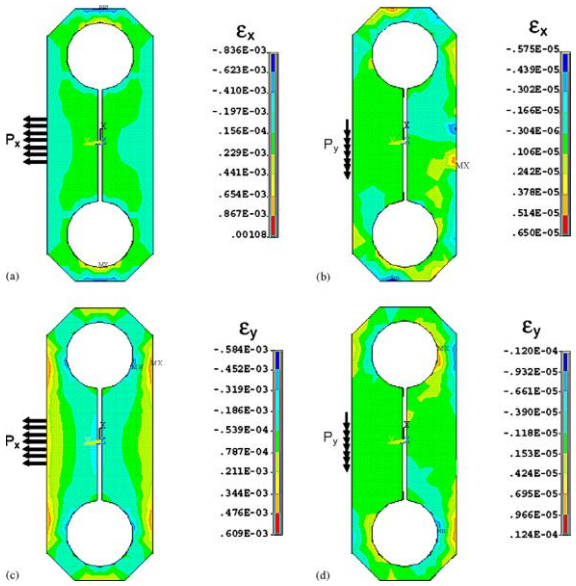


Figure 2.18 Strain distribution on an extended octagonal ring by Chen at al. when subjected to force in the axial and horizontal direction [5]

### *2.3.4 Design Deflection*

Circular force transducers has been designed to measure force by measuring its deflection [15]. Commercially available force transducers have also been developed. Proving rings with attached dial gauges require considerably more ring deflection than strain gauge-based rings. This is because deflections are preferably as high as possible for accurate measurement. A circular ring presented by Kumar et al. [22, 23] had a maximum deflection value of 1.770mm and 2.820 at 20kN.Generally a circular ring design has significantly more deflection compared to other shapes. However, recent literature has seen considerable number of rings of other shapes with improved deflection and therefore higher sensitivity. A square ring developed by Prasad et al. [66] has a reported deflection value of 0.927mm. A study by Kumar et al. [8] was done on an elliptical ring shape where computational deflection measurement was found to be 2.461mm compared to the experimental deflection of the fabricated ring found to be 2.488mm. Another study by the same author on a hexagonal ring design measured deflection at 1.900mm compared to an analytical value of 2.050mm [7].

Though proving rings are designed to be highly sensitive by maximizing its deflection, most common use of the proving ring in force measuring industries does not require large deflections. Due to size constraints in building a dynamometer, the deflection found in octagonal based shapes are very low and hence are usually not measured by means of a dial gauge. This is due to usage as rings are manufactured to be as small as possible as a component in dynamometer designs. This is an advantage though since some industries does not require rings with a significant deflection. These rings are mounted with strain gauges to measure strain instead of deflection for force measurements. Another advantage of using strain gauges over dial gauge is its effect on uncertainties in measurements. The use of strain gauges minimizes uncertainties which was proven by Kumar et al. [30] where an octagonal ring was fitted with a dial gauge and compared with strain gauges. They found sources of error and uncertainties to be higher when using the dial gauge compared to the strain gauges.

Force measurements in agricultural and machining applications does not rely on the deflection characteristics of the ring. This is due to the design of the whole dynamometer itself. Most dynamometer designs that has been reported does not intent to have a space to read a dial gauge due to small design. Also, rings used in these fields, such as the extended octagonal ring, has been reported to be extremely small to be measured. An example was provided by Thinley et al. [48] who reported deflection values of 0.034mm under a load of 1.05kN. Second is due to the nature of the application of smaller ring sizes. Forces measured in these applications typically ranges between 10-25kN. Hence, the use of a dial gauge to measure deflection is irrelevant for a smaller ring at lower capacity. Lower capacity measurements using a dial gauge was also reported to be of lower resolution [27]. Third is based on applications that does not permit deflection [44]. Deflection of the dynamometer might affect the cutting tool operation [39]. And lastly due to the dangers of being around the force transducer during applications such as machining, strain gauges allow users to read measurements at a further distance away during the force measuring time. This is done by connecting a data acquisition system based on attached strain gauges to measure the strain induced on the rings. Strain rings were used because it has high sensitivity to stiffness ratio [3, 38, 39].

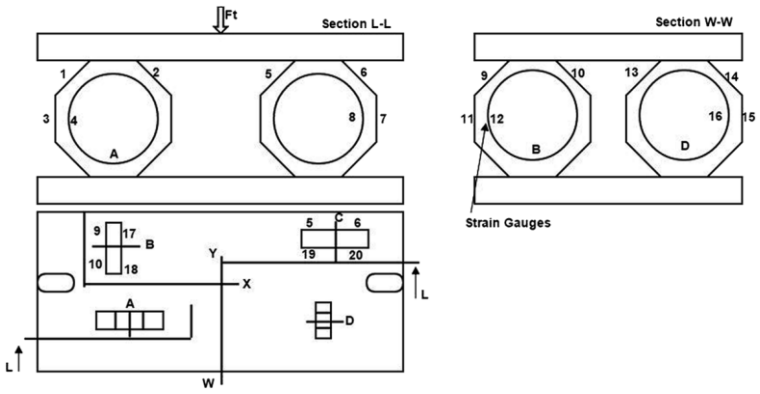


Figure 2.19 Compact dynamometer by Pathri et al. showcasing the use of multiple smaller sized rings. [33].

### *2.3.5 Measurement of Force*

Force measurement is commonly done with the use of a strain gauge. However, a cheaper and mechanical alternative is by measuring its deflection under load. The earliest known method of measuring the deflection was by using a vibrating reed. However, a simpler is way to measure the applied force using dial gauges. When load is applied, this causes a small diametral deflection onto the ring. Using a dial gauge or a vibrating reed, the deflection can be easily measured and read. Measuring load this way requires the ring and the gauge to be calibrated beforehand. Using the modulus of elasticity of the ring, the measured deflection value can then be used to obtain the load value by using the deflection equation derived from thin ring theory.

Dial gauges are used to measure the deflection of proving rings due to noticeable diametral change when force is applied [15, 30]. This would require a ring of considerable size to ensure the deflection is maximized and measurable. Literature tends to heavily favour strain gauges in a Wheatstone bridge configuration however as opposed to the dial gauge. The main difference is due to the nature of application between the two. Proving rings with dial gauges are more suitably used for static force measurements such as calibrations of dynamometers. Most applications such as machining operations however measures force dynamically which sees a constant change in forces. Strain gauges would therefore be more suitable for these types of applications.

### *2.3.6 Materials and Manufacturing Process*

Material and manufacturing of the proving ring depends on its intended use. Although the manufacturing process of proving rings has never been discussed in the present literature or design studies, a typical ring or cylindrical based metallic structure is commonly fabricated through metal rolling such as ring rolling. However, proving rings can also be manufactured by rough machining of an annealed forging, followed by heat treatment and grinding to obtain the final shape. Different types of metals have been used throughout literature, ranging from aluminum-based metals to the more commonly reported steel alloys. The use of alloys steels is common due to it being cheaper to manufacture and higher overall strength. The selection of steel depends on several criteria of the proving ring or the general dynamometer design of the study. Determination of material is usually done based on the maximum stress that is induced on the ring. Another, although was not directly reported in literature, could be the cost and availability of the desired material.

Karabay [3, 38] used the common and cost-effective SAE 1020 steel in his design of the force transducer. Korkut et al. [35] used AISI 1040 steel in their dynamometer design. They calculated maximum stress on the ring and found the value to be lower than the material yield strength. Yaldiz et al. [29, 36, 37] used AISI 4140 steel in their dynamometer design. This material is suitable due to high ductility and high yield strength. Kumar et al. [22, 26] reported in multiple studies the use of material EN24 in finite element studeis of their circular proving design. Other types of alloys have also been used in manufacturing the proving ring. Soliman and Abuhasel [41, 42] reported using the material Aluminum 1060 in their modified octagonal ring design. Another aluminum based proving ring design was reported by Thinley et al. [48] in their study on the extended octagonal ring. They used the alloy Aluminum 5056 due to the material characteristics which satisfies the maximum allowable stress induced on the ring.

## 2.4 Factors Affecting Proving Ring Design and Operation

### *2.4.1 Calibration*

Calibration of the ring is usually done to compare and validate the results of an analytical or finite element design approach to an actual experimental specimen. It is also done to assess and identify cross sensitivity effects due to strain gauge locations. Calibration process usually adheres to the calibration procedure according to ISO 376-2004. Cross sensitivity happens when a set of strain gauges measurements are affected by force application from another angle. Another is to measure cross effects, repeatability, hysteresis and various other parameters [8, 22-27]. Calibration process also affects strain gauge placements especially in special arrangements of proving rings. An example of this can be seen in the Godwins [64, 65] study. Initially, 50° and 90° based on strain gauges were placed at photo elastic methods. The author utilized the second set of angles initially. However, calibration test found that the output from the force bridge measuring force in the horizontal direction was not independent of the position of the force which results in cross effects during force measurements. This was rectified by inserting two plates; the first between the mounting and the transducer and the second between transducer and tine. Calibration test found that cross sensitivity was negligible when the horizontal force measurement gauge was at 34°. Sensitivity obtained was 1.35 times larger than the predicted value.

### *2.4.2 Uncertainty*

Uncertainty in measurement is a source of error that affects the reading of the force measurement. From calibration results found from literature, higher uncertainties in measurement tends to occur at lower force where the uncertainty value is the highest and decreases to a minimum at the rings maximum capacity. Multiple sources of uncertainties exist that may affect the performance of the ring. Uncertainties can also be affected by method of measurement. Earlier studies by Kumar reported that uncertainty is usually uncertainties at ± 0.025% [23, 26]. Other reported uncertainties were between 0.2-0.4% [27]. Kumar et al. [30] showed that with an octagonal ring, dial gauges tend to produce more uncertainties than strain gauges.

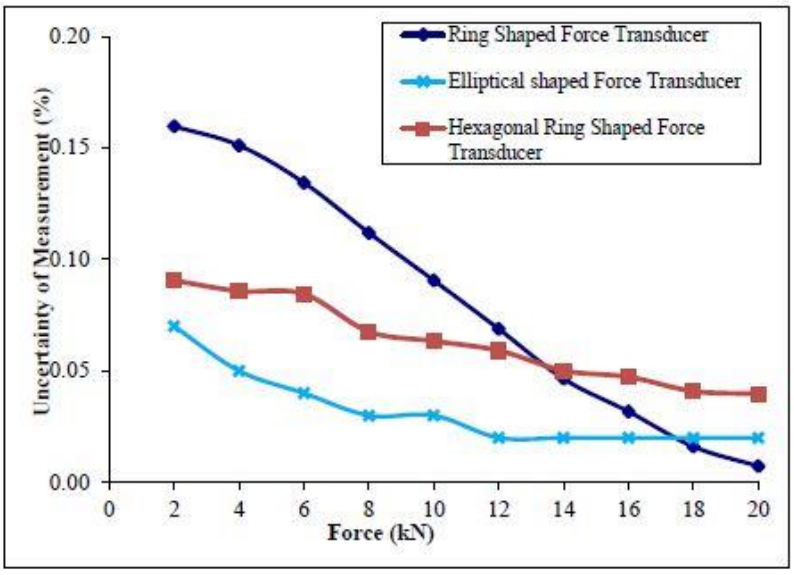


Figure 2.20 Comparison of uncertainties between different ring shapes [8].

### *2.4.3 Stability and Rigidity*

Stability is affected by the rigidity of the ring. Rigidity is affected by the width of the ring. The octagonal and its extended version usually has higher rigidity compared to the other types of proving ring. Uddin et al. [4] surmised that the rigidity of an octagonal ring tends to be significantly higher than a circular ring. This finding was corroborated by previous studies such as by Karabay et al. [3] where they stated that the popularity of octagonal rings in machining operations was due to its rigidity. A higher rigidity means that the frequency during machining operations such as turning and cutting would not affect the rings due to a higher natural frequency [38]. An extended octagonal ring is also thought to have a higher rigidity compared to both the circular and octagonal rings due to its larger overall structure, but its use is highly dependent on its intended application.

### *2.4.4 Ring Thickness and Curvature*

The thickness of the ring has been seen to affect the performance of the proving ring. Rahman et al. [68, 69] found that sensitivity of a variable cross section design of 6 sections per quadrant was increased. Abuhasel and Soliman [41, 42] found that edge radius or curvature showed no effects on the stiffness and sensitivity of the ring. Stiffness was observed to have influenced by the height and thickness of the ring whereas the sensitivity is influenced by the height, thickness and width of the ring. Increasing the height of the ring increases its sensitivity. Increasing thickness and width however has a negative effect on the sensitivity. In terms of stiffness, increasing thickness has a negative effect whereas increasing thickness results in higher stiffness.

Thickness to mean radius ratio based on the theory of thin rings has been adhered to by most design approaches. Kumar et al. [8, 27] states that a ratio of between 0.1-0.5 is suitable when designing a thin ring. This ratio can also be expressed as mean radius to thickness ratio in which to conform to the theory of thin rings, the ratio has to have a value of equal to or greater 3 although some authors have also reported a design with a slightly lower ratio [81]. Raheman and Sahu [58] found the sensitivity of an extended octagonal ring to nearly double when this ratio was increased as opposed to the length to mean radius ratio. Another factor that affects the performance of the proving ring was shown by O'Dogherty et al. [53] whereby they found the best results with optimal sensitivity for an extended octagonal ring was obtained when the width to mean radius ratio was between 1 and 3.

### *2.4.5 Effects of End Bosses or Attachment*

Bray at el [18] studied the effects end bosses and its dimensions on the measuring performance of the circular ring. The authors found that the end bosses dimensions and radius affect the performance of the ring in a wide variety of ways. Generally, end bosses introduce a stiffening effect on the ring and hence results in a slightly lower axial sensitivity compared to a circular ring without end bosses. This is due to the effect of the end bosses on the deflection and strain induced on the ring. They also noted horizontal diameter produces more axial sensitivity than the vertical

diameter. Rahman et al. [68, 69] found the deflection of the ring, and therefore its sensitivity, is lower with a top attachment then without. This could be due to the attachment or boss absorbing and spreading the load over a larger surface area as compared to directly loading at the tip of the ring itself. As far as studies on other non-circular shapes are concerned, the only study of end bosses on an octagonal ring shape was presented by Dhanal [43] but it's effect on the sensitivity or stress was not reported. Generally, however, end bosses and its effects were not studied on non-circular proving rings due to the geometry of these shapes that does not require any attachment or boss.

### *2.4.6 Ring Alignment and Arrangement*

Ring alignment and arrangement tends to differ on different rings due to their geometry being structurally different from one another. Rings such as the octagonal ring and its extended version has straight sides that makes alignment of the ring easier. For a circular ring, its alignment process tends to be slightly more complicated. Logically speaking the most optimal position for a ring to measure axial force is directly at the center point of the load. When doing force measurements where the ring is placed on a straight surface, its circular nature would require the use of an attachment or end bosses. This ensures the ring is positioned properly and directly at the center of the force acting on it. This is crucial especially when using a dial gauge as force is measured based on the deflection of the ring. The use of dial gauge, and to a certain extend strain gauges, requires the force acting on the ring to be right on top of the dial gauge to measure accurately. Misalignment will cause the ring to measure the force at an angle inaccurately and therefore causes the ring to rotate out of place. Some engineering operations, such as a CBR testing machine has the ring attached on a top beforehand by its manufacturers to ensure alignment issues are not encountered when operating the machine.

A typical machining dynamometer requires four octagonal rings with strain gauges attached. The octagonal rings are arranged in a way that allows it to measure the three component forces during any machining operations such as cutting and drilling. Typically, these forces are the thrust force, feed force, and main cutting force. From literature, the most common arrangement is shown in the figure below which was reported by multiple authors [34, 35, 37]. Although this

arrangement is very common in literature, reports have indicated that calibration is needed to ensure minimal cross sensitivity that might affect force readings. Different studies have reported different cross effects and have suggested ways to mitigate this. Some machining operations have certain requirements that must be met for force measurements. Zhao et al. [73] found that a simple octagonal ring has a lower natural frequency than the required frequency for measurement. Hence to increase its natural frequency, the force transducer was modified and designed with two octagonal rings combined perpendicularly at right angles to each other as shown in Figure 10.

Alignment and arrangement of extended octagonal rings are vastly different than its non-extended counterpart. Generally, alignment of the ring depends on the dynamometer design and its usage. Single extended octagonal rings are usually rigid and sensitive enough to measure forces during most engineering applications. Multiple reports have been presented by various authors mainly in the agricultural field which highlights the various ways the extended octagonal ring has been designed and used. McLaughlin et al. [54] designed two extended rings connected by drawbars and a hitch fixture. The arrangement of the ring is shown in Figure 2.22. This design allows the dynamometer to have a much longer lifespan as the total load acting on the rings are halved. The same extended octagonal ring arrangement was also used by Afzalinia and Roberge [6] in their design of a transducer to measure loads in a compression chamber of a large square baler. In designing an auto hitch dynamometer for tractor implements, Kheiralla et al. [47] presented a U bracket with the extended octagonal rings strategically placed at three different locations to measure the forces acting on the three-point auto hitch dynamometer. This configuration is shown in Figure 2.23. This designed allowed the dynamometer to have a total rated capacity of 50kN and 20kN for horizontal and vertical force respectively with optimal strain and minimal cross sensitivities between force components. Another extended octagonal ring design for tillage implements was presented by Abbaspour-Gilandeh and Khanramaki [63]. They presented a design of a triaxial dynamometer with two extended octagonal ring transducers rated at 20 kN each arranged back-to-back at right angles to each other with a tubular torque meter separating the rings. The transducers were placed in a dynamometer frame that was designed and analyzed using finite element method and found this arrangement to yield satisfactory results for its intended purpose. A similar design was also reported by Thinley et al [48].

Like the octagonal ring, the shape and geometry of its extended version also allows a modification on its alignment. Godwins [64, 65] study on a dynamometer design incorporated two double extended octagonal rings aligned perpendicularly as shown in the figure below. Each ring is an extended octagonal shaped transducer designed with two circular rings on opposite ends connected by a narrow slit. Calibration test found that cross sensitivity was negligible when the horizontal force measurement gauge was at 34° with higher sensitivity. A second study by Nalavade et al. [60, 61] utilized a similar design and strain gauge placements with optimal results, hence further verifying the effectiveness of this design arrangement.

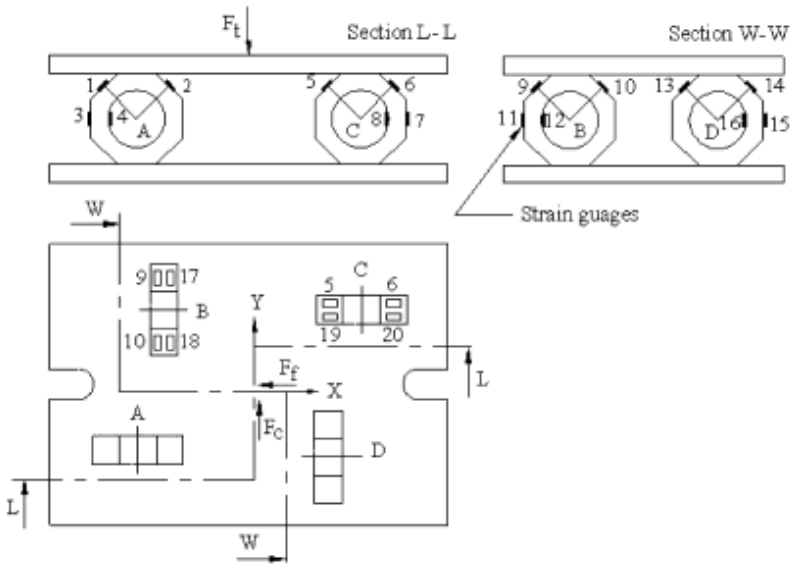


Figure 2.21 A typical machining-based dynamometer design incorporating four octagonal rings [37]

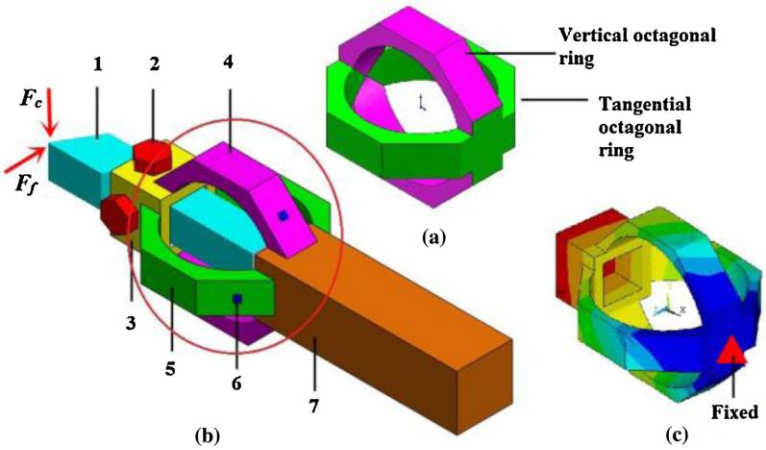


Figure 2.22 Design of the sensing element by Zhao et al.[71]

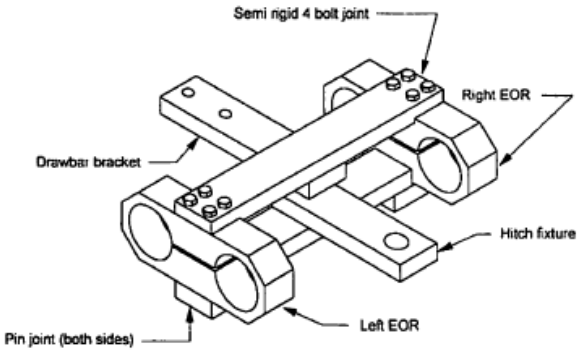


Figure 2.23 Design of a drawbar transducer by McLaughlin et al [54]

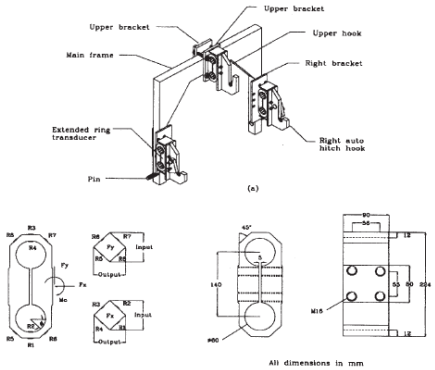


Figure 2.24 Auto hitch dynamometer design by Kheiralla et al. [47]

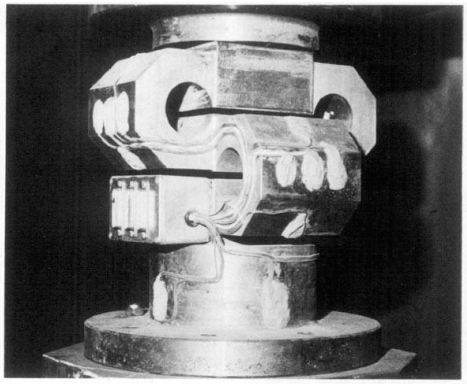

Figure 2.25 Dynamometer design showing the perpendicular arrangement of the extended octagonal rings by Godwin et al. [65]

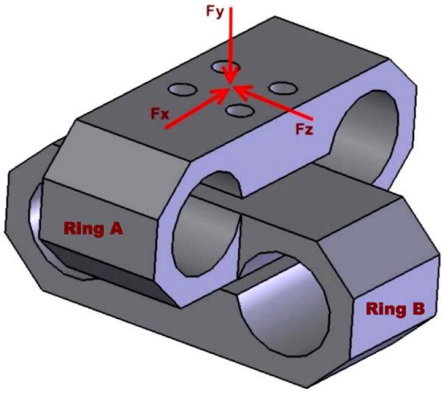


Figure 2.26 Force components measured on the perpendicularly arranged extended octagonal rings by Nalavade et al. [60]

### *2.4.7 Other Factors*

The effect of temperature on the performance of the proving ring itself has not been established in current literature. However, when strain gauges are used to measure the induced strain on the ring, the effects of temperature can have a significant effect on the ring. Patrick et al. [20, 21] reported their force transducers failed due to severe temperature that induces moisture in and around the strain gauges. This in turn causes a short in the strain gauge bridge which affect their results.

The effects of wear on the rings has not been studied extensively in current literature. Studies and research that have mentioned wear on a proving ring has been leaning more on prevention as opposed to the effects of wear itself. A common sign of wear is usually when the chrome coating, if any, starts to peel off. In terms of usage during force measurements however, rings are designed whereby its maximum load or capacity does not exceed the maximum load the material of the ring can withstand. In doing so, a factor of safety based on the material characteristics has been put in place to ensure wear such as plastic deformation during loading is avoided [58, 68, 70].

## 2.5 Applications of Proving Ring

### *2.5.1 Calibration of testing machine*

The circular proving has been used in calibration machines to calibrate different types of testing machines such as dynamometers. The standard of calibration most cited from literature is calibration based on the ISO 376:2011 or IS 4169 standards [30]. This standard has been applied to force measuring devices with an elastic member such as proving rings. The standard gives a guideline on calibration methods and procedures while assigning a precision class based on the metrological performance of the ring. Calibration of dynamometers has been shown in literature. An example was shown by Karabay [38] in their design of a dynamometer with octagonal rings. In the figure below, a circular proving ring was used to calibrate the dynamometer before use. A similar arrangement was also reported by the same author in a second study[39].

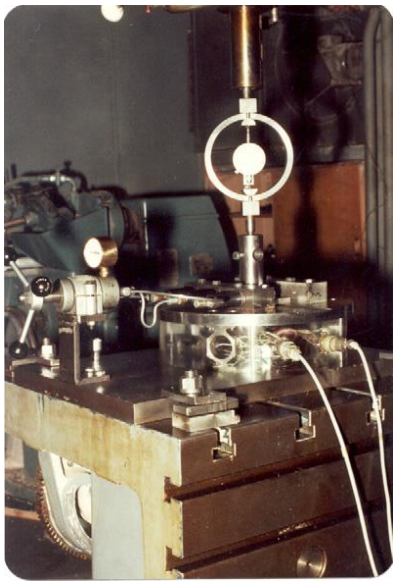

Figure 2.27 Calibration of a dynamometer shown by Karabay [39].

### *2.5.2 Drilling Milling and Turning (Machining operation)*

A machining dynamometer is used to measure forces such as feed force, thrust force and main cutting force. The dynamometer is placed in a position to measure these forces acting on the machining tool. Cutting force data can be used to create a theoretical model to predict tool wear [38]. This ensures that the tool condition is constantly monitored to improve tool life and maintain optimal efficiency during the machining process [34]. In designing a suitable dynamometer for force measurements in many machining processes, usage of octagonal rings as the main elastic member in a dynamometer design has been increasingly prevalent in machining operations such drilling, milling and turning. The usage of octagonal rings in fabricating and manufacturing machining-based dynamometers has been well documented by various authors. Octagonal rings are highly popular due to its flexibility in designing the rings considerably smaller in size which allows dynamometers to be easily built. It is also a popular choice due to its rigidity and as was mentioned in the previous sections.

Multiple examples have been reported on the design of a force measuring dynamometer for force measurements in machining operations. As was mentioned in previous sections, the most

common four ring arrangement is the one shown in Figure 2.20 by Yaldiz et al. [37]. Since then, multiple reports have shown on the success of this arrangement. Dandage and Bhagwat [32] reported this design arrangement with excellent linearity in measuring the three component forces and torque. Similar results with respect to linearity and cross sensitivity were also found by other authors utilizing this ring arrangement [2, 35]. A slightly different design arrangement was presented by Uddin and Songyi [4]. Their modified octagonal ring configuration is shown below. The increase in sensitivity of the dynamometer was noted in due part to their modified octagonal ring as opposed to the configuration itself.

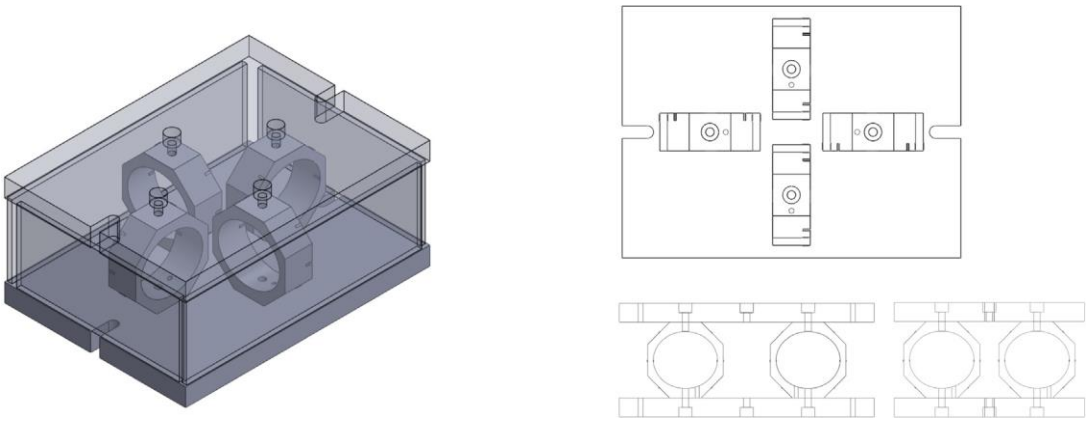

Figure 2.28 Cutting force measuring device with octagonal rings illustrated by Uddin and Songyi [4].

Another dynamometer design for drilling was suggested by Karabay [38]. The author presented two dynamometer designs involved a six-octagonal ring arrangement and a four-octagonal ring arrangement as shown in the figure below. The four-ring configuration was developed as a drill press dynamometer whereas the six-ring configuration was designed as a multi component dynamometer. A second report by the same author showed the four-ring configuration performed well when compared to a previous authors work with negligible cross effects [39]. Another report showed that the dynamometer performed well when working on SAE 1020 steel [3].

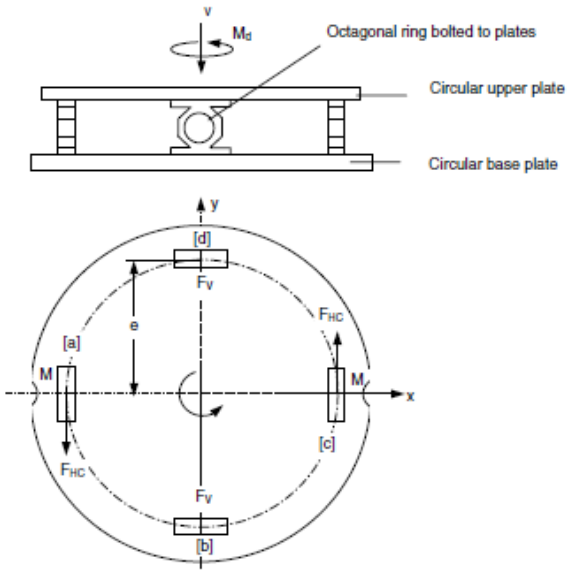


Figure 2.29 Four ring configurations [38].

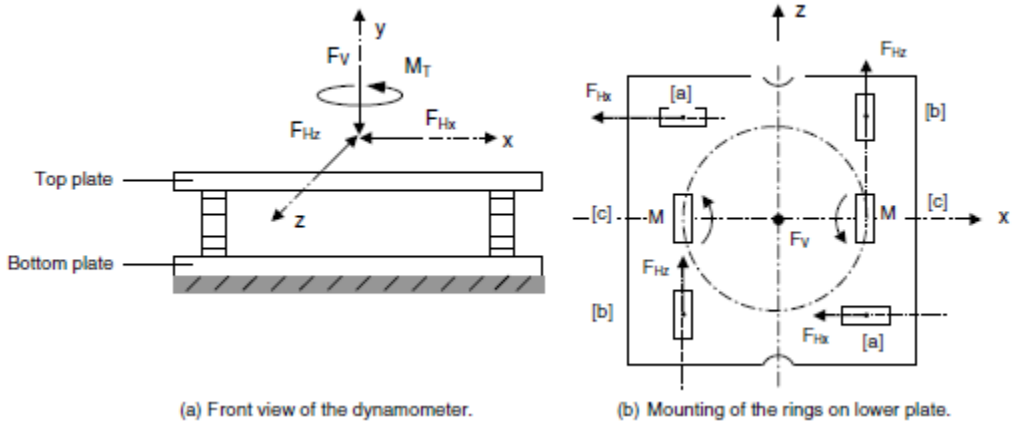


Figure 2.30 Six-ring configuration [38].

Although the octagonal ring has been highly popular as the main elastic member in a tool dynamometer design, an example of a circular ring or short hollow cylinder has also been shown by Jain et al. [28]. They designed a lathe tool dynamometer utilizing a short hollow cylindrical tube with a length of 35mm and diameter 15mm. The calibration results were deemed satisfactory by the authors however its performance was not compared to another octagonal based dynamometer.

### *2.5.3 Agriculture Engineering*

The extended version of the octagonal ring is almost exclusively used in the agricultural engineering field due to its durability and higher load capacity when measuring dynamic forces in relatively compact form factor compared to the octagonal ring. Multiple reports have been presented on its usage which states various characteristics of the ring. Similar to the octagonal rings used in machining operations, the force measuring instruments in agricultural usage are designed to measure the three force and moment components in all three directions.

Nalavade et al. [60, 61] perpendicularly aligned extended ring design was used to measure forces acting on a tillage disc. The extended octagonal rings were found to have minimal cross effects with calibration results providing excellent linear relationships. Girmas [44] heavily modified design of multiple extended octagonal rings provided desirable results with theoretical and measured strain values differing by less than 1.5%. The rings however were designed to morph into the plough bodies and not attached independently. As such, strain gauge placements differed markedly from previous studies on the extended octagonal ring. Thinley et al. [48] developed a force measuring instrument utilizing the extended octagonal rings to measure forces acting on an animal plough. Their design of two perpendicularly aligned extended octagonal rings connected to a torsion bar in the middle for ease of mounting onto the animal plough shows. Further calibration studies revealed all force and moment channels responded linearly with satisfactory results. Another tractor implement study was presented by Khan et al. [45] with the use of a bi-axial extended octagonal ring transducer. The transducer was designed to measure the forces and moments acting on a tractor linkage. The study however was more on the implementation of the extended octagonal rings and its performance for its intended use. The rings were already manufactured and procured from a third party instead of designing from scratch. A vibratory tillage tool dynamometer was designed and presented by Niyamapa et al. [50] in their study relating to soil pressure and oscillating frequency of the tillage tool. The extended octagonal ring was designed to measure forces in the horizontal and vertical direction acting on the vibratory tillage tool. Although the study was not focused on the design of the extended ring, it performed as expected and force readings were found to decrease as the oscillating frequency was increased.

### *2.5.4 Other Usage*

Multiple companies have fabricated and distributed the circular ring commercially for a variety of uses. Most of these rings are used in force calibrating machines or static force measurement devices. In civil engineering related industries, the California bearing ratio or CBR test requires a specialized machine. A CBR test measures the mechanical strength of soil, base courses or bitumen. A typical laboratory CBR test utilizes the ASTM Standards D1883-05 when measuring soil mechanical strength with a CBR testing machine. A proving ring is an essential component in this machine as it can measure a wide range of loading and very versatile since the ring attached on the machine is interchangeable depending on the specimen. Patrick et al. [20, 21] has also used circular rings with attached strain gauges in their study on the large borehole rocks.

Figure 2.31 A typical CBR testing machine by Cooper technology.

## 2.6 Research Gap

From the literature review conducted in the previous sections, it is clear that there are still certain aspects of the proving ring design that were not addressed. First, the significant stress imbalance throughout the ring was not addressed. The studies were mainly focused on showing the stress distribution in their design and did not suggest or study ways to address stress imbalance at certain locations around the ring design. Secondly, as was previously shown, various shapes

have various advantages. This is primarily due to the difference in geometry from one ring to the other. It is shown that the circular ring is used for high static force applications whereas the octagonal rings were mainly used in applications measuring dynamic forces. Therefore, there is a lack of ring design that could be used for different loading conditions.

## 2.7 Problem Statement

The current proving ring design practice imposes a non-uniform and nonlinear stress along the circumference of the ring which is also not ideal for its long-time operation. It has low level of sensitivity with small deflections under applied load. Therefore, there has been a lack of studies to address the significant stress imbalance found throughout the ring.

## 2.8 Hypothesis

From the critical review made of the literature above, it is clear that there is a need to address the stress distribution of the proving ring when axial load is applied. In order to address this, a hypothesis is made. It is expected that a varying cross section ring design where ring material is redistributed to optimize the ring shape will greatly reduce the stress levels and enhance the ring sensitivity. The design will provide a more balanced stress distribution where all ring materials are used efficiently. This means that regions or locations where stress levels are significantly lower to the average stress throughout the ring will be removed and redistributed to locations where stress levels are higher. This would also affect the strain distribution and therefore will enhance the ring sensitivity as well.

## 2.9 Aims and Objectives

The aim of this study is to improve the sensitivity of the proving ring while minimizing and optimizing the stress distribution. To address the problem statement and research gap, the objectives set for this study are:

1. To design a proving ring with uniform radial stress distribution
2. To design and modify the current proving ring design for improved sensitivity
3. To study the effect of cross-sectional dimensions on the stress distribution and sensitivity
4. To apply, analyze and compare various finite element-based shape optimization techniques that would yield an optimized ring shape design.

## 2.10 Scope of Study

The scope and limits of this study are:

1. Only ring-shaped force transducers will be studied in this research
2. Stress, strain and sensitivity studies and comparisons made will only be restricted to ring shapes only. Therefore, no comparisons will be made with other types of force transducers
3. With respect to ring material, it is assumed that an optimal shape would be deemed universal in its characteristics regardless of the ring material used. Therefore, no studies with regards to ring material will be discussed in this research.

## 2.11 Research Question

From the review, a few research questions were made.

- What are the effects of ring geometry on the stress levels on the ring?
- Can the sensitivity of the ring be enhanced further through geometric modifications?
- Can a universal ring shape be designed that would be sensitive irrespective of its size?

## 2.12 Literature Review Conclusion

Various authors have shown the strength and weaknesses of each ring design. The circular ring shape has been studied and its force measuring performance thoroughly evaluated. Octagonal rings have been shown to be capable force transducers in measuring dynamic forces in machining applications. The extended octagonal ring has been presented as a suitable force transducer particularly in the agricultural field. However, from the literature review, there are still some gaps in literature worth pursuing in this field, particularly in terms of stress distribution and enhancement of the ring sensitivity. It was determined that although each ring shape has its own unique characteristics, it was clear that the current ring designs suffer from the stress imbalance during load application. Also, there are still ways to improve ring sensitivity as opposed to relying on ideal strain gauge placement or type of strain gauge used. Therefore, as was previously mentioned, this research study will try to address the research problem and gap to design a proving ring with enhanced force measuring performances that would further benefit industries dependent on the use of proving rings.

# Chapter 3

# Methodology

## 3.1 Introduction

In designing the proving ring, multiple approaches were taken. An experiment was conducted on an existing circular proving ring. The results collected were then used as a basis for design improvements and a foundation for the optimization work later on. Based on the critical review work done in the literature section, the two conventional proving rings, circular and octagonal ring shape, were selected for finite element analysis. The results of the simulations were then used for further optimization and development of design ideas to address the research gap found in the current literature. A flowchart is presented below to summarize the methodology of the whole thesis.

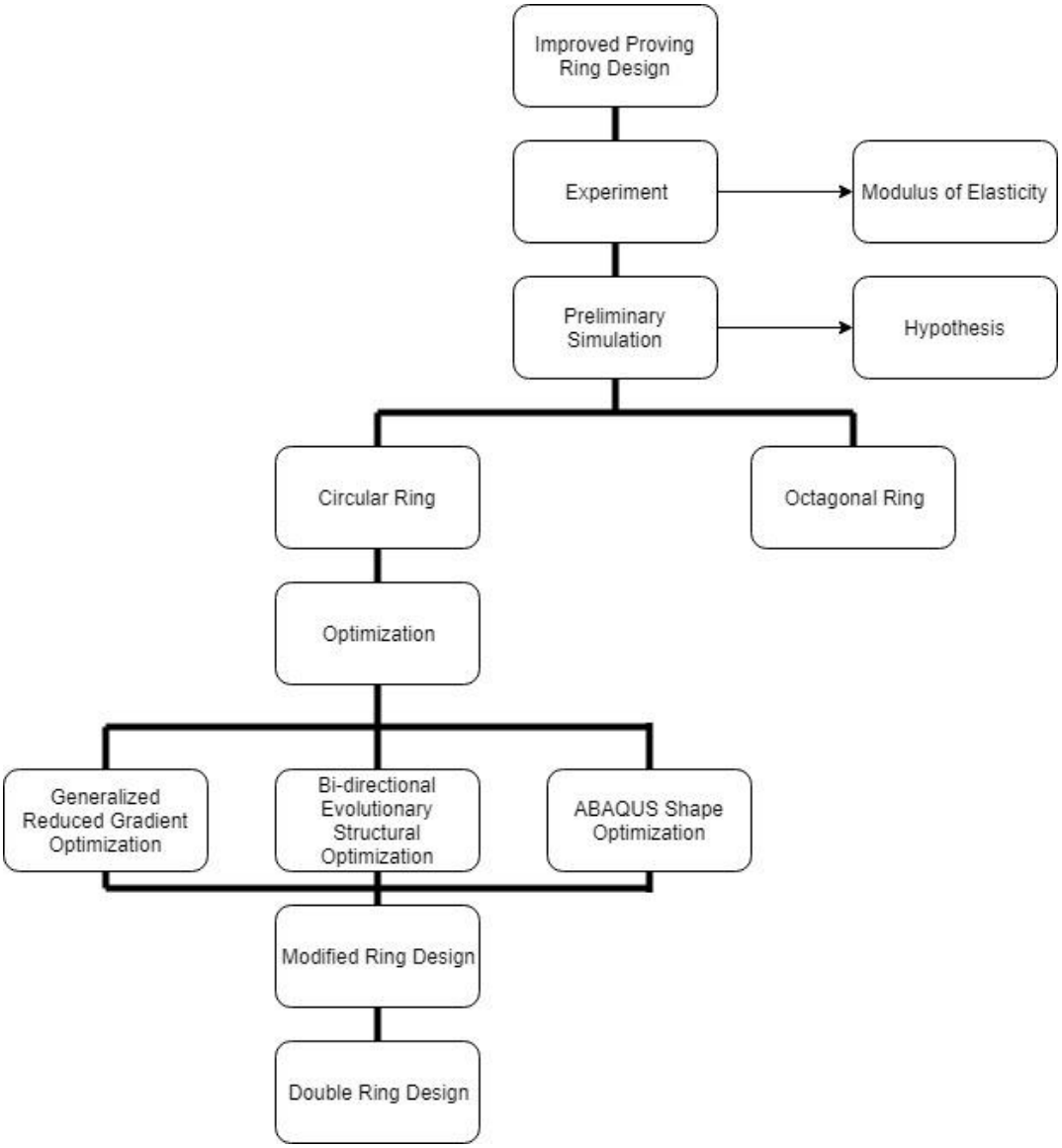


Figure 3.1 Research Methodology Flowchart

## 3.2 Experiment

The experiment was conducted on a conventional circular proving ring to identify the characteristics and performance of the ring as a basis for future design improvements. The dimensions of the ring were measured, and a static compressive load test was conducted. The load was set at step increments of 5kN up to 30kN with a 5 second pause at each interval to record the

corresponding deflection. The deflection values were read from the dial gauge attached to the proving ring as shown in Figure 3.3. The data was then collected, and a load vs deflection curve was plotted to identify the modulus of elasticity and stiffness of the circular ring using thin ring theory [17, 18][2].

## 3.3 Equipment

### *3.3.1 Circular Proving Ring*

As a basis for design improvements, a circular ring was found and experimented upon. The ring was obtained from the university laboratory as it was not in use. Figure 3.1 shows the circular ring during loading experiment. The dimensions of the ring are:

Table 3. Dimensions of experimental proving ring

| **Parameters** | **Dimensions, mm** |
|---|---|
| **Outer radius, $R_o$** | 89 |
| **Inner radius, $R_i$** | 79 |
| **Thickness** | 10 |
| **Ring width** | 60 |

Figure 3.2 shows the dimensions and two-dimensional representation of the proving ring used for the experiment.

[2] *The following section has been included in two published papers and a paper currently under preparation. The published papers are titled: Design of a proving ring with improved sensitivity and optimum stress distribution and Shape Optimization: Case Study on Design of a Ring Type Force Transducer*

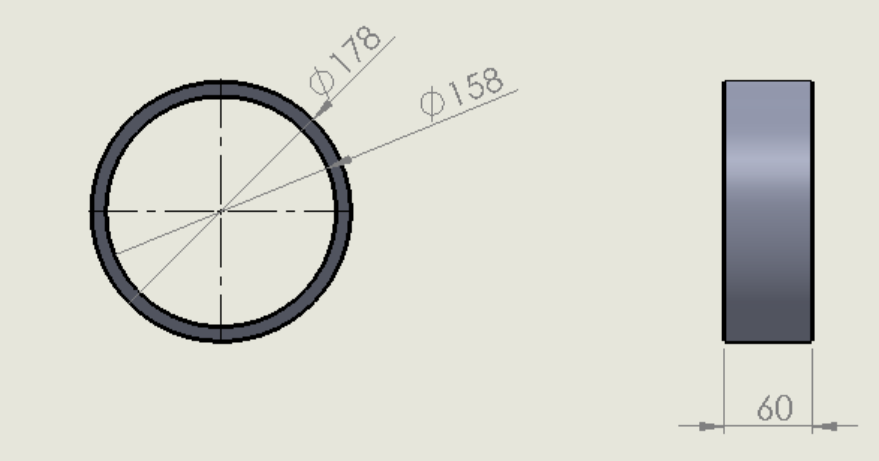


Figure 3.2 Dimensions in mm of the conventional proving ring

*3.3.2 Instron Testing Machine*

A static load testing machine was used to apply incremental static compressive load during the experiment. The static load machine used in the experiment was the Instron 5960 Series. Figure 3 shows the preparation of the circular proving ring in the between the Instron testing machines jaws during the experiment.

Figure 3.3 Experiment of the conventional proving ring

### *3.3.3 Other Equipment*

A measuring tape was used to measure the center of the Instron machine to ensure the force exerted on the ring center. A dial gauge seen in Figure 3.3 originally attached to the ring was used to measure the ring deflection. The dial gauge was calibrated to zero before use.

## 3.4 Analytical Analysis

### *3.4.1 Dimensional Analysis*[3]

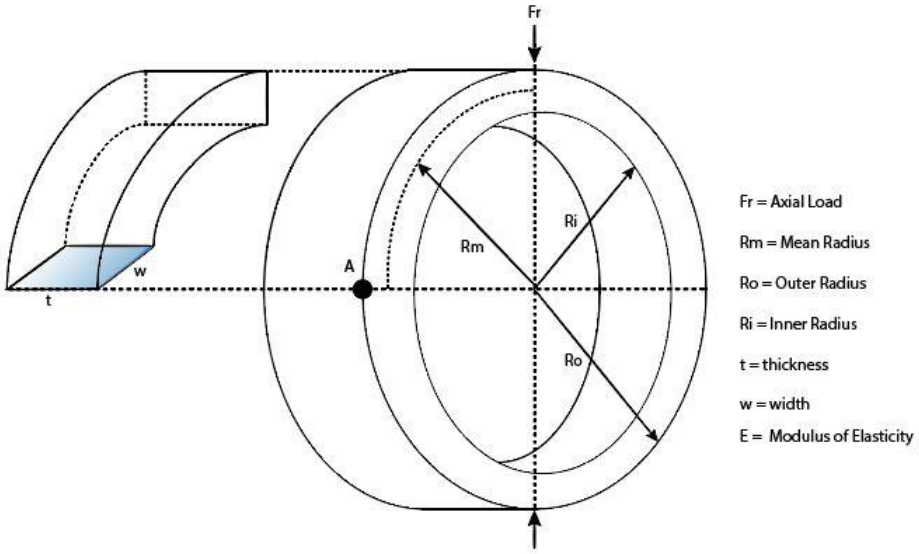


Figure 3.4 Cross section of circular ring

Figure 3.4 illustrates the cross section of a conventional circular ring rotated to the right of its horizontal axis. Point A is a fixed location of interest where all parameters were measured such as stress and strain for fair comparisons of different geometry. Dimensional analysis was performed to establish the relationships of the ring dimensions with factors such as applied force, the resulting deflection and the modulus of elasticity.

[3] *The following section has been published in the methodology part in ICMEA 2018 conference paper titled Design of a Proving Ring with Improved Sensitivity and Optimum Stress Distribution.*

$$\delta = F_1(F_r, E, R_i, w)$$

$$F_2(\delta, F_r, E, R_i, w) = 0$$

$$\delta^a {F_r}^b E^c {R_i}^d w^e = 0$$

$$(L)^a\ (F)^b\ (\frac{F}{L^2})^c\ (L)^d\ (L)^e = 0$$

$$\therefore L^{a-2c+d+e}\ {F_r}^{b+c} = 0$$

Let c = 1, d = e = 0. Therefore,

$a = 2\ and\ b = -1$

Hence, the first $\pi$ group is obtained as

$$\pi_1 = \delta^2 {F_r}^{-1} E^1 = \frac{\delta^2 E}{F_r} \tag{3.1}$$

Let e = 1, d = -1 and c = 0. Therefore,

$a = 0\ and\ b = 0$

Hence, the second $\pi$ group is obtained as

$$\pi_2 = {R_i}^{-1} w^1 = \frac{w}{R_i} \tag{3.2}$$

Let c = 0, d = -1 and e = 0. Therefore,

$a = 1\ and\ b = 0$

Hence, the third $\pi$ group is obtained as

$$\pi_3 = \delta^1 {R_i}^{-1} = \frac{\delta}{R_i} \tag{3.3}$$

From the dimensional analysis above, it is clear that the width of the ring was not taken into consideration. This is because the ring width plays no part in the sensitivity or stress levels due to the downward action of force acting on the ring. As such this analysis has been treated as a

plain strain problem. For a circular proving ring, strain at 0° angle from the horizontal axis point A can be calculated using the following formula [10].

$$e_A = \pm \frac{1.09 F_r R_{mean}}{Ebt^2} \tag{3.4}$$

And sensitivity is defined as,

$$\frac{e_A}{\delta / R_i} = 0.61 \frac{t}{R_{mean}} \tag{3.5}$$

Hence, the term on the left hand-side represents the sensitivity on the outer side at point A of the ring. Sensitivity is taken as the ratio of strain in the circumferential direction with respect to the ratio of deflection per inner radius for the fact that strain in that direction can be physically measured by a strain gauge.

### *3.4.2 Castigliano's Theorem and the Theory of Thin Rings*

The theory of thin rings has been used to develop the analytical solutions in designing rings of various shapes. Due to the symmetry in the horizontal and vertical axes, the ring deflection analysis can be simplified by only considering a quarter ring. Deflection of the ring is derived using Castigliano's theorem and strain energy theory. Castigliano's first theorem derives the equation needed to calculate force on an elastic member by calculating the partial derivative of internal strain energy with respect to deflection. In the case of a known force acting on a curved beam, which in this case represents the quarter ring, the second theorem is more appropriate. Castigliano's second theorem states that the partial derivative of the structures internal strain energy with respect to the force is equal to the deflection of the beam in the direction of the applied force. This second theorem can be represented as

$$\frac{\partial U}{\partial F} = \delta \tag{3.6}$$

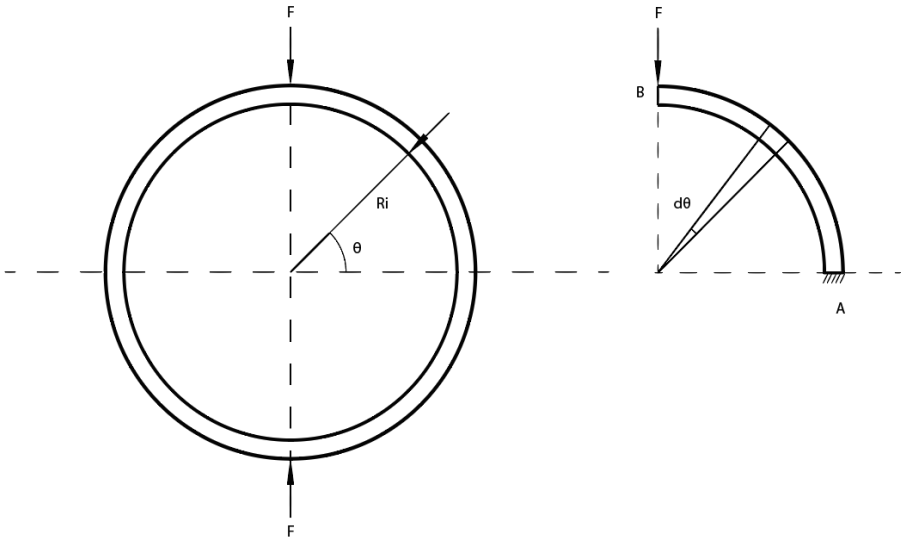


Figure 3.5 Circular and Quarter Ring

Figure 3.5 above representing the quarter ring. Point A is fixed whereas the point of axial load application B is free. Taking moment at point A,

$$\frac{\partial U}{\partial M_A} = 0 \tag{3.7}$$

The equation above returns the value of zero since at point A there is no vertical displacement. Considering a section θ, the bending moment is defined as

$$M = M_A - \frac{F(R - x)}{2} \quad where\ x = R\cos\theta$$

Therefore, the above equation becomes

$$M = M_A - \frac{FR(1 - \cos\theta)}{2} \tag{3.8}$$

From strain energy theory, the strain energy of a ring under axial loading with respect to the moment induced is defined as

$$U = \int \frac{(M^2 R d\theta)}{2EI} \tag{3.9}$$

The partial derivative of the equation above with respect to the moment at point A becomes

$$\frac{\partial U}{\partial M_A} = (\frac{R}{EI}) \int_0^{\pi/2} M(\frac{\partial M}{\partial M_A}) d\theta \tag{3.10}$$

At 90°,

$$\frac{\partial M}{\partial M_A} = 1$$

$M_A$ can be obtained as

$$\int_0^{\pi/2} M d\theta = 0$$

Thus

$$\int_0^{\pi/2} M = \int_0^{\pi/2} M_A - \frac{FR}{2}(1 - \cos\theta) d\theta = 0$$

Solving the above equation with respect to the limits,

$$\frac{\pi}{2} M = \frac{FR}{2}[\theta - \sin\theta]$$

Which yields

$$M_A = FR\left(\frac{1}{2} - \frac{1}{\pi}\right) \tag{3.11}$$

Therefore, the moment equation now becomes

$$M = \left(\frac{FR}{2}\right)\left(\frac{1}{2} - \frac{1}{\pi}\right) - \frac{FR(1-\cos\theta)}{2}$$

$$M = \left(\frac{FR}{2}\right)\left(\cos\theta - \frac{2}{\pi}\right) \tag{3.12}$$

Substituting the above equation into the second theorem definition, the deflection of the ring at the point of axial load application becomes

$$\delta = \frac{\partial U}{\partial F} = \int_0^{\pi/2} \left(\frac{MR}{EI}\right)\left(\frac{\partial M}{\partial F}\right) d\theta$$

$$\delta = \frac{\partial U}{\partial F} = \int_0^{\pi/2} \left[\frac{FR^2}{2}\left(\cos\theta - \frac{2}{\pi}\right)\right]\left[\frac{R}{2}\left(\cos\theta - \frac{2}{\pi}\right)\right] d\theta$$

$$= \frac{FR^3}{4EI}\int_0^{\pi/2} \left(\cos\theta - \frac{2}{\pi}\right)\left(\cos\theta - \frac{2}{\pi}\right) d\theta$$

$$\delta = \left(\frac{FR^3}{EI}\right)\left(\frac{\pi}{4} - \frac{2}{\pi}\right) \tag{3.13}$$

*3.4.3 Natural Frequency*

Modal analysis will be conducted using finite element analysis code ABAQUS to compare the natural frequency of the designed ring against conventional shaped rings. Knowing the natural frequency of a ring is crucial to ensure it meets certain frequency requirements usually related to applications where vibration can affect the ring performance. Frequency is defined as the inverse of time period. This is expressed as

$$f = \frac{1}{T} \tag{3.14}$$

Whereby the time period T represents

$$T = 2\pi\sqrt{\frac{m}{k}}$$

Hence, the natural frequency equation becomes

$$f_d = \frac{1}{2\pi}\sqrt{\frac{k}{m}} \tag{3.15}$$

Whereby K is defined as the bending stiffness of a beam. The stiffness of the ring k is defined as the ratio of force per unit deflection which is also the gradient value in a force displacement curve.

$$k = \frac{F}{\delta}$$

## 3.5 Shape Optimization

### *3.5.1 Generalized Reduced Gradient Optimization*

*Analytical Equation*

Generalized reduced gradient optimization method, or GRG, is an optimization code based on the gradient method [83]. The GRG method is a type of first order numerical optimization method which finds the optimal point that satisfies the objective function curve and the input constraints. This method is especially useful when dealing with nonlinear based optimization problems. The algorithm follows a list of steps to find the optimal point. Visual Basic was used for ease of calculation in the analytical process.

The generalized reduced gradient method is used to optimize the stress levels on the ring by sections. For this analysis, due to symmetry, only a quarter of the ring is considered. It has been established that the moment of the ring at any point from θ is

$$M = \frac{FR_m}{2}\left(\cos\theta - \frac{2}{\pi}\right) \tag{3.16}$$

Whereby in this instance mean radius is considered. Combined total stress induced on the ring with respect to moment at an angle is

$$\sigma = \pm K\frac{M\,{}^{w}/_{2}}{I} + \frac{F}{wt}\cos\theta \tag{3.17}$$

The first term is the bending stress induced on the ring. The second term is the normal stress acting on the ring at θ. K represents the correction factor that was obtained by a modified equation for computing stresses in a curved beam [82]. This was done by plotting a logarithmic curve of mean radius $R_m$ against ring width w. The correction factor K is expressed as

$$K = 0.1405\ln\frac{2R_m}{w} + 0.6113 \tag{3.16}$$

And moment inertia of a ring

$$I = \frac{bh^3}{12} = \frac{tw^3}{12}$$

Combining the three equations above yields,

$$\sigma = 0.843\frac{M}{w^2}\ln\frac{2R_m}{w} + 3.668\frac{M}{w^2} + \frac{F}{w}\cos\theta \tag{3.17}$$

The value of stress σ is then calculated for each section between 0 - 90° at 15° interval. The obtained value will be the stress at that location with respect to angle. However, the goal of this optimization work is to lower the total stress levels of the ring by at least 20%. The stress value at angle 0° is multiplied by 80% and is then substituted back into each equation at different angle. The objective function is therefore the stress equation at an angle set to 0 or

$$\sigma = 0.843\frac{M}{w^2}\ln\frac{2R_m}{w} + 3.668\frac{M}{w^2} + \frac{F}{w}\cos\theta - 0.8\sigma_0 = 0 \tag{3.18}$$

Where $\sigma_0$ represents the stress taken at angle 0°. This ensures that the stress at any given angle is similar to the stress at point 0° which essentially creates a uniform stress distribution throughout the ring. To achieve the optimization goal with respect to the objective function, the constraint is taken as the sensitivity of the ring improved by 20%. Consider the following sensitivity equation at 0°,

$$\frac{e_A}{\delta/_{R_m}} = 0.61\frac{w}{R_m} \tag{3.19}$$

Substituting the value of the initial ring parameters,

$$\frac{e_A}{\delta/_{R_m}} = 0.61\left(\frac{10}{84}\right) = 0.073$$

Multiplying the value above by 120% yields 0.0871. Hence, the constraint equation becomes

$$0.61\frac{w}{R_m} \geq 0.0871 \tag{3.20}$$

The objective and constraint equations above are then used in the optimization task using the generalized reduced gradient method.

*Algorithm*

Generalized reduced gradient (GRG) method is a simple generalized optimization process based on the Frank-Wolfe algorithm or reduced gradient [84]. The algorithm is suitable for solving nonlinear optimization problems. The algorithm solves the optimization problem by applying an equality constraint to find the optimal points. For most engineering process however, behavourial

variables such as stress and sensitivity are treated as implicit functions to the design parameters which forms inequality constraints. From the previous section, the objective function has a natural logarithm in its equation which implies a nonlinear function. Hence, the GRG method is suitable for solving a nonlinear equation coupled with an inequality constraint. The following equation defines the optimization problem for the GRG code to solve.

$$\begin{cases} 0.843\frac{M}{w^2}\ln\frac{2R_m}{w} + 3.668\frac{M}{w^2} + \frac{F}{w}\cos\theta - 0.8\sigma_0 \; equals \; to \; 0 \\ Subject \; to \;\; 0.61\left(\frac{w}{R_m}\right) \geq 0.0871 \end{cases}$$

In the optimization procedure, only the ring width is varied to maintain a constant mean radius. This is important to avoid large variations in size and ensure a smooth transition between sections. The optimization starts at (w,Rm) = (10,84). The algorithm will then solve iteratively until it can find a solution to solve the objective function subject to the given constraint. From the previous section, the aim of this optimization procedure is to reduce the stress at each section by 20% while increasing the ring sensitivity by at least a similar amount. The second part indicates a problem subject to an inequality constraint. To solve this, solver adds a slack variable to the inequality constraint to form an approximate equality constraint. This is done by introducing a non-negative value to the inequality constraint. Therefore,

$$0.61\left(\frac{w}{R_m}\right) - 0.087143 = S \tag{3.21}$$

Where S > 0

Finally, the solver finds a solution that satisfies both the objective function and the constraint based on the initial points. Stopping condition can either be when a solution is found that satisfies the objective function and the constraint or when a global convergence is obtained. A global convergence happens when the change in the first order derivative of the objective function is too small for every step length. By default, the convergence value is set to 0.001. For this problem, a centralized step change or central derivative is used as global convergence can be

more accurately reached. The following diagram summarizes the whole GRG optimization procedure.

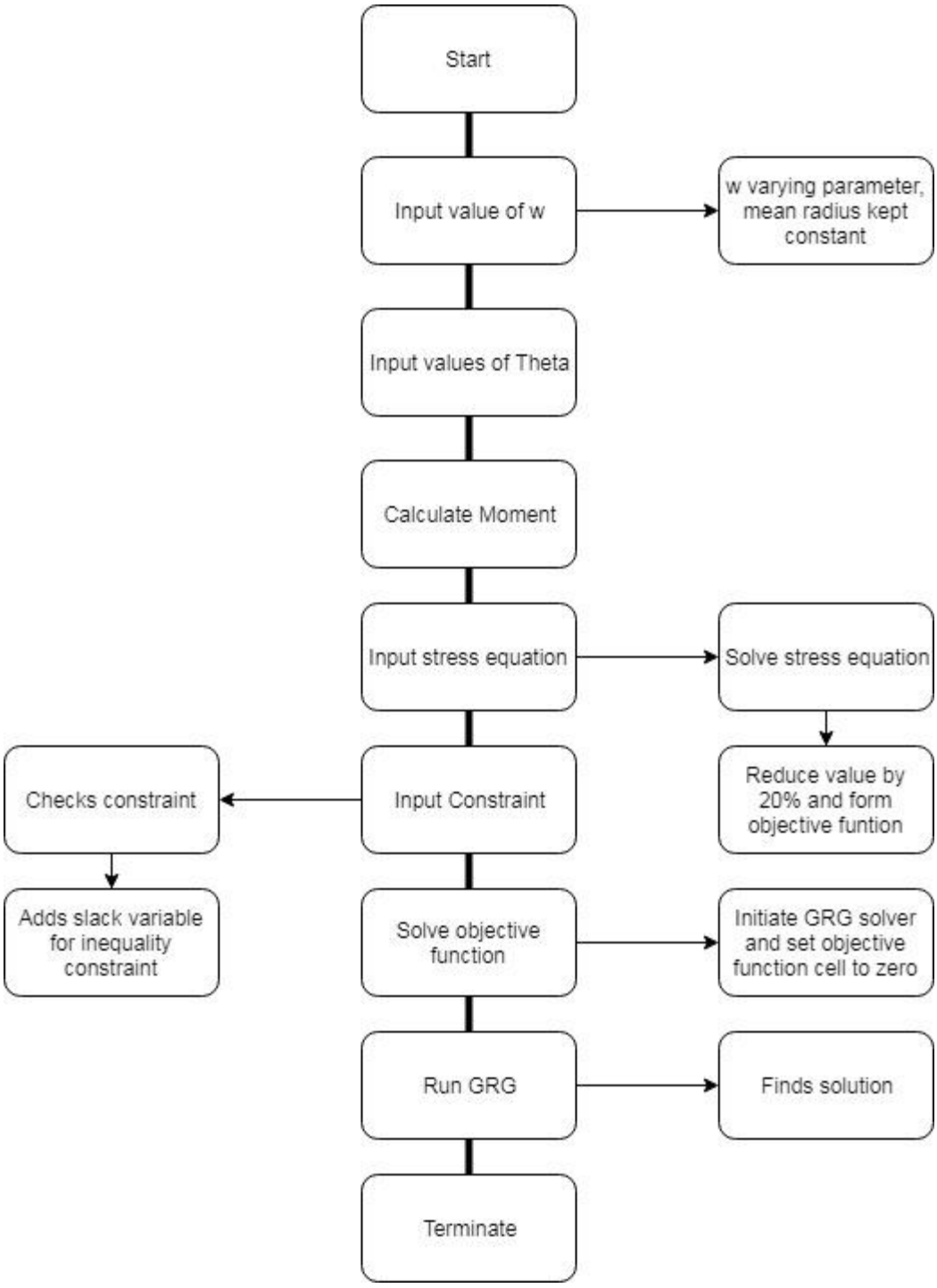


Figure 3.6 Flowchart detailing the GRG algorithm steps

### *3.5.2 Finite Element Analysis*

*FEA Parameters*

A 2D finite element analysis was conducted on the conventional circular ring. The boundary condition has been applied at the bottom of the ring where it is fixed as no movement and rotation is permitted. A constant load of 30kN was applied in the axial direction at the top point of the ring. A 2D solid continuum 4 node rectangular plain strain element with reduced integration (CPE4R) was employed in meshing the model as the width of the ring not taken into consideration in the analysis. The width of the ring was not considered because it does not affect the deflection or strain on the ring. Therefore, the analysis is treated as a plain strain problem. A mesh sensitivity study was conducted by varying the seed element value around the ring to determine the suitable mesh size for the models. Due to the different geometries of the different ring shapes studied, a range of mesh sizes was considered. For the conventional shape, a suitable result was obtained with a total of 1280 element and 1600 nodes. Other ring shapes designed in this thesis will meshed to be as similar to this as possible. This is done by seeding the model by edges which offers greater meshing control compared to seeding by part. These element values were selected to save computational time as any more increment did not yield much variation in the simulation response. The element size had a length of 1.18mm with varying width. Material properties in the simulation is set with Young's Modulus of 205 GPa and Poisson ratio of 0.3. These properties were based on the initial experiment conducted as described later in section 4.2.

The preliminary finite element analysis is to study the validity of the research hypothesis. To test the hypothesis, a circular ring and octagonal ring will be simulated for comparison. The circular ring represents a constant cross section design whereas the octagonal ring will represent a varying cross section design. The rings are designed to have similar mass for fair comparison. Stress and strain levels, as well as its distribution around the ring, will be compared. For this

preliminary study, the sensitivity of the ring will be taken as the deflection of each rings. Higher deflection value shows a higher resolution when measuring force hence higher sensitivity.

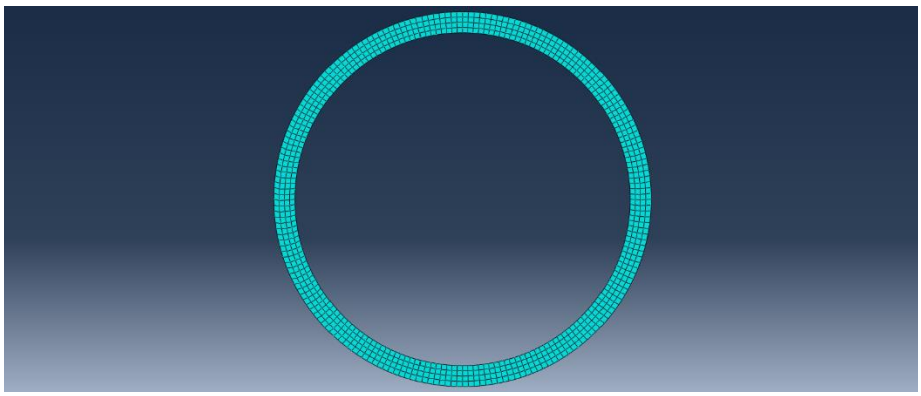

Figure 3.7 Screenshot of finite element analysis of a circular ring using ABAQUS

*TOSCA Shape Optimization*

Shape optimization through finite element method can be conducted by using the ABAQUS shape optimization algorithm found in its optimization suite TOSCA. The TOSCA optimization algorithm used in ABAQUS is based on topology optimization by distribution of isotropic material. The purpose of this optimization technique is to find the optimum shape for the structure based on a certain set of parameters determined by the algorithm which minimizes the stress induced on the structure while minimizing its volume.

This is achieved by finding a solution that has an optimal structure with increased stiffness. The structure obtained generally has a much more optimal stress distribution characteristics due material efficiency. Materials that do not contribute to sustaining the force or pressure acting on it will be removed or redistributed to locations where high stress is present. To achieve this, compliance is a major factor in determining the direction of the optimization. Compliance is the inverse of stiffness. In the case of a concentrated load acting on a structure such as a proving ring, it is highly advisable to minimize the strain energy in the ring which leads to lower compliance and therefore a stiffer structure. The TOSCA optimization suite contains a general topology

optimization-based algorithm that can be used to conduct topological, shape and sizing optimization. The algorithm optimizes by distribution of isotropic materials. Although a common algorithm is used by the suite, shape optimization defers slightly as the optimization process only does minimal changes to the structure as opposed to large material removal in topology optimization. The main difference is in the execution of the algorithm in obtaining the results while the general process leading towards the optimization goal is quite similar.

Shape optimization is typically performed at the end of a finite element analysis to make slight tweaks or refinement to the geometry. Since the general outline of the ring is already determined, this optimization task is more suitable. The optimization procedure is similar to topology optimization but at a much smaller scale. However, unlike topological optimization, shape optimization generates an optimized shape by making slight modifications to the surface nodes by moving it around to reduce the stress within the vicinity of the node instead of by removing material. The solution is therefore much simpler and shortens time considerably. After the finite element analysis was conducted on the conventional circular shape from the previous section, the shape optimization is performed based on the simulation results. Before the optimization procedure is initiated, sensitivity analysis will be carried on. Sensitivity numbers of each element will be compared against the average sensitivity of the structure as a whole and a low pass filter will be applied to elements with sensitivity numbers that do not fit. The optimization process is then conducted based on material redistribution and the method of moving asymptotes. The objective function in this case will be to minimize the strain energy and increasing the stiffness of the ring. The algorithm will continue the process until both convergence and volume constraints are met.

Using the ABAQUS software, a conventional circular ring will be designed with dimensions based on the proving ring used in the experiment. Finite element simulation will be conducted on the conventional circular shape. After the finite element analysis is complete, shape optimization will be conducted. The following is a list of parameters in the optimization process. Finally, the results of the initial finite element simulation will be combined with the results of the shape optimization which will show a more optimized shape with respect to stress.

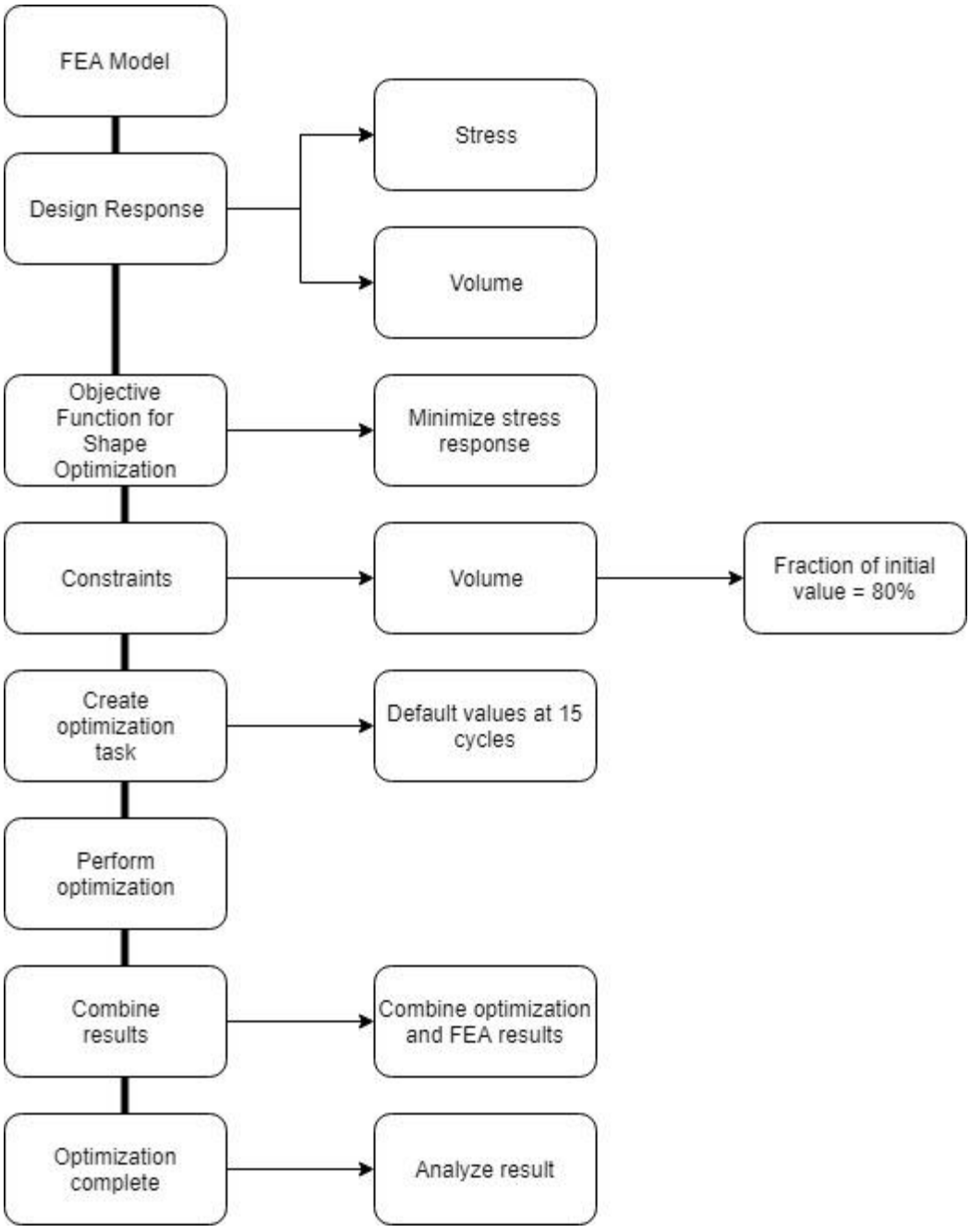


Figure 3.8 Flowchart of TOSCA shape optimization method

### *3.5.3 Evolutionary Algorithm*

*Evolutionary Structural Optimization*

Multiple optimization codes exist for various engineering problems and applications. In optimizing the proving ring, which requires structural or shape optimization, it was determined that the evolutionary algorithm to be suitable for this type of problem. Standard ESO or evolutionary structural optimization codes are based on evolutionary algorithm which optimizes the structure through material subtraction using a determined rejection ratio to find an optimal shape [85]. The optimization procedure aims to ideally puts all stress values of each element on the structure to as close as possible. This ensures efficient material usage throughout the structure. To achieve this, materials with low stress levels, which is assumed to be negligible and under-utilized, are subsequently removed. A rejection criterion or rejection ratio is therefore employed to carry out this procedure. After a discretization of the structure has been established through finite element analysis, stress levels of each element are then compared to the maximum stress levels of the structure as a whole. The rejection ratio is defined as

$$\frac{\sigma_e^{vm}}{\sigma_{max}^{vm}} < RR_i \tag{3.22}$$

Whereby $RR_i$ is the rejection ratio, $\sigma_e^{vm}$ is the stress value of the element and $\sigma_{max}^{vm}$ is the maximum stress of the whole structure. Therefore, at this point it is clear the main objective of the optimization procedure is to remove as much void elements or elements that does not contribute to sustaining the stress induced on the structure. This results in a much stiffer structure as a whole. Although useful, this method however does have certain restrictions. The most obvious is that material subtraction alone will not yield a completely optimized shape. The resulting shape from the optimization procedure could be largely different than the true optimized shape the algorithm is supposed to reach. Essentially, this means that the results of the optimization are rendered inadequate. This is especially true if the constraint or rejection ratio applied is too large or

inappropriate. This approach is usually catered more towards designing certain structures such as a bridge or a support column where the simulation starts with a block of material and results in a skeletal-like structure significantly thinner than the starting material. The result is a much smaller and stiffer structure.

*Bi-directional Evolutionary Structural Optimization*

As was mentioned in the previous section, optimization through material subtraction alone is insufficient. A second, much appropriate approach for this type of simulation is the bi-directional evolutionary structural optimization or (BESO). This algorithm is similar to the ESO approach. However, just as the name implies, the algorithm optimizes in a bi-direction method i.e. material subtraction and addition [86]. The main difference is the use of evolutionary volume ratio ER instead of RR. The elemental and sensitivity numbers are calculated first. A filtering procedure is then put in place. The sensitivity numbers of each element are then compared to either addition or removal threshold sensitivity value. If the solid element has a lower sensitivity number than the threshold it will be removed. The opposite is true for void elements with higher sensitivity number than the threshold value. An averaging of the sensitivity numbers is then calculated. This is done to ease convergence. The target volume for the next iteration is then determine and material addition or subtraction is conducted. The whole process repeats itself until the volume constraint and convergence is achieved.

A program code developed by Mike Xie [85] from RMIT University called BESO2D will be used to simulate and run the BESO optimization algorithm. A square ring model with length 178mm as well as an inner ring diameter of 79mm was created. Finite element analysis with nodal distance set at 4 was performed before the BESO optimization. The evolutionary parameters are set at material removal rate ER% 2%. Material reduction or volume constraint is set at 80%. Maximum iteration number is set at 200. Other parameters such as the filter radius and convergence tolerance are set at default values of 12 and 0.10 respectively. Finite element simulation parameters are similar to the ones used in the ABAQUS simulation with axial load set at 30kN. The basic optimization procedure is presented in the flowchart below.

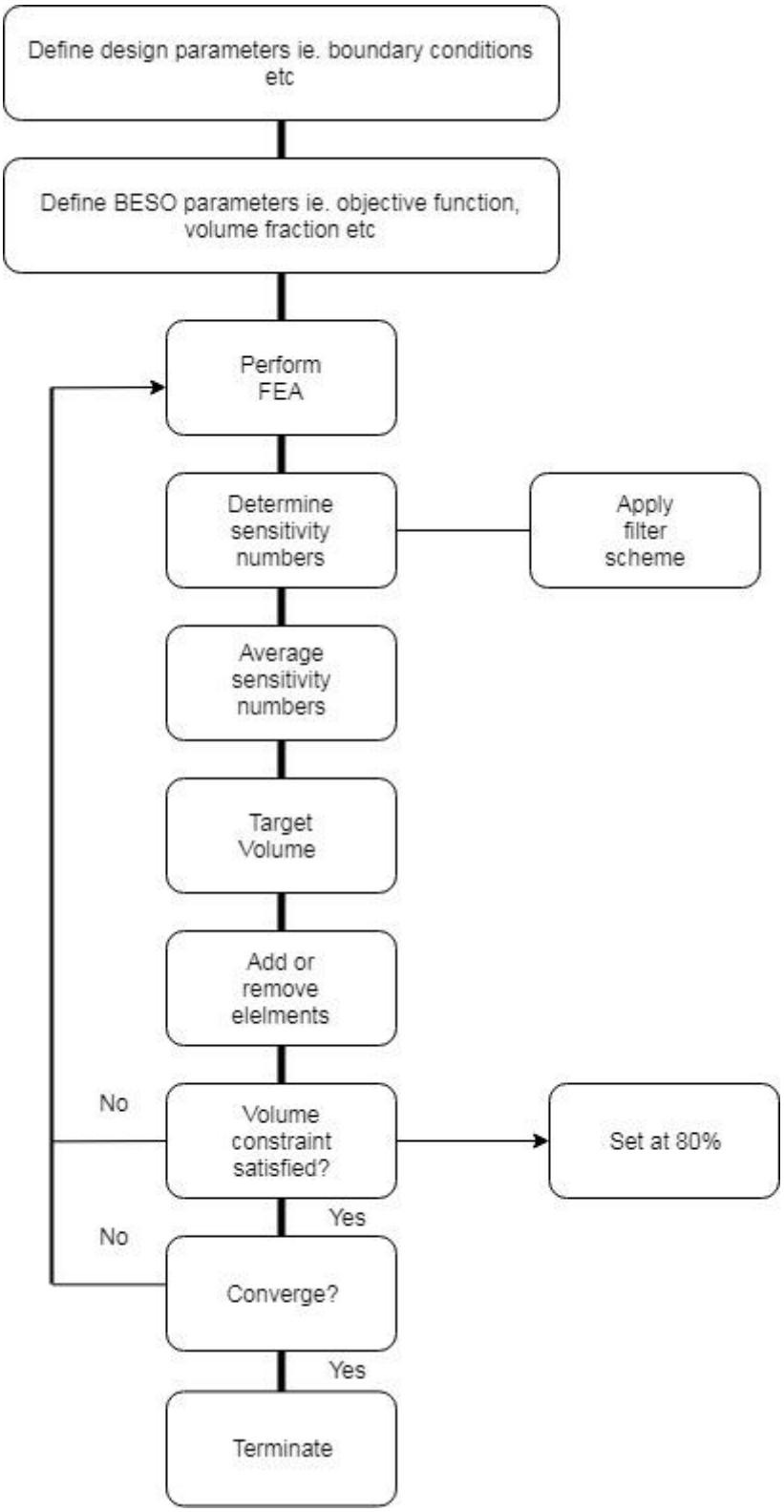


Figure 3.9 Flowchart of BESO optimization method

### 3.6 New Ring Design

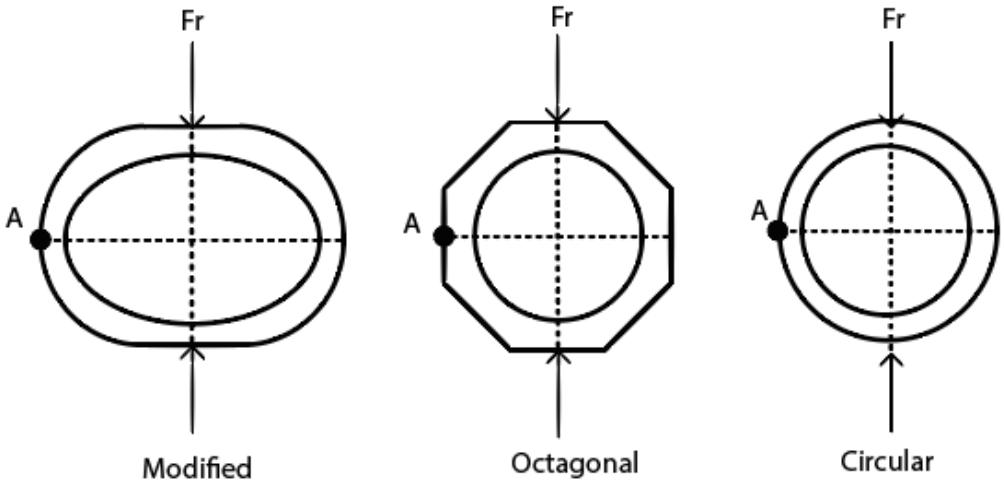


Figure 3.10 Three rings. Point A is the reference point in which stress and strain in the S11 or $\sigma_x$ and E11 or $\varepsilon_x$ respectively are measured.

From the optimization work conducted, a general varying cross section shape is observed. Using this combined general shape from the optimization results, where material seems to concentrate more at the top and bottom portion of the ring followed by the horizontal sides, two new ring designs are proposed. The first sees a combination of a circular shape and octagonal shape. This was done based on the optimization results where the top and bottom portion were similar to an octagonal ring with the sides curving akin to a circular shape. Also, straight sides at the point of load application means the need for clamps are negated. The inner shape remains circular or elliptical depending on the inner radius. The second is an extension of the first but with a double ring design. The first modified ring design is a novel idea proposed by the author which combines two conventional shapes into one. The ring has a varying cross section design with ring material mostly concentrated at locations where high stress levels are expected based on the optimization results found earlier. The top and bottom portion of the ring has straight sides of fixed length 50mm. The width of the ring will be varied primarily from the horizontal axis. This in turn would also affect the ring thickness at the vertical axis. The modified ring design as well as dimensions with width w = 12.41mm are shown in Figure 3.11. The modified ring mesh is similar to the circular ring with 1600 nodes and 1280 elements. Comparison of the modified ring

against the other two conventional rings will be made. This is done by utilizing the developed equation formed from the second $\pi$ group or Equation (3.2) in the analytical section. Using this equation, the width w and inner radius, $R_i$ of all three rings are varied to have similar $w/R_i$ values. This ensures the rings are fairly compared. The ring sensitivity in the E11 and E22 directions are defined based on Equation (3.5) and plotted against the $w/R_i$. Stress in the S11 and S22 direction are also compared and plotted against $w/R_i$. Both sensitivity and stress values are taken at point A as shown in Figure (3.10). Ring deflection studies will also be conducted by comparing calculated values based on the first $\pi$ group. Finally, frequency analysis was conducted to determine and compare the natural frequency of the three rings. This is to determine the suitability of the ring for various applications where the natural frequency of the ring plays a vital role in the force measuring dynamometer design. After comparisons of the rings are conducted, another study to study the effects of varying the length of the straight edges on the stress, sensitivity and deflection of the ring.

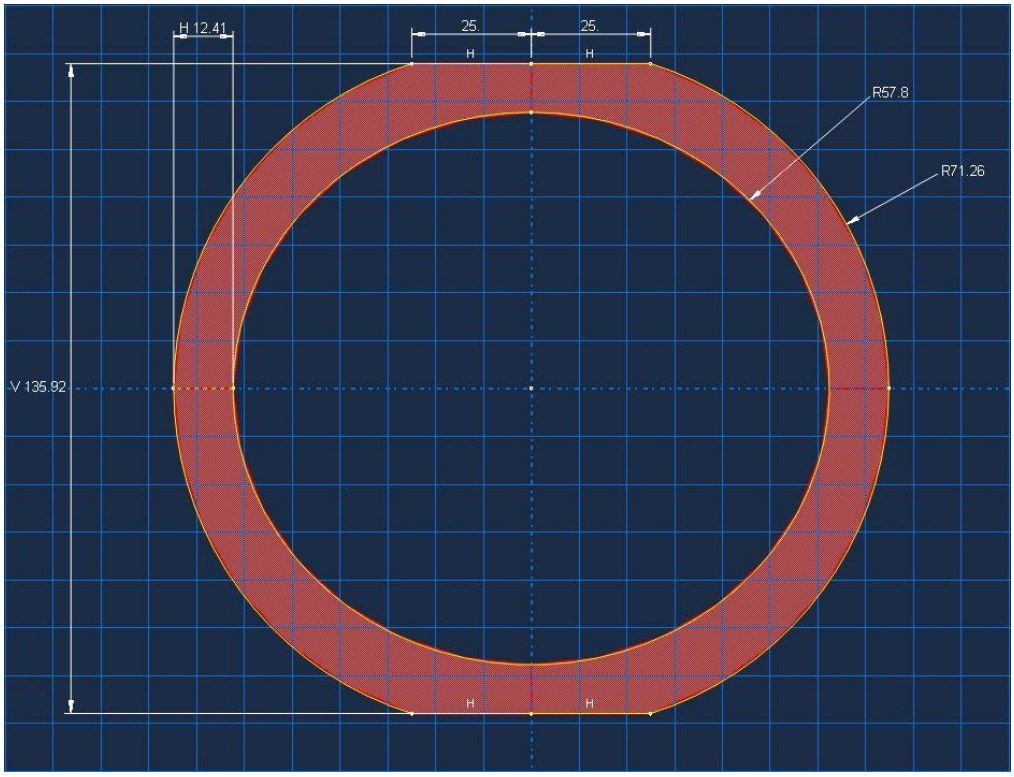


Figure 3.11 Modified ring design at ring thickness 12.41mm. Dimensions are in mm.

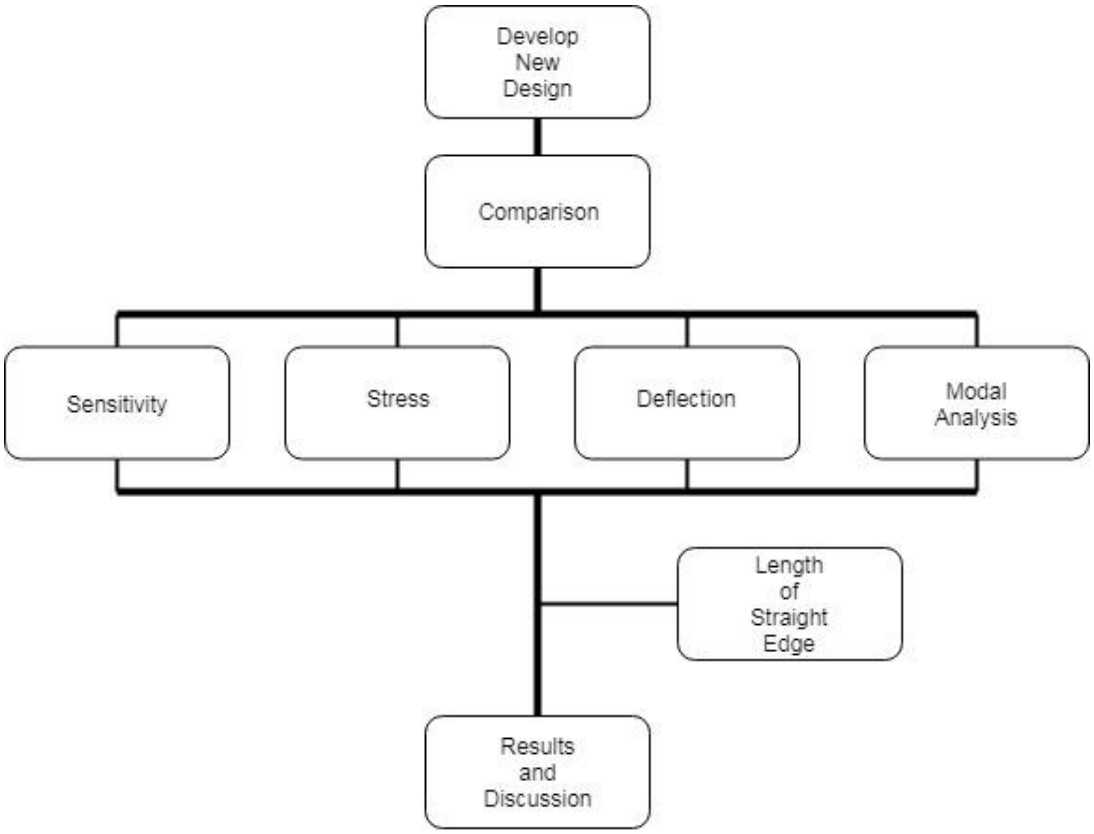


Figure 3.12 Flowchart of modified design analysis

From the design comparison studies conducted on the new ring, it will be shown that the overall modified ring can be said to have a universal design. Taking this into account, after the new modified design is compared and verified to have better stress levels as well as improved sensitivity, a second design modification is implemented. The second design will also have a similar overall structure but with a double ring on each side instead. This means that the second modified ring will have two curved sections on each side. Figure 3.13 shows the proposed second design with the double ring concept. Stress, sensitivity as well as deflection will be studied to see if this second design can further improve the first new rings' characteristics.

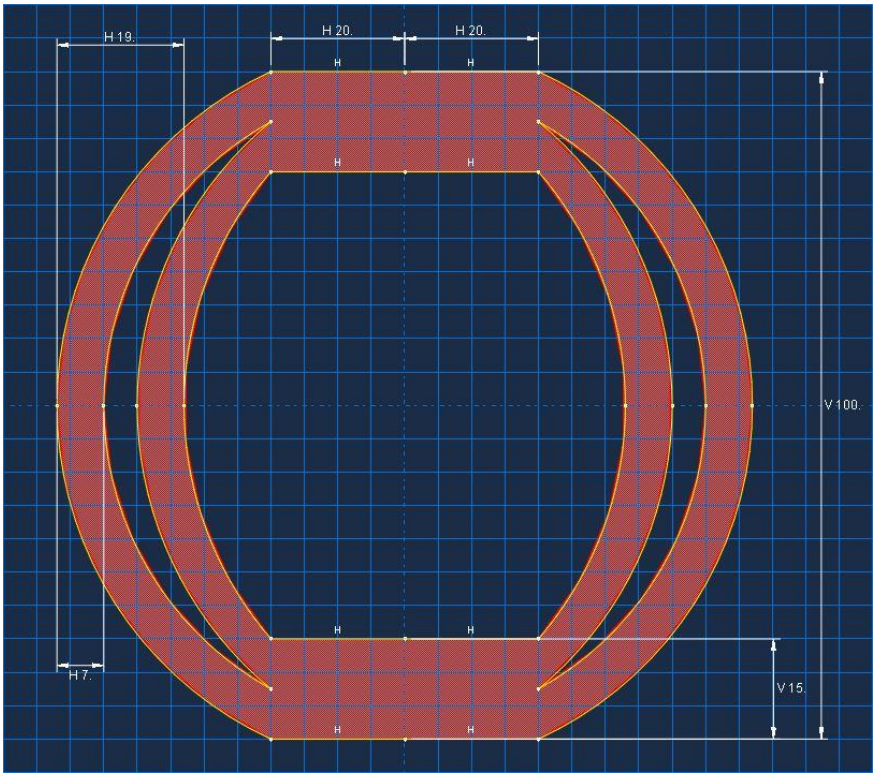


Figure 3.13 Model of proposed double ring design. Dimensions in mm.

## 3.7 Conclusion

In conclusion, the designed methodology was done to ensure that the objectives of this research study are met. The first or earlier sections were done to create a base understanding of the problem at hand. Identifying the initial response of the ring through an experiment as well as numerical research helps to determine the direction of this study. The optimization sections help to understand and roughly design the general shape of an optimized ring with respect to stress induced. The final stage establishes a design idea proposed from the various results and findings from this study. Here, a definite ring shape taking the optimization results into account was designed and evaluated against other conventional ring shapes. It can be observed that the necessary steps have been taken to design a proving ring with optimized stress distribution and enhanced ring sensitivity that meets all objectives stated in the previous chapter.

# Chapter 4

# Results and Discussion

## 4.1 Introduction

In this chapter, all results obtained based on the developed methodology are presented and discussed. Experimental work was done to identify material properties such as modulus of elasticity as well as the deflection characteristics of the ring. Using finite element simulation, initial preliminary work was done by comparing a circular ring with an octagonal ring to test the hypothesis. Next, an optimization technique based on GRG code written in Visual Basic is then used. Optimizations based on simulations using finite element analysis and evolutionary algorithm shows the legitimacy of a varying cross section design with a more optimized shape. The results of these three optimization techniques were then used to develop a modified ring with a varying cross section design. Lastly, the proposed modified design was enhanced further by applying a double ring design.

## 4.2 Experiment

A preliminary experiment was done on a conventional proving ring. The proving rings' material data sheet however was not available and therefore its modulus of elasticity was unknown. The experiment was conducted on a conventional circular proving ring to identify the characteristics and performance of the ring as a basis for the design improvement. The dimensions of the ring were measured, and a static compressive load test was conducted. The ring was loaded

at step increments of 5kN up to 30kN with a 5 second pause at each interval to record the corresponding deflection. The final ring deflection at 30kN was found to be 2.55mm. The data was then collected, and a load vs deflection curve was plotted to identify the modulus of elasticity and stiffness of the circular ring using thin ring theory [17, 18].

Table 4. Experimental results

| **Load, F (kN)** | **Deflection, δ (mm)** |
|---|---|
| **5** | 0.39 |
| **10** | 0.86 |
| **15** | 1.25 |
| **20** | 1.69 |
| **25** | 2.13 |
| **30** | 2.55 |

$$\delta = \frac{PR^3}{EI}\left(\frac{\pi}{4} - \frac{2}{\pi}\right) \tag{4.1}$$

$$E = 0.149\frac{PR^3}{\delta I} \tag{4.2}$$

$$E = \frac{30000 \times 89^3}{2.55 \times \frac{60 \times 10^3}{12}}\ 0.149$$

$$E = 245.708\ \frac{N}{mm}^2$$

$$E = 245.708\ GPa$$

$$E \approx 246\ GPa$$

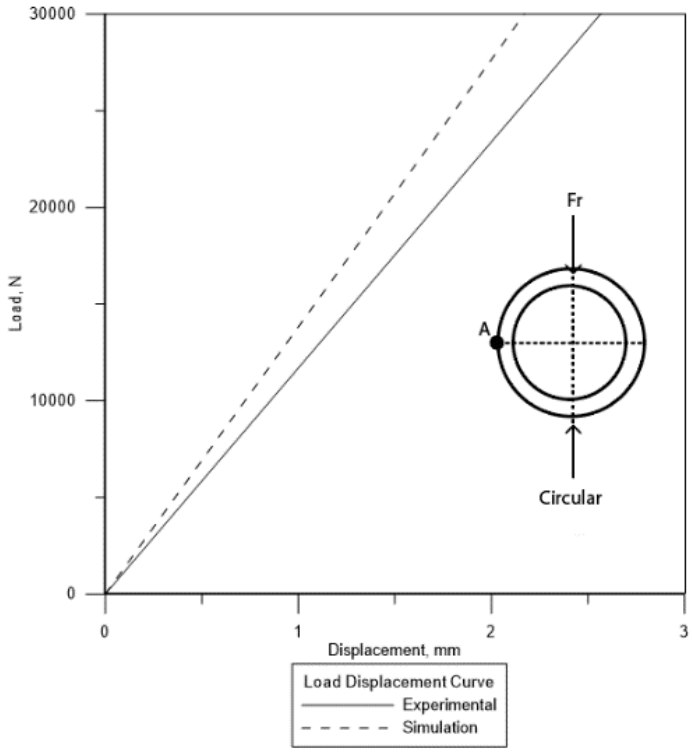


Figure 4.1 Load vs displacement response

Figure 4.1 shows the load displacement curve comparing experimental and finite element response. The experimental and finite element analysis responses differed by a significant margin. It is because the modulus of elasticity used in finite element analysis was calculated based on the experimental response which was not closely matching due to factors such as the chrome coating and the effects of the clamps on the ring were not taken into consideration. The experimental deflection was then taken and used to calibrate the load displacement curve through finite element analysis to obtain an adjusted response. This was done by applying a displacement load on the top point of the ring instead of an axial load of 30kN. The modulus of elasticity obtained through this method was found to be 205GPa.

## 4.3 Initial Finite Element Analysis and Simulation

For this simulation study, the objective is to study the stress distribution in a circular ring and compare it with a variable cross section design represented by the octagonal ring. From literature, varying cross section rings such as the octagonal and extended octagonal ring shape

designs were frequently discussed due to their suitability in various applications. The extended octagonal ring was not considered due to a largely different geometric design compared to the constant cross section circular ring. The dimensions of the finite element simulation circular shape were similar to the ring used in the experiment section. The mass of the circular ring without attachment was determined by using Solidworks. The octagonal ring was designed to have similar mass to the circular ring. This was to ensure a fair comparison between both rings. In this analysis, stress in the S11 or $\sigma_x$ direction, strain in the E11 direction and deflection are the design responses considered for comparison. Along with the stress and strain levels, the distribution pattern of each response was noted as well. The following figure shows the comparison of each rings' stress, strain and deflection distribution.

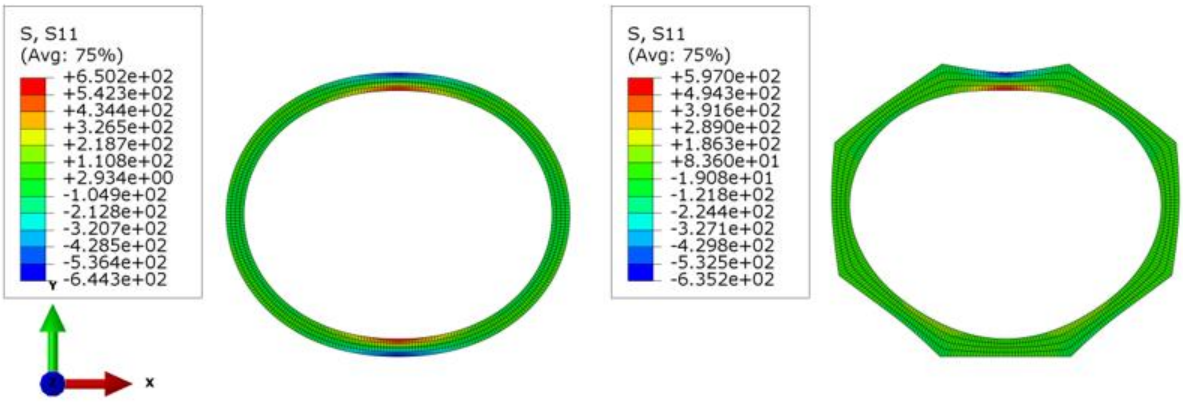


Figure 4.2 Comparison of stress in the S11 or $\sigma_x$ direction for circular and octagonal rings

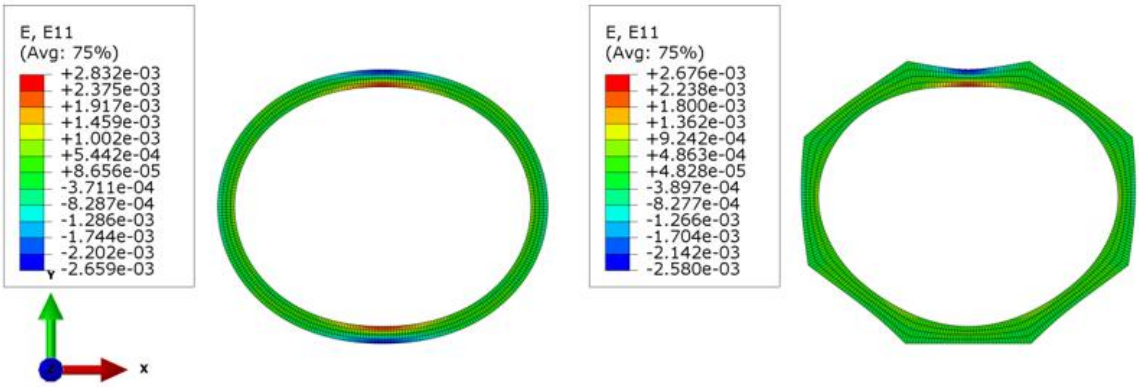


Figure 4.3 Comparison of strain in the E11 or $\varepsilon_x$ direction for circular and octagonal rings

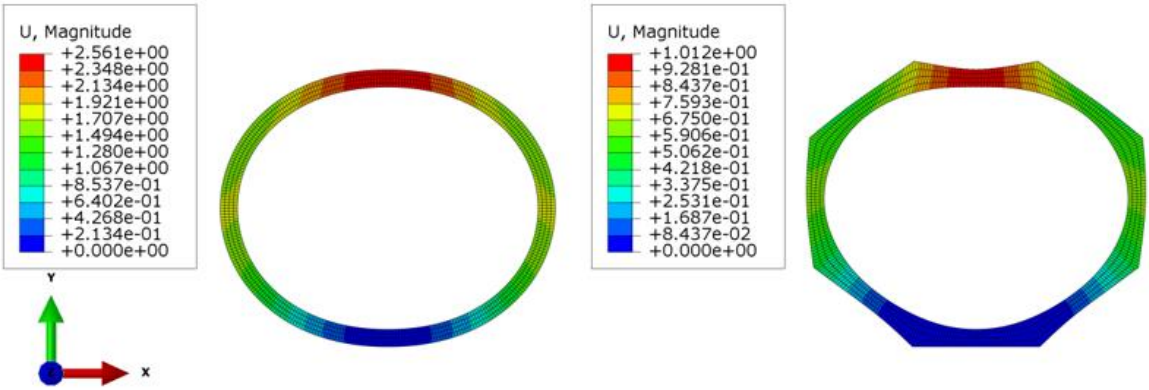


Figure 4.4 Comparison of deflection for circular and octagonal rings

In the stress and strain analysis, the maximum stress strain values as well as stress strain at horizontal point A where $\theta = 0°$ in the S11 direction was taken. From Figure 4.2, the radial stress in the S11 direction induced by the applied load is mostly concentrated at the inner fibre of the top and bottom portion of both rings. The application of a point load creates a bending stress induced in the ring. This causes tension on the inner fibre and compression on the outer fibre of the ring. The observations made from the finite element modelling however shows that the stress due to tension is significant compared to the compression. S11 stress is seen to be minimum at the horizontal sides of the ring. The stress levels in the circular ring however is slightly higher compared to the octagonal ring. This indicates that a varying cross section design such as the octagonal ring produces lower stress levels than a constant cross section design. Figure 4.3 shows the elastic strain induced on the ring. Similar to the stress distribution, the maximum elastic strain was located on the inner fibre of the top and bottom portion of the ring. The circular ring has a slightly higher strain value compared to the octagonal ring. Comparing the deflection values of the rings in Figure 4.4, the circular ring has a much higher deflection than the octagonal ring. This reveals that the stiffness of the octagonal ring is much higher than the circular ring. Moreover, this indicates that in terms of measurable deflection, the circular ring is more sensitive. Table 5 summarizes the findings in this initial finite element analysis.

Table 5. Comparison between circular ring and octagonal ring

| Design Response | Circular Ring | Octagonal Ring | Difference |
|---|---|---|---|
| **Maximum Stress, (MPa)** | 650.2 | 597.0 | 8.2% |
| **Stress at point A, (MPa)** | -6.18 inner,<br>-4.75 outer | -3.60 inner,<br>-0.97 outer | |
| **Maximum Strain, (μ)** | 2.832E-3 | 2.676 x 10-3 | 5.5% |
| **Strain at point A, (μ)** | $7.31 \times 10^{-4}$inner,<br>-6.54 $\times 10^{-4}$outer | $6.33 \times 10^{-4}$ inner,<br>$-5.37 \times 10^{-4}$outer | |
| **Deflection, (mm)** | 2.561 | 1.012 | 60.5% |

The results obtained from simulation show that there is legitimacy in applying a varying cross section design to the conventional rings to improve its stress levels. The octagonal ring has significantly reduced stress levels compared to the circular ring with constant ring thickness. However, the octagonal ring has a significantly lower sensitivity based on measurable deflection. This is expected as the moment area of inertia at the point of load application has been increased. It is known that stress is directly proportional to the strain in a structure given a constant modulus elasticity. From this relationship, the increase in bending stress in the ring will result in the increase in strain of the ring given a constant modulus of elasticity. The increase in strain is measurable using a strain gauge connected in a Wheatstone bridge configuration. Therefore, increasing the stress levels can increase the strain and sensitivity of the ring. However, a balance of these two factors must be achieved. The next few sections will try to address this by utilizing various optimization algorithms.

## 4.4 Generalized Reduced Gradient Optimization Code

GRG or generalized reduced gradient is an optimization algorithm for general first order optimization work. In this section, the GRG code was used to find an optimal width based on the stress equation. The ring was segmented into sections of 15° intervals. Only a quarter of the ring was considered due to symmetry. The objective function and constraint have been defined in the previous chapter. The initiation of the algorithm starts with a width of 10mm. Mean radius was kept constant to ensure a smooth ring geometry with minimal variations between sections of different thickness. Hence, with the width varied, the mean radius is controlled. The following table illustrates the results obtained from the GRG optimization work.

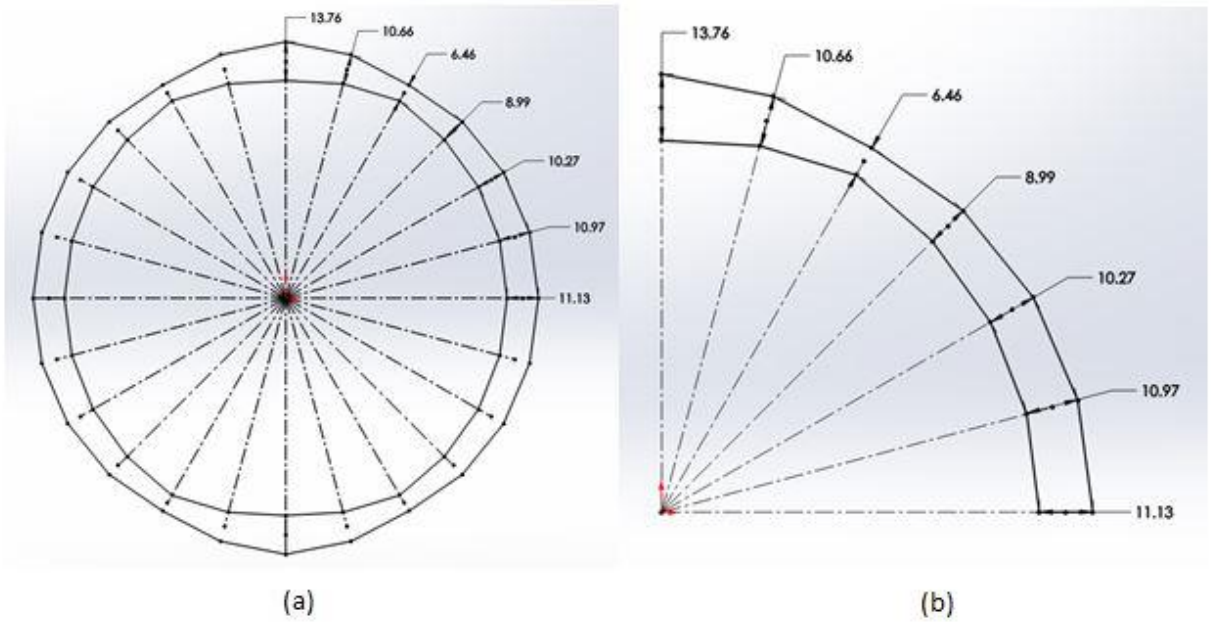


Figure 4.5 GRG optimization results for a) quarter ring and b) full ring

The optimization process was conducted in a way that ensures stress level at each section is similar to stress value at section 0°. From Figure 4.5, a varying thickness ring design can be observed. From Table 6, it was found that stress at all sections have been made uniform. The results therefore indicate that the objective function has been successfully achieved with each section sustaining the same amount of induced stress after the ring thickness was modified. Also, it is observed that the ring width decreases considerably by nearly half as it approaches from 0° to 60°

from 11.14mm to 6.46mm. This is expected since bending moment reduction results in lower stress levels at those sections. Hence, less material is required to sustain the stress induced. Between 45-60°, there is a change in sign from positive stress value to negative. A sign change from one angle to another suggest a change from tensile stress to compressive stress which is indicated from positive to negative. Lastly, highest sensitivity with respect to measurable strain was obtained at 90° with the minimum found at 60°. The second largest sensitivity was located at 0° which is a more ideal location for strain gauge placement than the section where axial force is applied.

Table 6. Results of GRG Optimization

| Angle, ° | Width, w | Stress, MPa | Sensitivity |
|---|---|---|---|
| **0** | 11.14 | 24580 | 0.0809 |
| **15** | 10.98 | 24580 | 0.0797 |
| **30** | 10.27 | 24580 | 0.0746 |
| **45** | 8.99 | 24580 | 0.0653 |
| **60** | 6.46 | -24580 | 0.0469 |
| **75** | 10.66 | -24580 | 0.0774 |
| **90** | 13.76 | -24580 | 0.0999 |

## 4.5 Bi-directional Evolutionary Structural Algorithm Results

The second optimization technique was the bi-directional evolutionary structural optimization algorithm BESO2D developed by Mike Xie of RMIT University [85]. The parameters for the finite element simulation section in BESO was similar to the ones used in the ABAQUS finite element simulation. The optimization settings have been discussed in the Methodology section of this thesis. The design approach in starting with a square ring shape is called an Initial Guess Approach [85]. This design approach starts with initial material volume as close to the final objective volume as possible. To do so, a square ring with significantly more material is used in the initial guess. The square ring approach was also taken as starting directly from a circular ring design results in a structure too thin to be considered ideal which in part is due to the coarse mesh. From numerous simulation trials, a finer mesh results in program error which

could be due to computer memory problems. Hence, a coarser mesh is used for the simulation. This means that since less materials are added or removed to achieve the target volume, the number of iterations can be significantly reduced which saves computational time. Lastly, a volume constraint of 80% was selected to maintain the mean radius of the ring. A lower volume constraint would result in a thinner ring structure.

Figure 4.6 (a) shows the finite element simulation result of the square ring shape. It can be observed that high stress levels tend to concentrate at the upper and lower portion of the ring. Slightly lower stress levels were seen at the sides of the ring predominantly on the inner surface. This is in accordance to previous simulation results where high stress concentration levels were at similar locations around the circular ring. Also, stress levels are lowest at locations between 30-60° from the horizontal axis. In summary, there are large variations in stress levels between elements in different locations of the ring. These observations indicate that the ring material has not been fully utilized to sustain the stress induced on the ring. In Figure 4.6 (b), the optimization result observed a drastic reduction of materials from the edges of the ring towards the center where stress levels are highest. Based on the simulation results, this outcome was to be expected. The optimized shape shows a kind of modified ring shape with most ring materials concentrated at the upper and lower portion of the ring as well as at the horizontal sides where stress levels are the highest. Thinner structure was observed at the curved edges connecting the vertical and horizontal portion of the ring. It was also found that the stress levels around the ring were more evenly distributed compared to the initial simulation results. This indicates ring material has been optimally redistributed throughout the cross section of the ring.

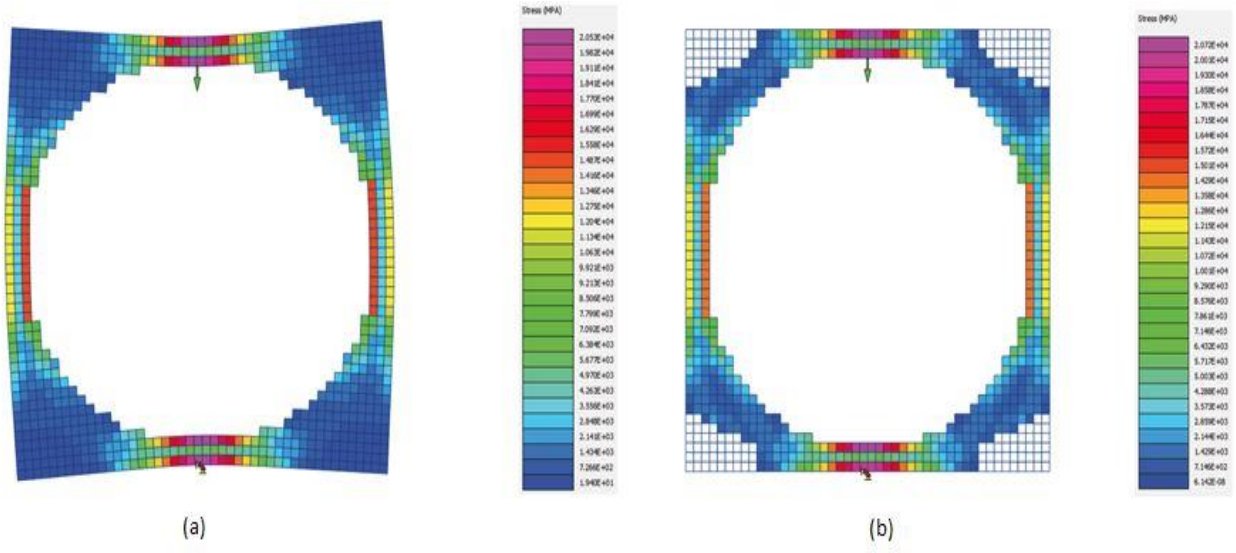


Figure 4.6 (a) Finite element analysis and (b) optimization results of a square shaped ring using BESO2D code

## 4.6 Finite Element Shape Optimization (TOSCA)

TOSCA optimization was conducted on the circular ring from the previous finite element simulation. The objective function was set at minimizing stress. The volume constraint was set at 80% of a fraction of the initial volume. Similar to previous optimization method, there is a distinct pattern of materials concentrated at the four sides of the ring. The vertical sides of the ring that is perpendicular to the applied load indicates thicker sections from the middle that gradually thins out as it reaches 45°. At around 45°, there is a necking pattern where ring material is minimum. Ring width is smoother and more even on the horizontal sides of the ring. This shows that material is least required at this location to support the stress induced on the ring.


Figure 4.7 Result of TOSCA shape optimization

From the Figure 4.8, it can be observed that the stress levels have been significantly reduced. The initial ring geometry was identical to the ones simulated from section 4.3. Comparing the results of the conventional ring to the optimized one shown above, the optimized ring shows a maximum stress reduction from 650.2 MPa down to 557.2MPa. This is a reduction of 125.8MPa or 14.3%. In terms of the stress distribution, unlike the circular ring which concentrates over a smaller area directly under the axial load application point, the stress is more evenly distributed over a larger area at the inner surface of both the top and bottom portion of the ring. This would explain why the stress levels can be decreased as the area is more densely packed with ring material to withstand and support the stress induced. Slightly higher stress levels can also be seen on the periphery of the ring on the horizontal sides which was not observed in the circular ring (Figure 4.2). This indicates that stress is much more evenly distributed throughout the ring thereby ensuring ring material is optimally used. Figure 4.9 shows the strain distribution in the E11 of the optimized ring. It is observed that the maximum strain levels have been reduced from $2.832 \times 10^{-3}\mu$ to $2.504 \times 10^{-3}\mu$ or by 11.6%. This indicates that the sensitivity of the ring in terms of measurable strain has been slightly reduced. The reduced strain levels however were expected as the stress levels has been reduced. Similar to the stress results, the strain distribution pattern shows a more evenly distributed strain over a larger inner surface as opposed to the circular ring. In Figure 4.10, the deflection of the ring has been significantly increased from 2.561mm to 4.043mm or by 72%. Table 7 summarizes all findings made from this optimization technique.

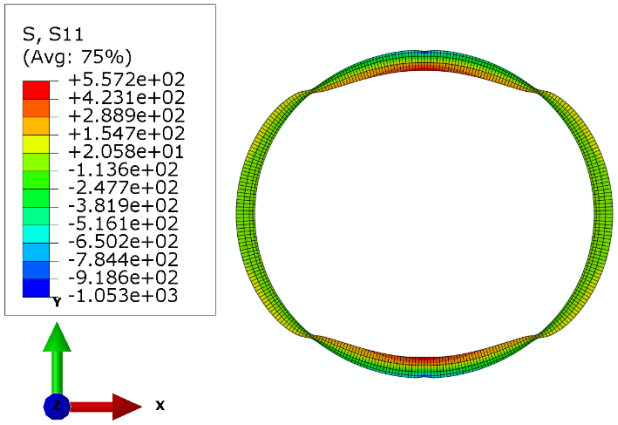


Figure 4.8 Stress in S11 or $\sigma_x$ direction of optimized ring

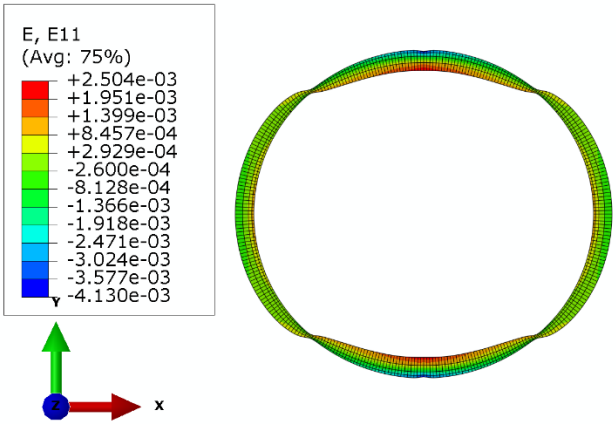


Figure 4.9 Strain distribution in the E11 or $\varepsilon_x$ of the optimized ring

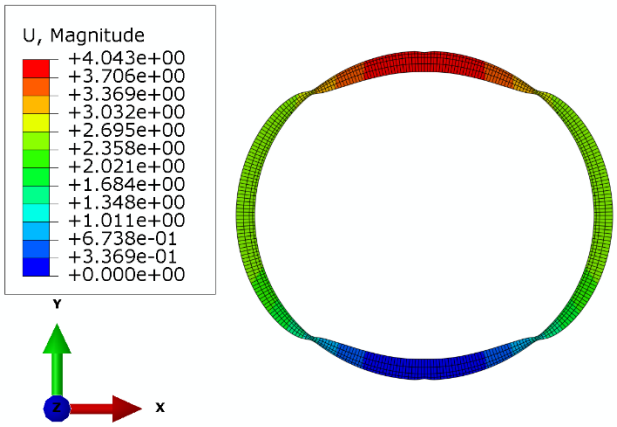


Figure 4.10 Displacement of the ring in the U2 or vertical direction

Table 7. Summary comparing conventional circular ring and optimized ring.

| Design Response | Optimized | Circular | Difference, % |
|---|---|---|---|
| **Maximum Stress, MPa** | 557.2 | 650.2 | 14.3 |
| **Maximum Strain, μ** | $2.504 \times 10^{-3}$ | $2.832 \times 10^{-3}$ | 11.6 |
| **Deflection, mm** | 4.043 | 2.561 | 57.9 |

## 4.7 Comparison of Optimization Techniques

The following section discusses the results obtained from the optimization process. Stress and strain values were measured at point of load application Fr and at the horizontal point A as is shown in the following figure below. Literature shows that different ring shapes were found to have different optimal strain gauge locations for accurate force measurements. To highlight the differences between ring geometries in terms of the various measured parameters such as stress and strain, location point A was identified as the referral point for comparison between different ring shapes. This ensured comparisons between the different ring shapes were fair. Shapes and geometries from each optimization technique were discussed and results obtained were later compared based on various design response.

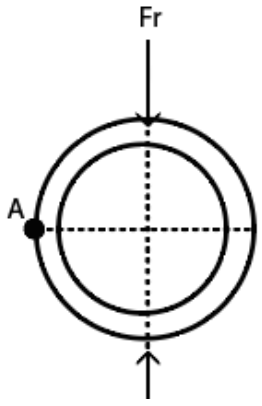


Figure 4.11 Circular ring illustrating where design responses were measured

### *4.7.1 Effect of Shape Optimization Codes on Ring Stress*

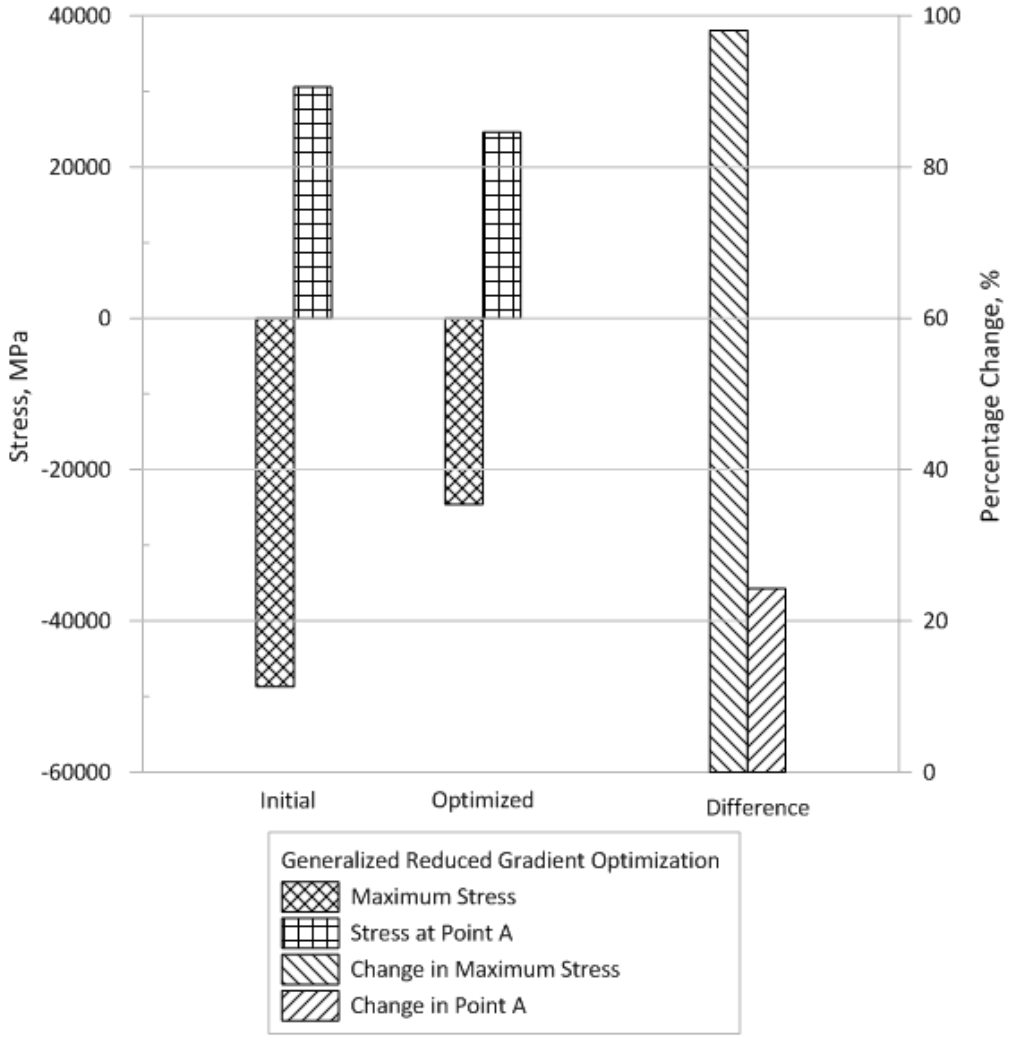


Figure 4.12 Changes in stress at various points for S11 stress GRG optimization

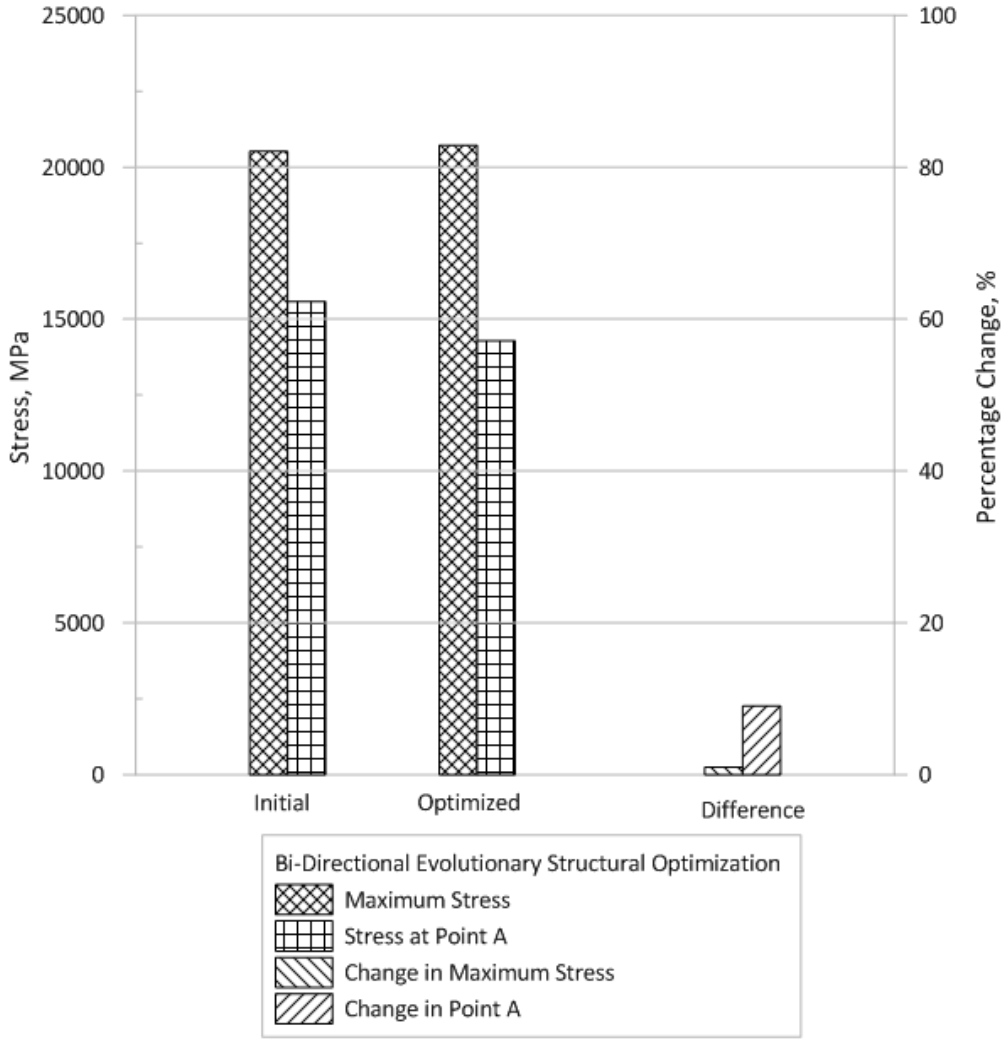


Figure 4.13 Changes in stress at various points for von Mises stress in BESO optimization

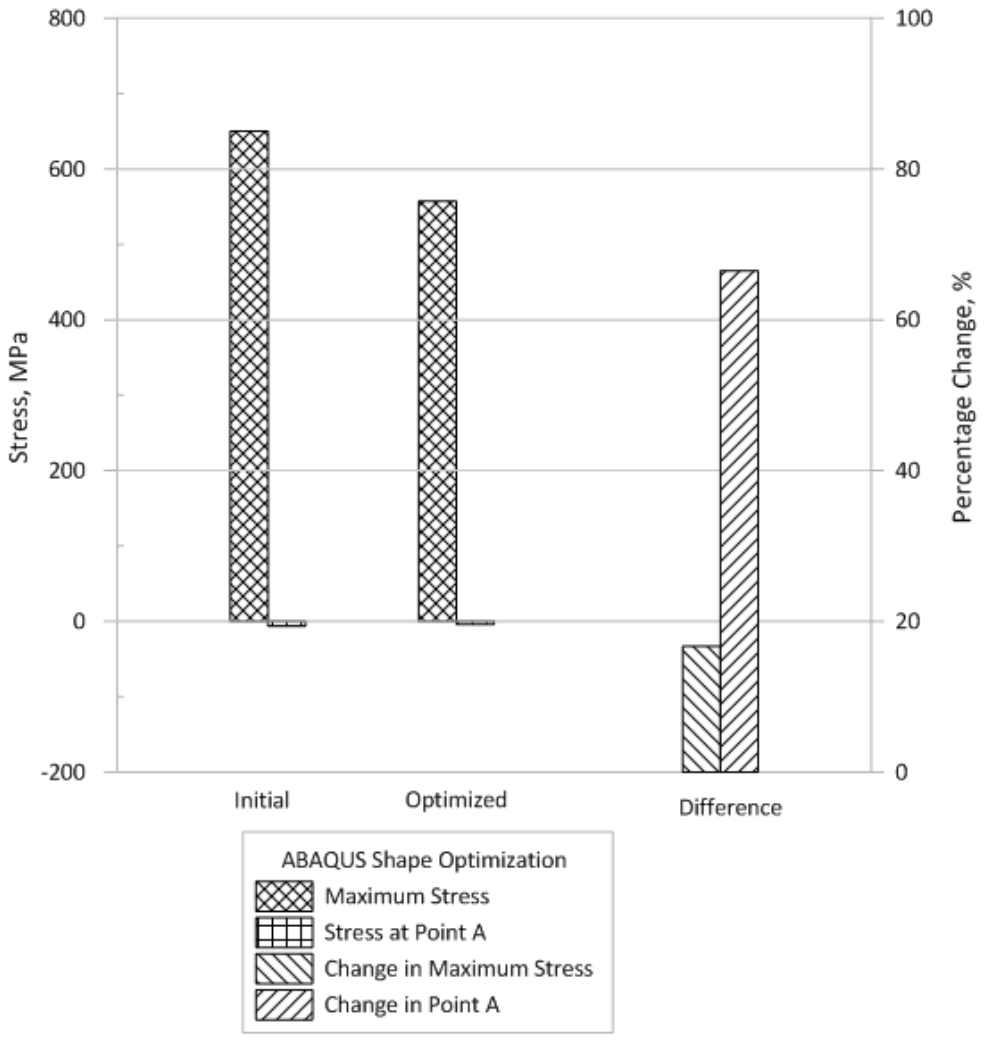


Figure 4.14 Changes in stress at various points for S11 or $\sigma_x$ stress ABAQUS shape optimization

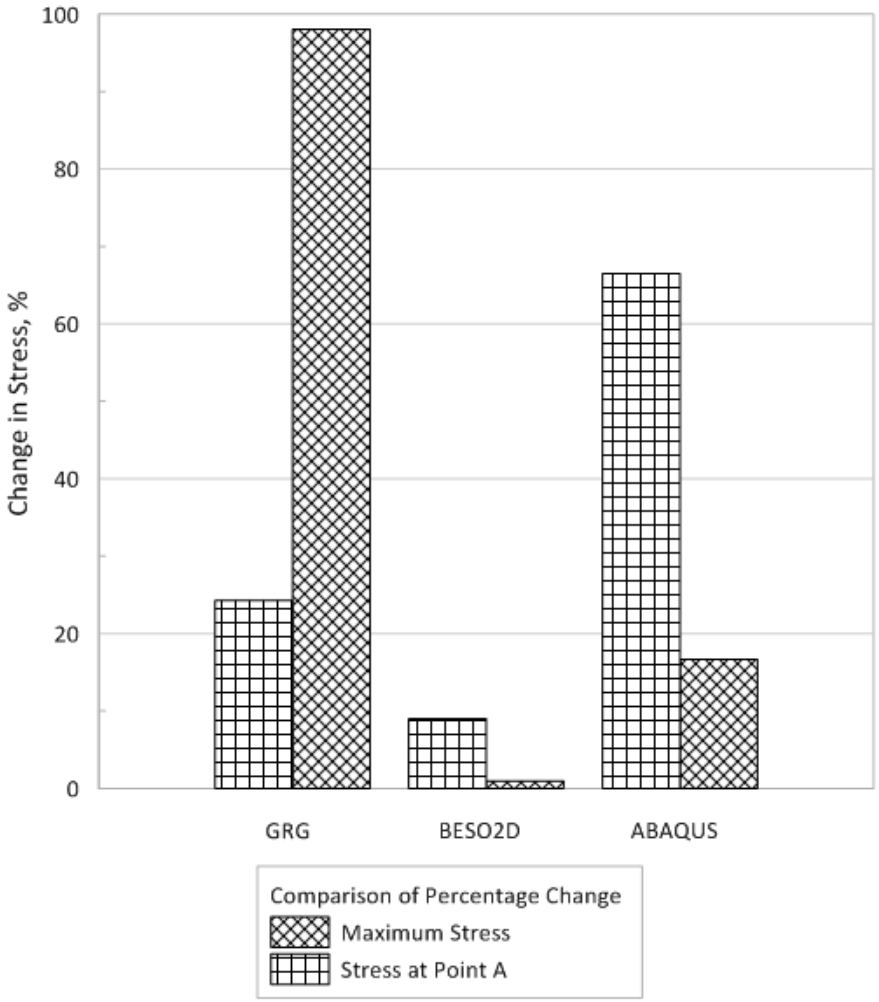


Figure 4.15 Comparison in percentage of all three optimization methods

The figures above show the percentage changes in stress for all three optimization methods. Stress in BESO is represented in the von Mises form whereas stress in the X direction or $\sigma_{xx}$ is represented in the GRG and ABAQUS optimization. From the GRG optimization method, it is observed that both maximum stress and stress at point A were significantly reduced. The maximum S11 stress was found to reduce by 98.0% with stress at point A reduced by 24.3%. The maximum von Mises stress at point of load application was found to have slightly increased by 1.0% in the BESO optimization. This small increase can be deemed negligible. Slight reduction of 9.0% was also observed at point A. This indicates that BESOs' optimization aim of finding the stiffest

possible structure was achieved. The slight increase and decrease in stress at both locations shows that stress is more optimally distributed between the point of load application and horizontal point A. Similar to the GRG optimization, the ABAQUS shape optimization sees reductions in both maximum stress and stress at point A. Stress reduction in the S11 direction was more pronounced at point A with a reduction of 66.5% whereas the maximum S11 stress was reduced by 16.7%. The results indicate that all three optimization techniques successfully reduced the stress levels in the rings.

### *4.7.2 Effect of Shape Optimization Codes on Ring Strain*

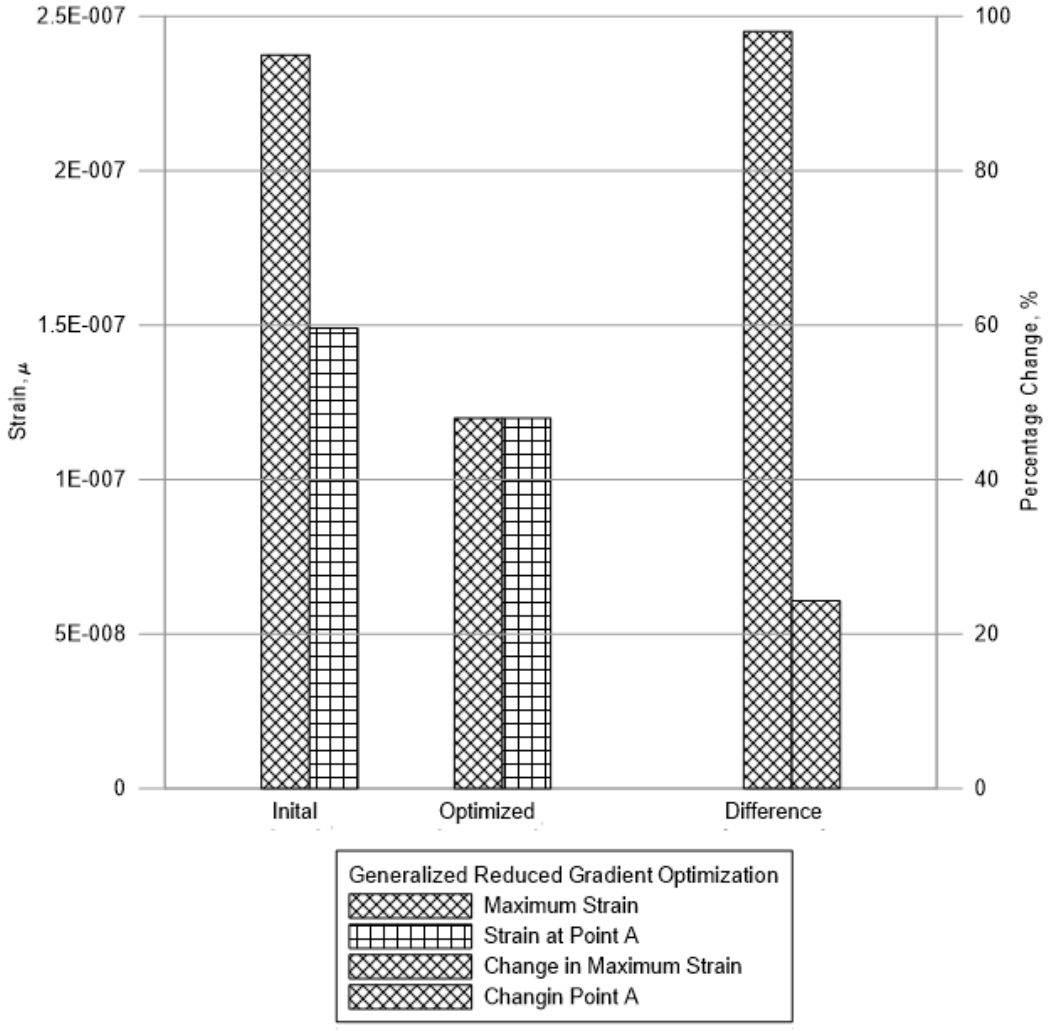


Figure 4.16 Changes in strain at various points for GRG optimization

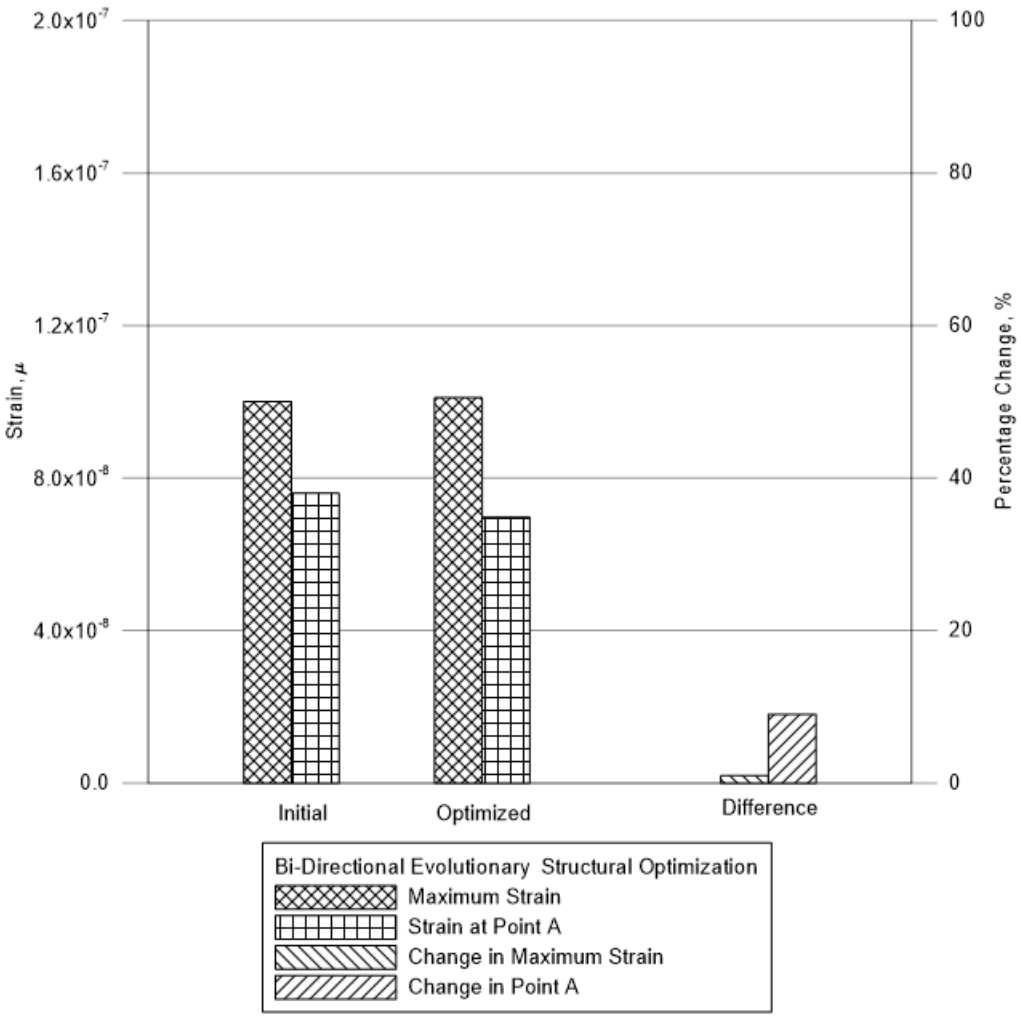


Figure 4.17 Changes in strain at various points for BESO optimization

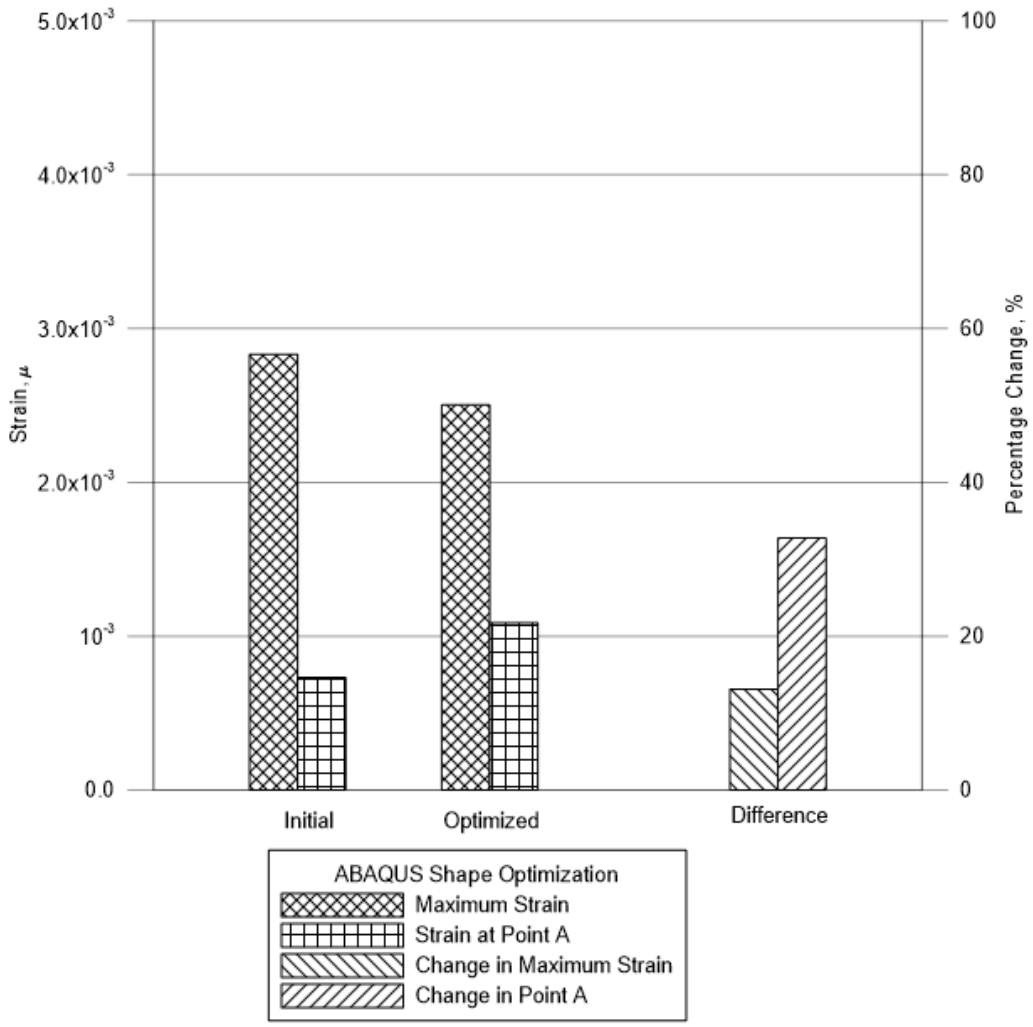


Figure 4.18 Changes in strain at various points for ABAQUS shape optimization

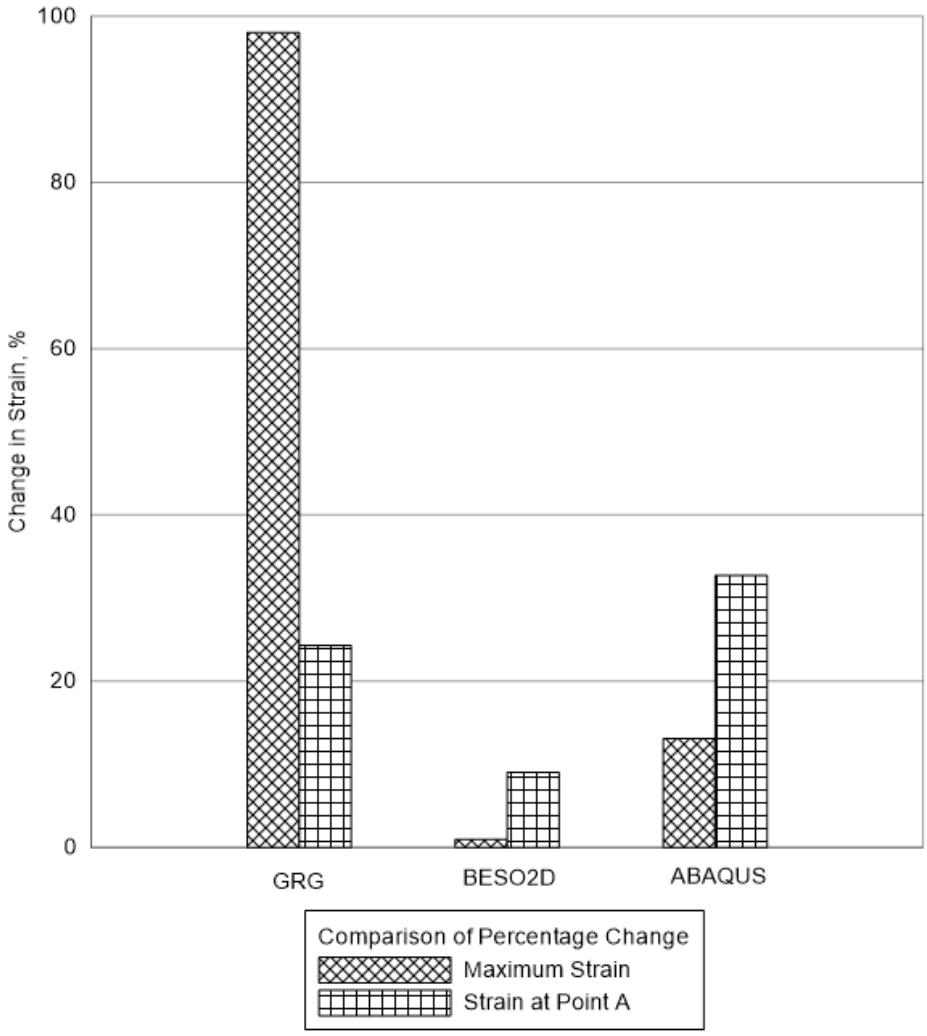


Figure 4.19 Comparison in percentage of all three optimization methods

It was observed that there is an overall trend of strain reductions across all three optimization techniques with a one exception. The general trend of strain reductions is expected however as a reduction in stress would result in strain reductions. Both GRG and BESO optimization experienced strain reduction similar in value to the stress reductions from the previous section. However, the BESO method shows a very slight increase in maximum strain value and a decrease in strain at point A. Similar to the stress results, this is due to the optimization method finding a stiffer overall structure. The ABAQUS results shows an increase in strain at point A and a decrease in maximum strain value. The positive change in strain at point A indicates a potential location for ideal strain gauge placement.

### *4.7.3 Effect of Shape Optimization Codes on Ring Sensitivity*

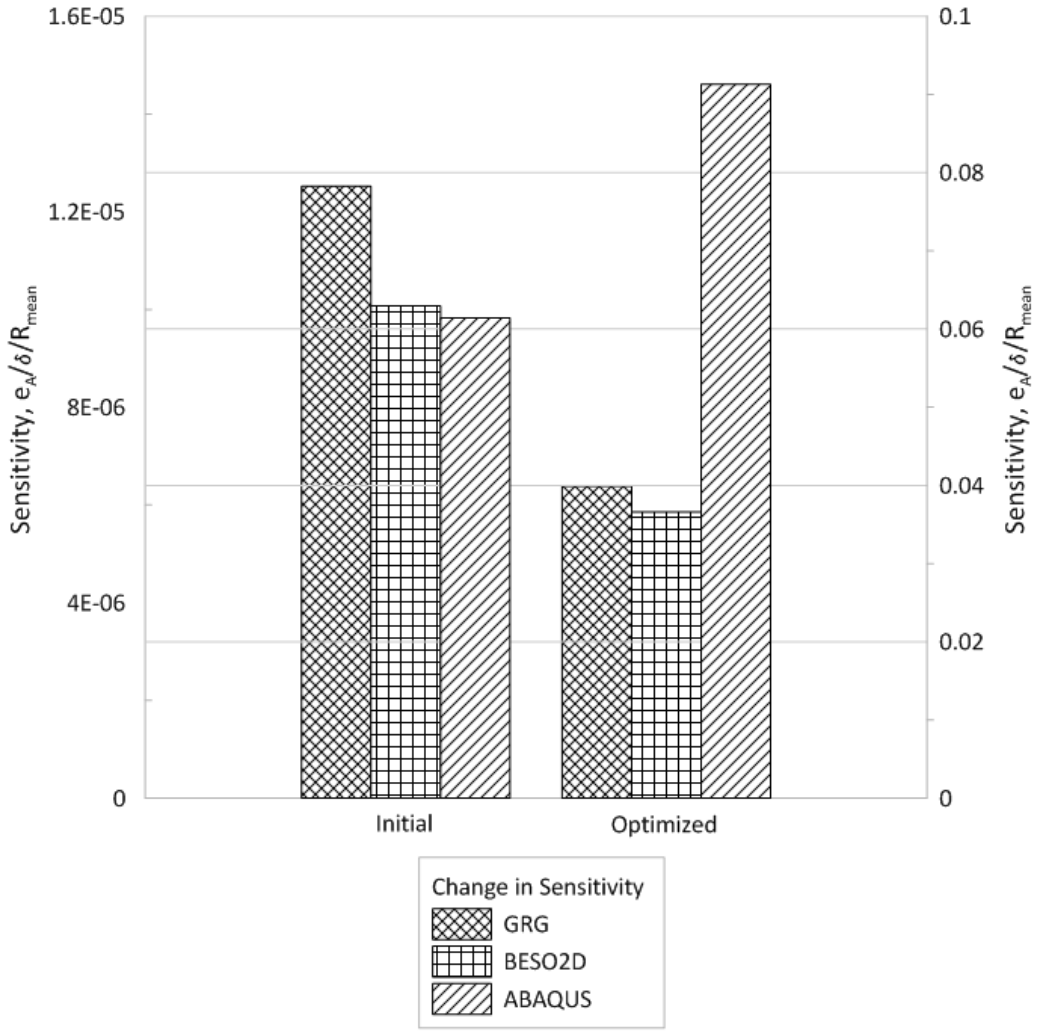


Figure 4.20 Effect of optimization codes on change in sensitivity

The figure above compares the changes in sensitivity in all three optimization codes. Ring sensitivity was calculated using the following equation [10]:

$$\frac{e_A}{\delta/R_{mean}} = 0.61\frac{w}{R_{mean}} \tag{4.3}$$

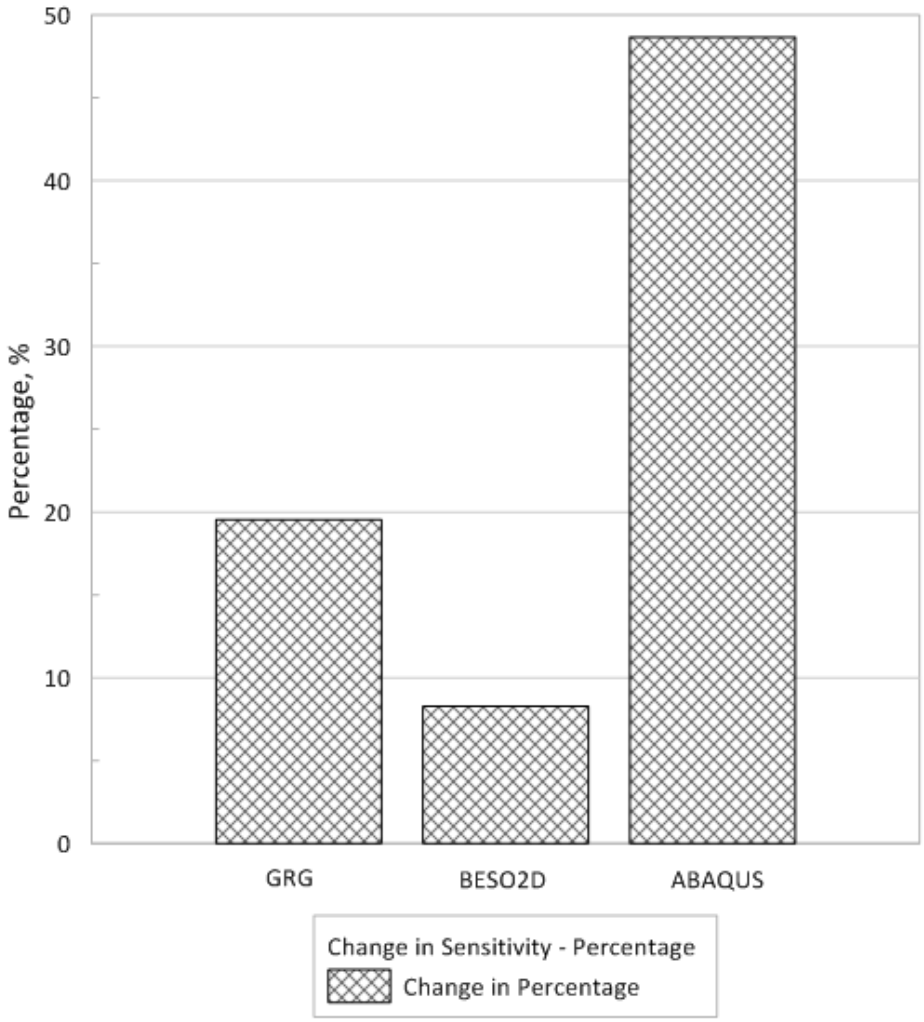


Figure 4.21 Percentage change in sensitivity

In this case, the ring deflection is taken as 1 to ensure unity and fair comparison. There is no effect on the mean radius of the ring at all three optimization techniques. Hence, sensitivity was affected only by the change in strain. Ring sensitivity was measured at point A. From Figure 4.21, it can be observed that ring sensitivity has been significantly increased in all three optimization codes. GRG optimization increases ring sensitivity from $1.25 \times 10^{-5}$ to $1.01 \times 10^{-5}$ or by 19.5%. BESO2D optimization sees sensitivity increase by 8.3%. ABAQUS shape optimization produced the largest increase of the three optimization codes by 48.7%. The positive results in all three optimization codes were the result of increase in strain at point A.

### *4.7.4 Mean Compliance comparison*

In Figure 4.22, it can be observed that the volume constraint was immediately achieved at the first iteration t = 2.0 with no changes after. The first iteration sees a large increase in the objective function value at the first iteration. A gradual downward trend was then observed as the iterations continued until both objective function and volume constraint lines intersect. The optimization process stopped when convergence was achieved. This was indicated as both objective function and volume constraint lines see minimal changes past the iteration t = 10.0. Figure 4.23 shows the BESO evolution history of the mean compliance and volume fraction from the BESO optimization process. It is observed that the mean compliance increases up to iteration number 10 before stabilizing. Volume fraction stabilizes to 80% at the same iteration number. Convergence occurred at iteration number 20.

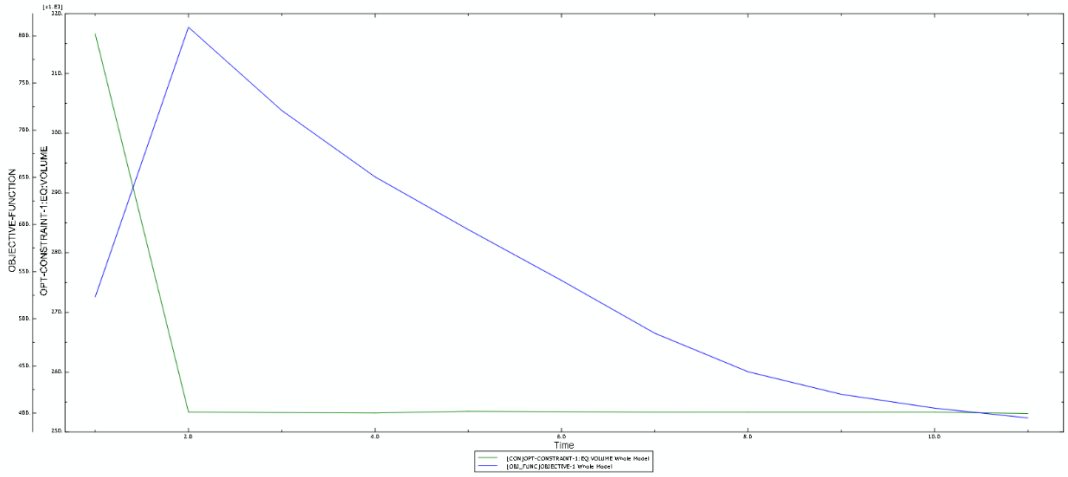


Figure 4.22 History output of ABAQUS shape optimization

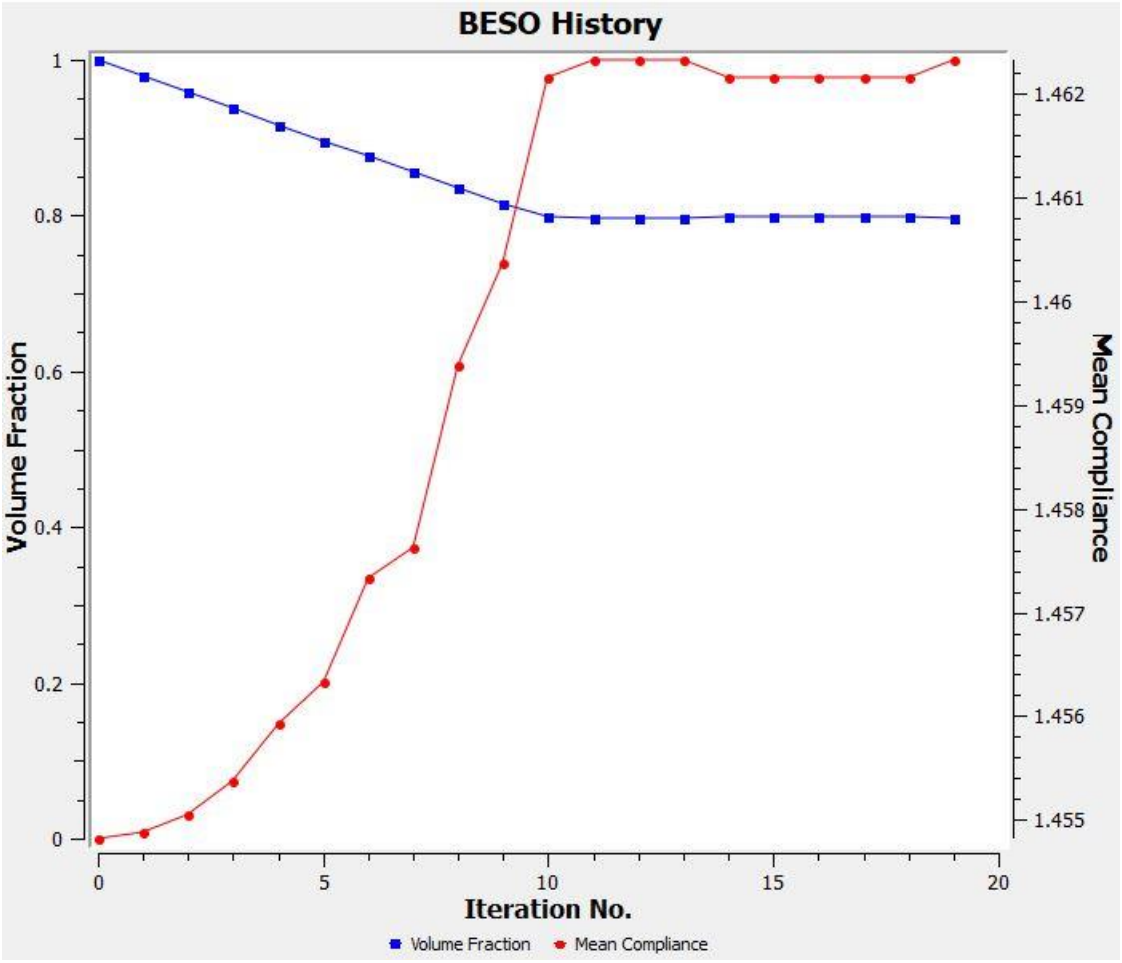


Figure 4.23 BESO history output

## 4.8 Continuous Varying Cross Section Ring Design[4]

### *4.8.1 Effects of modified design on ring sensitivity*

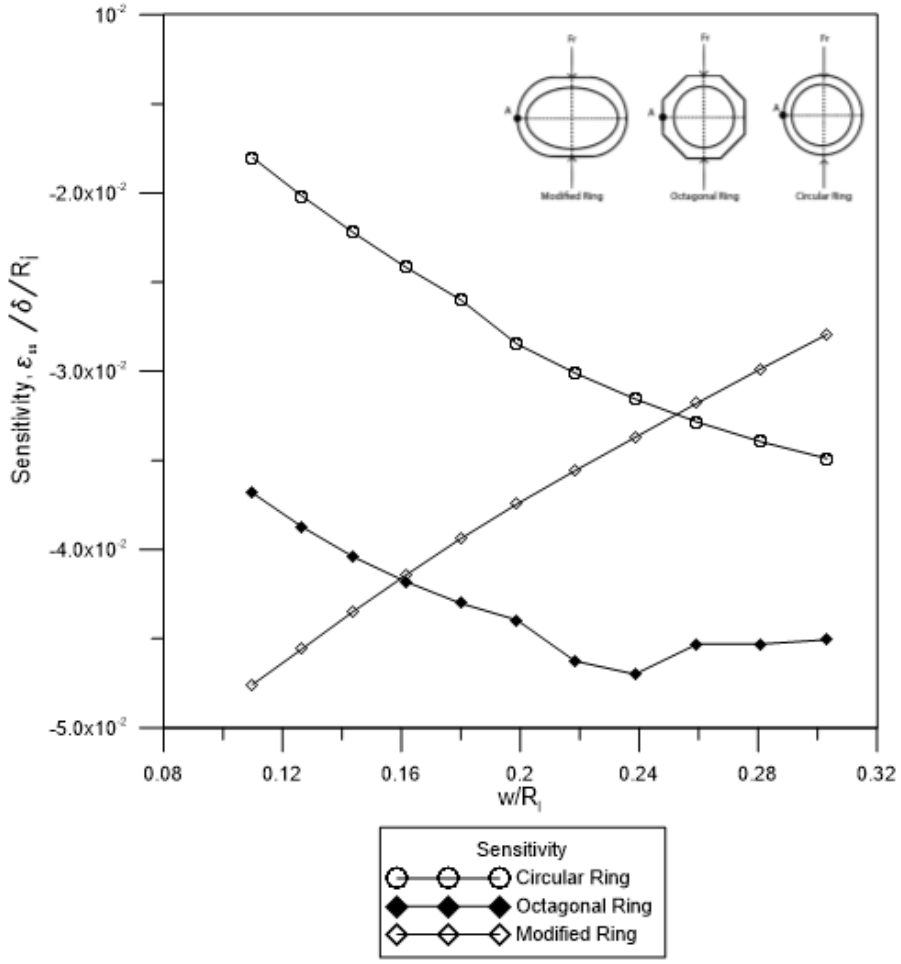


Figure 4.24 Relationship between $\frac{\varepsilon}{\delta/R_i}$ and $\frac{w}{R_i}$ for modified and conventionally designed proving rings by finite element analysis for sensitivity in the E11 or $\varepsilon_x$ direction.

[4] *The following section was accepted and presented in a conference paper titled "**Design of a Proving Ring with Improved Sensitivity and Optimum Stress Distribution**" submitted to ICMEA 2018. The last two sections however were added solely as part of this thesis and will not be published.*

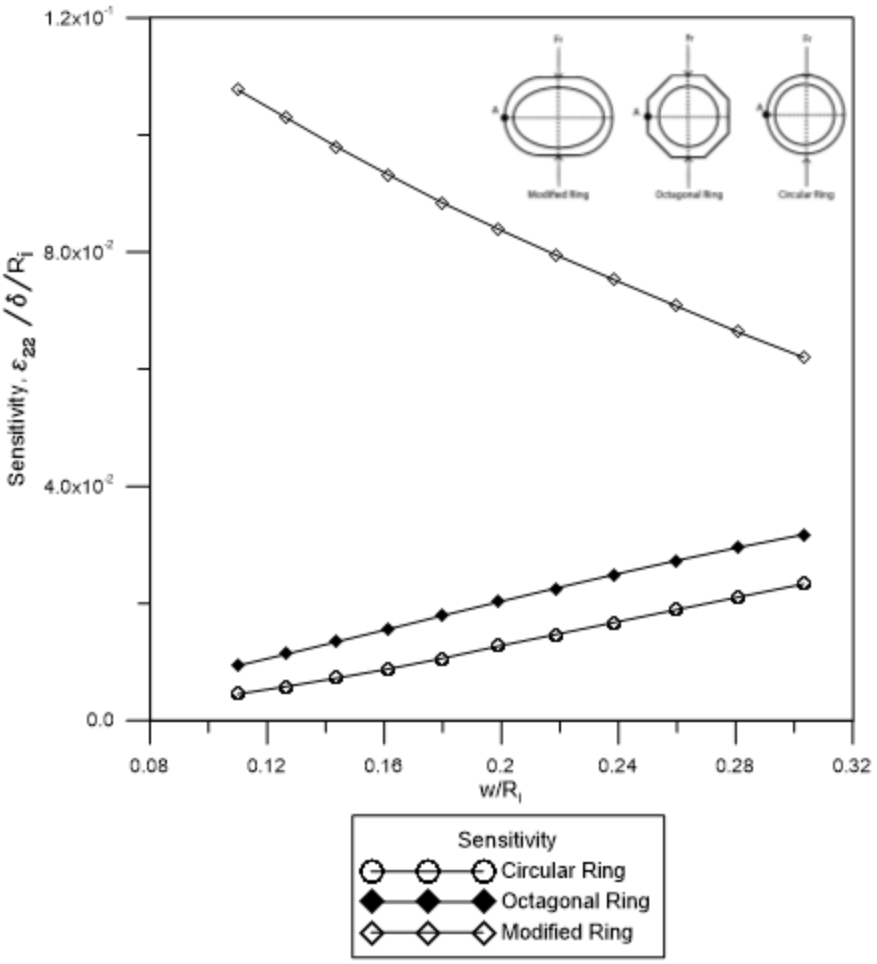


Figure 4.25 Relationship between $\frac{\varepsilon}{\delta/R_i}$ and $\frac{w}{R_i}$ for modified and conventionally designed proving rings by finite element analysis E22 or $\varepsilon_y$ direction

Based on the derived ratios through dimensional analysis, the finite element simulations comparing circular, octagonal and modified shape were performed. Strain in the circumferential and radial direction were measured at point A. Sensitivity response based on strain in the E11 and E22 direction of all three rings were compared in Figure 4.24 and Figure 4.25. For strain in the E11 direction, it was observed that the modified ring has a lower sensitivity compared to the other two rings at lower size. However, at these lower sizes, the rings are considered too thin to be practical. Conversely, the modified ring design shows an increasing sensitivity when size is increased. At larger size, where the ring is thicker, the modified ring has increased strain which

results in higher sensitivity compared to the other conventional rings. Sensitivity for strain in E22 direction shows that the modified proving ring is much more sensitive compared to the other two proving rings irrespective of ring size. The maximum sensitivity achieved is higher than an octagonal based design from literature [4].

*4.8.2 Effect of modified design on ring stress*

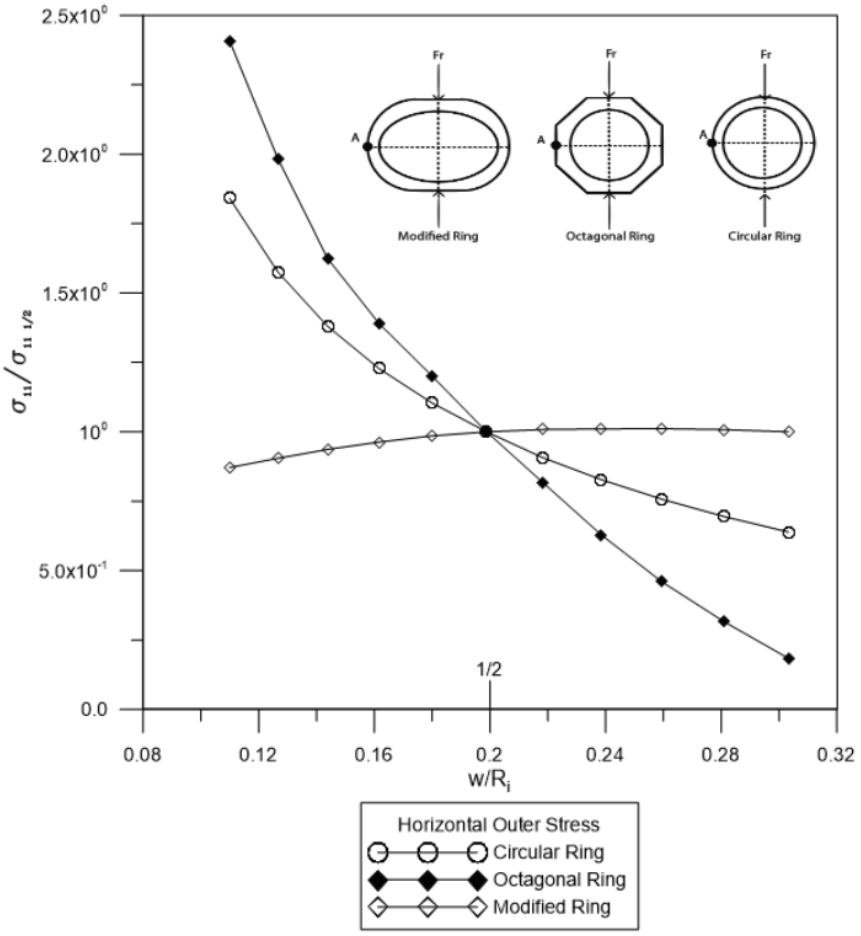


Figure 4.26 Relationship between stress and $\frac{w}{R_i}$ for modified and conventionally designed proving rings by finite element analysis in the S11 or $\sigma_x$ direction

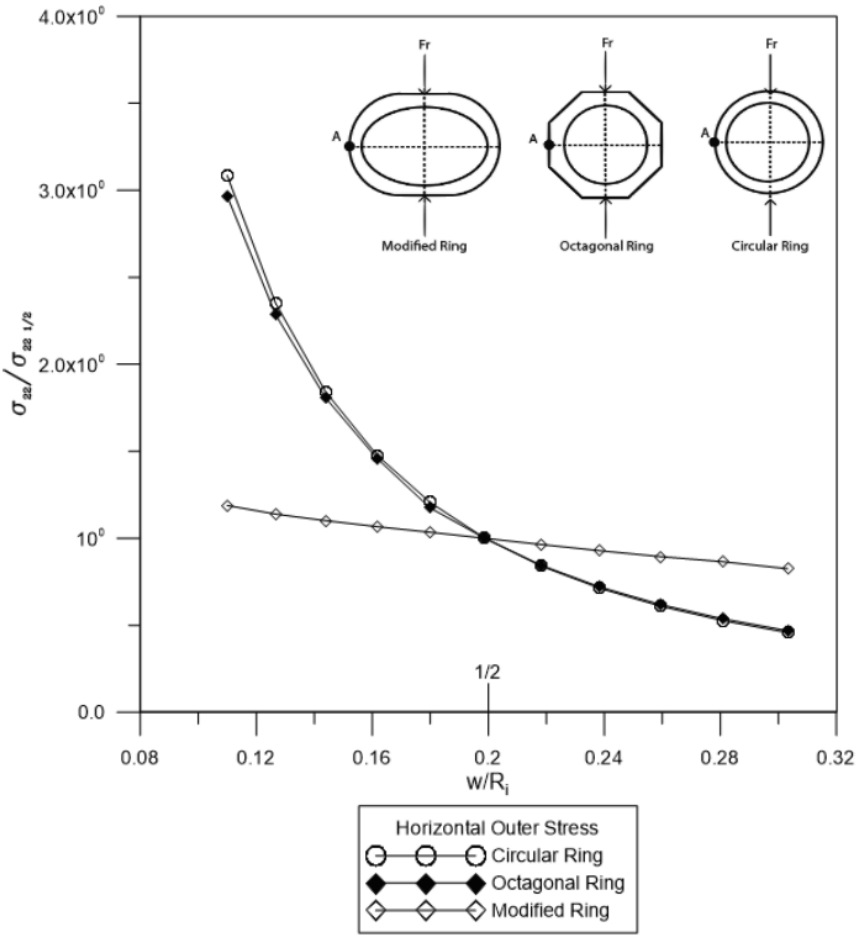


Figure 4.27 Relationship between stress and $\frac{w}{R_i}$ for modified and conventionally designed proving rings by finite element analysis in the S22 or $\sigma_y$ direction

Figure 4.26 and Figure 4.27 shows the maximum horizontal stress values at point A in the S11 and S22 direction with respect to Equation (3.2). It was observed that when the ring size increased, both stress components decrease significantly for the circular and octagonal proving rings. The modified proving ring however showed a slight increase in the S11 direction (+14.7%) and a slight decrease in the S22 direction (-30.6%) as the ring size increases. Compared to the large changes seen in the other two conventional rings however, these changes can be deemed negligible. Although most literature reported on the von Mises stress, the results obtained here still shows that

without compromising the stress levels and with respect to varying ring size, the modified ring design is universal [4, 19, 41].

*4.8.3 Effect of modified design on ring deflection*

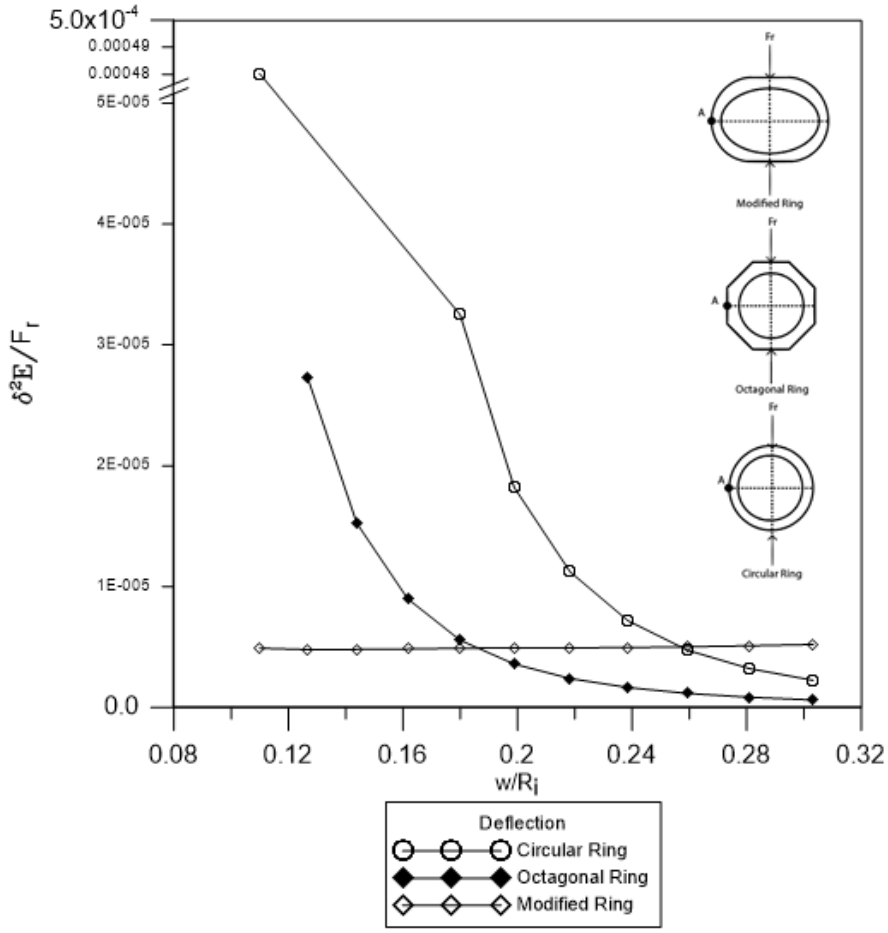


Note: E is taken as 1GPa for all ring types as material are similar

Figure 4.28 Relationship between $\frac{\delta^2 E}{F_r}$ and $\frac{w}{R_i}$ for modified and conventionally designed proving rings by finite element analysis

Based on Equation (3.1) and Equation (3.2), deflection characteristics for all three rings were compared as shown in Figure 4.28. Deflection results for the circular and octagonal rings vary

considerably when the ring size is increased. However, the deflection of the modified ring did not vary much when the ratio is increased. This result shows that compared to the other two rings, the modified ring can be said to have a universal design because of its deflection characteristics. The negligible variation of the ring deflection shows that the effects of ring dimensions does not affect the deflection of the ring. Most studies reported similar deflection values for the conventional rings which verifies the comparison made [26, 41, 67].

*4.8.4 Effect of Modified design on strain distribution*

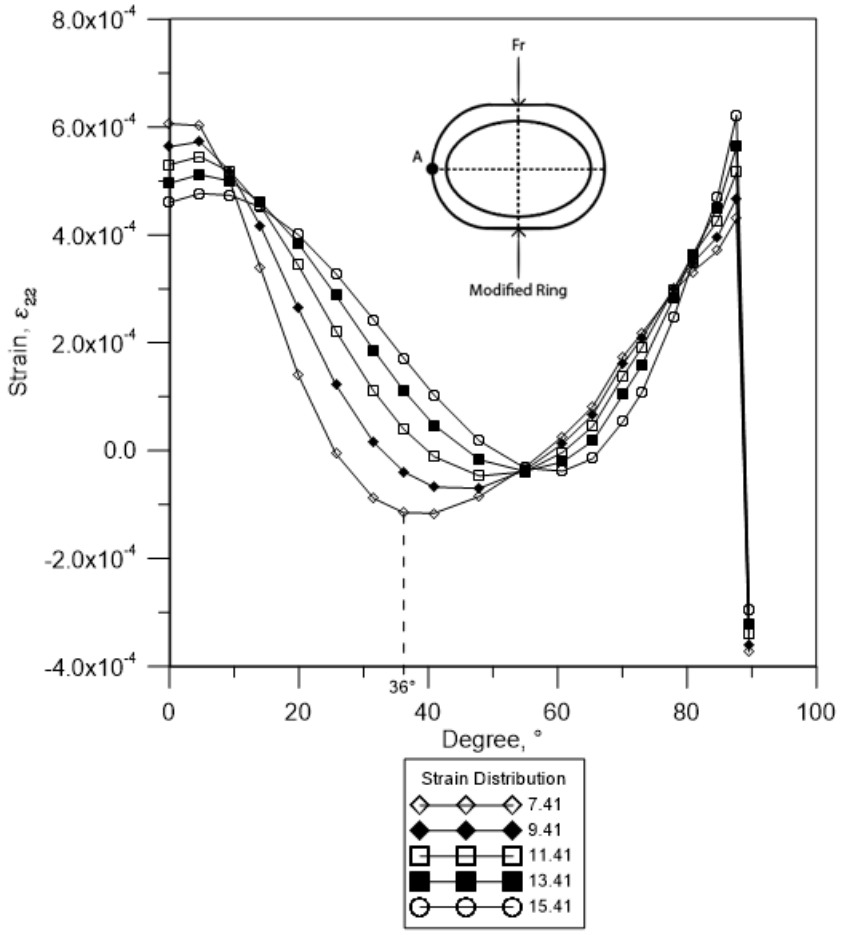


Figure 4.29 Strain distribution in the E22 or $\varepsilon_y$ direction along the quarter ring.

From Figure 4.29, it was observed that the ring has a positive strain value at 0° up to 26° indicating tensile strain at these locations. Negative strain values appeared from 26° to 60° which indicates compressive strain. At 90°, the strain is compressive due to it being at the location of load application. This point is not suitable for strain gauge placement. Between 36° to 56°, compressive strain is maximum for all rings of varying thickness. The most sensitive ring is seen to peak at 36° with thickness 7.41mm. This is the ideal strain gauge location to measure the strain induced by axial loading. From literature, the ideal strain gauge placement for circular ring by Kumar et al. [22, 23] and Chen et al. [19] was stated at 39.6°. The ideal octagonal strain gauge placement was reported to be at 45° by Soliman and Abuhasel [41, 42].

### *4.7.5 Frequency analysis*

Frequency analysis was conducted on the new ring design. Identifying the natural frequency of the ring is essential when designing for applications where the force measuring device can be affected by tool vibrations such as those in the machining field. The natural frequency of the ring is determined from the following equation:

$$f = \frac{1}{2\pi}\sqrt{\frac{k}{m}} \tag{4.4}$$

Where stiffness *k* is calculated as [3]:

$$k = \frac{Etw^2}{1.8r^3} \tag{4.5}$$

The calculated value obtained through the equations above is then compared to the finite element simulation of the new ring design and other ring types. The compared rings have similar mass for fair comparison. Table 8 shows the results of modal analysis through simulation with the final entry showing the natural frequency of the modified design based on analytical calculation for verification. It is observed that the modified design has a significantly higher natural frequency

compared to the conventional circular and octagonal rings. From stiffness equation, the stiffness k has an inversely proportional relationship with cube radius r with the rest of the term's constant. This shows that as the radius decreases, the stiffness increase. The increase in stiffness results in the increase in natural frequency. Therefore, given the rings are of equal mass, the lower diameter design of the modified ring is expected to have a higher natural frequency.

Table 8. Comparison of natural frequency of different ring types

| Ring Type | Natural Frequency, Hz | Horizontal Diameter, mm |
|---|---|---|
| **Circular** | 183.48 | 178.00 |
| **Octagonal** | 219.92 | 158.60 |
| **Modified Design (FEA)** | 591.50 | 144.82 |
| **Modified Design (Analytical)** | 589.4 | 144.82 |

*4.8.6 Effect of varying length of straight edge*

The previous studies show the effect of the modified ring design on various aspects with the length of the straight edge kept constant at 50mm. The following table shows the effect of varying the straight side length on the maximum stress in the S11 direction and the resulting sensitivity. Strain value was taken at the horizontal inner side of the ring where $\theta = 0°$. The straight sides were varied from 25mm up to 75mm with the total edge to edge length or diameter of the ring kept constant. From Table 9, it was observed that the maximum stress in the S11 direction of the ring decreases as the length of the parallel straight edges increase. This can be attributed to the decrease in bending stress applied on the straight edge as its length was increased. Conversely, strain at point A was found to increase as the length increases which in turn increases the ring sensitivity. The increase in sensitivity can also be attributed to the increases in strain induced on the ring. Deflection was

found to decrease as the length was increased. An optimum straight side length of 50mm was selected due to a balance of maximized strain and minimized stress.

Table 9. Effect of different straight side length

| Straight side Length | Deflection at top ring, mm | Strain at point A, μ | Sensitivity, μ/mm | Maximum S11, MPa |
|---|---|---|---|---|
| **25** | 0.5498 | $-2.95118 \times 10^{-4}$ | 0.0335 | 314.1 |
| **50** | 0.3847 | $-2.30842 \times 10^{-4}$ | 0.0375 | 289.3 |
| **75** | 0.2787 | $-1.7592 \times 10^{-4}$ | 0.0393 | 252.4 |

## 4.9 Double Ring Design

From the previous sections, it was observed that a continuous variable cross section significantly improves the stress levels as well as enhance the ring sensitivity. This is due to ring material redistributed at optimal locations around the ring. In this section, the last ring design approach is studied. In the previous section, the modified ring design had a varying cross section design with straight sides at the point of load application and boundary condition. Taking this design even further, this section will study the effect of having a double ring design on the previous modified ring. A double ring design is applied at the circular end of the ring to form four curved sections. Unlike all other previous ring studies however, the double ring design was meshed by seeding the part as a whole using a global size number. This is due to the largely differently geometry of the double ring design. The mesh has 1645 nodes with 1356 elements which is a close to the circular ring mesh as possible. From the finite element analysis of the design, it was found that the stress levels were decreased significantly when this design procedure was applied. Stress levels reduced from 381.6 MPa in the previous modified ring design to 196.0Mpa or nearly 49% reduction. From the previous modified ring design and conventional rings, it was observed that the stress distribution was mostly concentrated at the inner surface of the top and bottom sections of the ring which decreases along the periphery before increasing again to a second maximum

stress level at the horizontal side. However, in the double ring design, it was observed that the stress distribution was evenly distributed along the inner surface of the top and bottom portion of the ring. Maximum stress levels were found to be concentrated at the location where the straight and inner curved section meet. Of the two curved sections, it was observed that the inner section experienced higher stress levels compared to the outer section.

The ring sensitivity based on the strain equation from the previous section was found to have increased slightly. Similar to the observations made of the stress distribution, the strain distributions were also more evenly distributed along the straight sections of the ring compared to the previous modified ring design and conventional rings. Finally, the double ring design has a lower deflection value of 0.2146mm compared to 0.5183mm from the modified design which indicates that the former has higher stiffness than the later. The results indicate that although stress levels have been significantly lowered, it was at the cost of the ring sensitivity which was found to have reduced significantly. Therefore, the modified ring would be the better choice of the two. Table 10 compares the double ring design with the most optimal modified design (width 12.41mm).

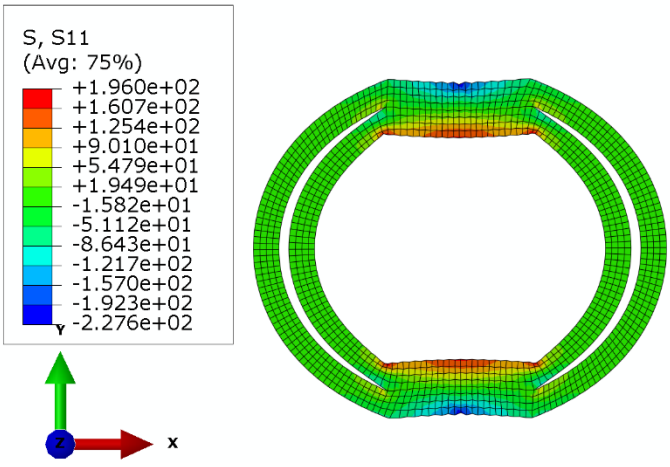


Figure 4.30 Stress distribution in the S11 or $\sigma_x$ direction

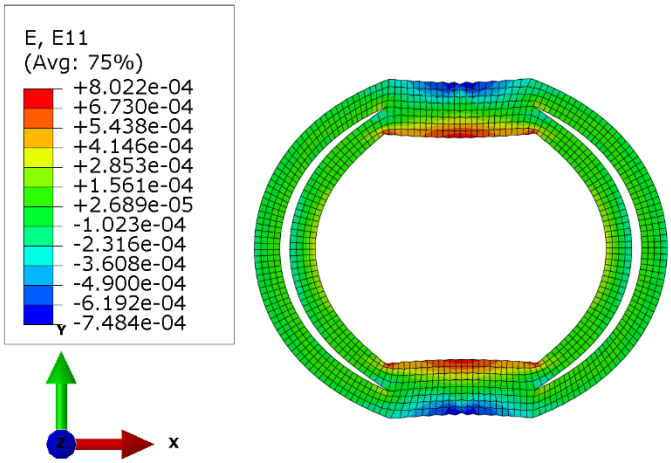


Figure 4.31 Strain distribution in the E11 or $\varepsilon_x$ direction

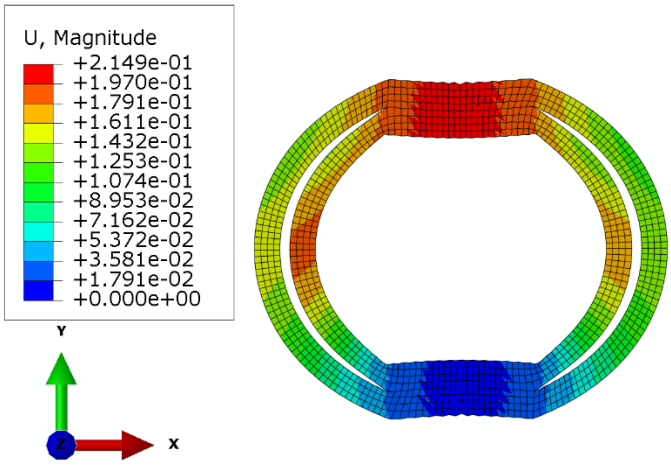


Figure 4.32 Deflection characteristics of the double ring design

Table 10 Summary of double ring design

| **Factors** | **Double Ring Design** | **Modified Design** | **Difference, %** |
|---|---|---|---|
| **Maximum Stress** | 196.0 | 381.6 | 48.6 |
| **Maximum Strain** | $8.022 \times 10^{-4}$ | $1.732 \times 10^{-3}$ | 53.7 |
| **Deflection** | 0.2149 | 0.5183 | 58.5 |
| **Outer Sensitivity** | 0.01945 | 0.03745 | 48.1 |
| **Inner Sensitivity** | 0.050311 | 0.047961 | 4.9 |

## 4.10 Results Summary

To conclude, it can be observed that the objectives of this research were successfully achieved. All optimization codes produced a varying cross section design to achieve better stress levels. The optimization codes were found to have improved stress levels significantly with GRG code resulting the largest decrease in maximum stress by 98% while the ABAQUS TOSCA shape optimization yielded the largest increase in sensitivity by 48.7% and decrease in stress at point A by 66.5%. The modified ring design was found to have significantly lower stress levels compared to the conventional circular and octagonal ring shape designs as well as having higher sensitivity levels especially at higher ring size. With no significant effect with respect to deflection and changes in stress as the ring size increases, the ring can be said to have a universal design. Finally, in the double ring design study, it was found that the proposed ring geometry saw large decrease in stress levels. The deflection value was also found to have decreased considerable owing to the enhanced stiffness of the ring geometry. Overall, the author believes the modified design to be best suited for most loading conditions. Although the double ring design was shown to have a stress reduction by nearly 50%, it is noted that this is at the cost of significant reduction in sensitivity as well. Due to this, and the fact that the modified ring itself does have optimal stress levels already, the modified design was chosen.

# Chapter 5

# Conclusion

## 5.1 Summary

This thesis concerns the research of ring type mechanical force transducer or proving ring. Experimental characterization on a proving ring was conducted to find a reference design for future improvements. From the experiment, it was found that the calculated modulus of elasticity yielded a finite element force displacement response that differed by a significant margin compared to the experimental curve (Figure 4.1). To correct this, a displacement load was imposed at the top point of the ring instead of a constant axial load of 30kN. The value of modulus of elasticity was than calibrated between 190-210 GPa. A force displacement curve that closely resembles the experimental response was obtained when the modulus of elasticity value was 205GPa. In the subsequent analyses, the value of E = 205GPa was used in all finite element simulations and optimization work conducted in this research. The simulations were all elastic simulation. Hence, all results within the elastic range were validated. In conclusion, the research objectives have been successfully achieved. To summarize, the following conclusions were found:

- In the preliminary experiment, it was shown from Figure 3.2 and Table 4 that reduced stress levels as well as a more balanced stress distribution were seen in the octagonal ring which indicates the varying cross section hypothesis is valid. This hypothesis was then used as the fundamental basis for design improvements.
- In the first optimization part using the generalized reduced gradient optimization code, the objective was to evenly distribute stress with similar levels at all sections. The resulting

optimized shaped shows a varying design with maximum ring thickness at the point of axial load application. Minimum thickness was seen an angle 45° from the horizontal axis. These results can be seen in Figure 4.5 (a) and (b).

- From Figure 4.7, as expected, the BESO algorithm removed material from the outer corners of the ring with ring thickness mostly maintained on the horizontal and vertical sides where stress levels are highest.
- Similar results were also seen in Figure 4.8 where the ABAQUS shape optimization produces a ring geometry with minimum thickness between 45-50°. These three results show that since bending stress is minimum at 50° and highest at the point of load application, ring material can be rearranged to be more optimally placed around the ring to account for the major stress imbalance.
- From Figure 4.13, the optimization results show that stress levels were reduced significantly except for the BESO result. All three optimization codes successfully produced a design with uniform radial stress distribution. These results successfully achieved Objective 1. The effect of varying thickness and mean radius throughout all three optimization results also confirms Objective 3.
- In Figure 4.15, it was observed that all three optimization codes increased ring sensitivity. BESO optimization sees the least amount of increase by 8% whereas the ABAQUS shape optimization code increases sensitivity by almost 49%. These results indicate that Objective 2 and 4 have been achieved.
- In the new design study, from Figure 4.19, it was shown that the modified ring compared favourably against the circular and octagonal shape with ring size having minimal effect on the stress levels. It was also shown that stress in the modified ring was notably much lower compared to the other two ring shape when ring size is smaller. In Figure 4.18, when considering strain in the $\varepsilon_{22}$, modified ring sensitivity was much higher than the other two rings. Sensitivity in the $\varepsilon_{11}$ direction however showed that the sensitivity of the modified ring was higher when ring size was larger. Based on the deflection comparison, ring size does not seem to affect the deflection characteristics of the modified ring. Taking all the results into account, the modified ring can be said to have a universal design, that is the change in ring size does not affect the ring stress levels or deflection characteristics. Here, the results indicate Objective 2 has been achieved.

- By applying the double ring design approach, stress levels were again significantly reduced. More importantly, as was shown in Figure 4.22 and 4.23, the stress and strain are more evenly distributed on the inner surface or the ring on the top and bottom portion of the ring. This indicates a more optimized ring design. These results show that Objective 1 of this research work has also been achieved.

## 5.2 Limitations

The previous sections show that the proposed methodology were successful in obtaining the desired results. An optimized proving ring design was obtained through the various optimization codes which were then used to propose a simple ring modification that showed significant enhancement over the current circular and octagonal ring designs. However, although the results were promising, these were achieved with certain limitations that were unavoidable.

1. Fabrication of the proposed proving ring design was not possible due to time constraints placed on the project.
2. The lack of a fabricated ring meant that further experimental studies and verification were not conducted.

## 5.3 Future work

Although the objectives of this research study has been achieved, there are still other possible solutions to improve the performance of the proving ring as a force transducer even further. However, due to the limitations in time as well as resources in doing this thesis, other possible modifications can be made to the ring. The following are suggestions for future work to further improve the proving ring:

1. Manufacture the prototype of the modified ring for further studies.

2. Optimization of the double proving ring design using the bi-directional evolutionary structural optimization code.
3. Optimization of the double proving ring design using the ABAQUS TOSCA shape optimization code.
4. Using the generalized reduced gradient code to optimize sensitivity based on each individual section instead of only at 0°.

# References


1. Hayashi, T., et al., *Evaluation of tuning fork type force transducer for use as a transfer standard.* Measurement, 2008. **41**(9): p. 941-949.
2. Parida, B., S.D. Vishwakarma, and S. Pal, *Design and development of fixture and force measuring system for friction stir welding process using strain gauges.* Journal of Mechanical Science and Technology, 2015. **29**(2): p. 739-749.
3. Karabay, S., *Performance testing of a constructed drilling dynamometer by deriving empirical equations for drill torque and thrust on SAE 1020 steel.* Materials & design, 2007. **28**(6): p. 1780-1793.
4. Uddin, M. and D. Songyi, *On the design and analysis of an octagonal–ellipse ring based cutting force measuring transducer.* Measurement, 2016. **90**: p. 168-177.
5. Chen, Y., N. McLaughlin, and S. Tessier, *Double extended octagonal ring (DEOR) drawbar dynamometer.* Soil and Tillage Research, 2007. **93**(2): p. 462-471.
6. Afzalinia, S. and M. Roberge, *An extended octagonal ring transducer for the compression chamber of a large square baler.* 2009.
7. Kumar, H., et al., *Development and Characterization of a Modified Ring Shaped Force Transducer.* MAPAN, 2015. **30**(1): p. 37-47.
8. Harish Kumar, M.K., Pardeep Pardeep, Pawan Kuamr Arora, *Investigations on metrological characterization of elliptical shaped force measurement.* Engineering Solid Mechanics, 2015. **3**(4): p. 263-273.
9. Kumar, H. and C. Sharma, *Experimental investigations of different force measuring systems.* 2013.
10. Shaw, M.C. and J. Cookson, *Metal cutting principles*. Vol. 2. 2005: Oxford university press New York.
11. Timoshenko, S., *XCI. On the distribution of stresses in a circular ring compressed by two forces acting along a diameter.* The London, Edinburgh, and Dublin Philosophical Magazine and Journal of Science, 1922. **44**(263): p. 1014-1019.
12. Filon, L.N.G., *THE STRESSES IN A CIRCULAR RING.* Selected engineering papers, 1924. **1**(12).
13. Srinath, L.S. and Y.V.G. Acharya, *Stresses in a circular ring.* Applied Scientific Research, Section A, 1954. **4**(3): p. 189-194.
14. Silverman, I.K. and W.T. Moody, *Displacements in closed circular rings subject to concentrated diametral loads.* Journal of the Franklin Institute, 1965. **279**(5): p. 374-386.
15. Libii, J.N., *Design, analysis and testing of a force sensor for use in teaching and research.* strain, 2006. **2**(1): p. 1.
16. Ito, S., S. Sakai, and M. Ishikawa, *A Study on a Two Dimensional Dynamometer for Surface Grinding.* Journal of the Japan Society of Precision Engineering, 1978. **44**(521): p. 634-639.
17. Ito, S., S. Sakai, and M. Ishikawa, *A Study on a Two Dimensional Dynamometer for Surface Grinding.* Bull. Jpn. Soc. Precis. Eng., 1980. **14**(1): p. 25-30.

18. Bray, A., *The role of stress analysis in the design of force-standard transducers.* Experimental Mechanics, 1981. **21**(1): p. 1-20.
19. Chen, B., X. Wu, and X. Peng, *Finite element analysis of ring strain sensor.* Sensors and Actuators A: Physical, 2007. **139**(1–2): p. 66-69.
20. Patrick, W.C. and T. Butkovich, *Application of proving-ring technology to measure thermally induced displacements in large boreholes in rock*. 1984, Lawrence Livermore National Lab., CA (United States).
21. Patrick, W. and N. Rector, *Measurement of Displacements in Large Boreholes with a Strain-Gaged Proving Ring.* Experimental Techniques, 1985. **9**(2): p. 17-19.
22. Kumar, S., et al., *Finite Element Analysis of a force Transducer*. 2011. 2011.
23. Kumar, H., C. Sharma, and A. Kumar, *Design and development of precision force transducers.* 2011.
24. Kumar, H., et al., *Design studies of ring shaped force transducers.* Int. J. Engg. Sci. & Technol, 2011. **3**(3): p. 1536-1541.
25. Kumar, H. and C. Sharma, *Role of finite element analysis in improving hysteresis error of force transducers.* Transactions of the Institute of Measurement and Control, 2012. **34**(8): p. 1019-1024.
26. Kumar, H. and C. Sharma, *Performance evaluation of force transducers.* 2012.
27. Kumar, H., et al., *Design, development and metrological characterization of a low capacity precision industrial force transducer.* ISA Transactions, 2015. **58**: p. 659-666.
28. Jain, R., J. Rathore, and V. Gorana, *Design, Development and Testing of a Three Component Lathe Tool Dynamometer Using Resistance Strain Gauges*, in *CAD/CAM, Robotics and Factories of the Future*. 2016, Springer. p. 13-21.
29. Yaldız, S. and F. Ünsaçar, *Design, development and testing of a turning dynamometer for cutting force measurement.* Materials & Design, 2006. **27**(10): p. 839-846.
30. Kumar, H., et al., *Development and metrological characterization of a precision force transducer for static force measurement related applications.* Measurement, 2016. **88**: p. 77-86.
31. Kroencke, M. and M.L. Hull, *A method for designing multiload component dynamometers incorporating octagonal strain rings.* Experimental Mechanics, 1989. **29**(2): p. 195-204.
32. Dandage, R., S. Bhatwadekar, and M. Bhagwat, *DESIGN, DEVELOPMENT AND TESTING OF A FOUR COMPONENT MILLING TOOL DYNAMOMETER.* 2012.
33. Pathri, B.P., et al., *Design and Fabrication of a Strain Gauge Type 3-axis Milling Tool Dynamometer: Fabrication and Testing.* International Journal of Materials Forming and Machining Processes (IJMFMP), 2016. **3**(2): p. 1-15.
34. Saglam, H. and A. Unuvar, *Three-Component, Strain Gage Based Milling Dynamometer Design And Manufacturing.* J. Integr. Des. Process Sci., 2001. **5**(2): p. 95-109.
35. Korkut, I., *A dynamometer design and its construction for milling operation.* Materials & design, 2003. **24**(8): p. 631-637.
36. Yaldız, S. and F. Ünsaçar, *A dynamometer design for measurement the cutting forces on turning.* Measurement, 2006. **39**(1): p. 80-89.
37. Yaldız, S., et al., *Design, development and testing of a four-component milling dynamometer for the measurement of cutting force and torque.* Mechanical Systems and Signal Processing, 2007. **21**(3): p. 1499-1511.

38. Karabay, S., *Design criteria for electro-mechanical transducers and arrangement for measurement of strains due to metal cutting forces acting on dynamometers.* Materials & design, 2007. **28**(2): p. 496-506.
39. Karabay, S., *Analysis of drill dynamometer with octagonal ring type transducers for monitoring of cutting forces in drilling and allied process.* Materials & design, 2007. **28**(2): p. 673-685.
40. Sun, Y.J., et al. *An Alternative Method to Optimize Octagonal-Ring Transducer*. in *Applied Mechanics and Materials*. 2012. Trans Tech Publ.
41. Soliman, E., *Performance analysis of octal rings as mechanical force transducers.* Alexandria Engineering Journal, 2015. **54**(2): p. 155-162.
42. ABUHASEL, K.A. and E. SOLIMAN, *Statistical Analysis of Octal Rings as Mechanical Force Transducers.* 2016.
43. Dhanal, S.V., *Finite element analysis of octagonal ring for a three component milling tool dynamometer.*
44. Girma, G., *Multicomponent dynamometer for measurement of forces on plough bodies.* Journal of Agricultural Engineering Research, 1989. **42**(2): p. 85-96.
45. Khan, J., et al., *Design and calibration of a bi-axial extended octagonal ring transducer system for the measurement of tractor-implement forces.* J. Eng. Appl. Sci, 2007. **2**(1): p. 16-20.
46. Onwualu, A., *An Extended Octagonal Ring Dynamometer for Measurement of Forces on a Simple Tillage Tool.* Nigerian Journal of Technology, 2002. **21**(1): p. 46-59.
47. Kheiralla, A., et al., *Design and development of a three-point auto hitch dynamometer for an agricultural tractor.* ASEAN Journal on Science and Technology for Development, 2003. **20**(3&4): p. 271-288.
48. Thinley, K., et al., *Development of Three-Dimensional Force Measurement Instrument for Plough in Mountain Region.* AGRICULTURAL MECHANIZATION IN ASIA, AFRICA, AND LATIN AMERICA, 2016. **47**(4): p. 66.
49. Bhowmick, T., N. Dhar, and J. Rana, *DEVELOPMENT OF A GRINDING DYNAMOMETER FOR AN INDUSTRIAL MODEL.*
50. Niyamapa, T. and V.M. Salokhe, *Force and pressure distribution under vibratory tillage tool.* Journal of Terramechanics, 2000. **37**(3): p. 139-150.
51. Pitla, S.K., L.G. Wells, and S.A. Shearer, *Integration of an Extended Octagonal Ring Transducer and Soil Coulterometer for Identifying Soil Compaction.* 2009. **25**(5).
52. O'Dogherty, M., *A dynamometer to measure the forces on a sugar beet topping knife.* Journal of Agricultural Engineering Research, 1975. **20**(4): p. 339-345.
53. O'Dogherty, M.J., *The Design of Octagonal Ring Dynamometers.* Journal of Agricultural Engineering Research, 1996. **63**(1): p. 9-18.
54. McLaughlin, N., S. Tessier, and A. Guilbert, *Improved double extended octagonal ring drawbar transducer for 3-D measurement.* 1998.
55. McLaughlin, N., B. Patterson, and S. Burtt, *Effect of load fixture design on sensitivity of an extended octagonal ring (EOR) transducer.* Canadian Biosystems Engineering, 2012. **54**.
56. McLaughlin, N. and Y. Chen, *Effect of strain gage misalignment on cross sensitivity of extended ring (ER) transducers.* Canadian Biosystems Engineering, 2013. **54**: p. 2.23-2.31.

57. Ortiz-Laurel, H. and P.A. Cowell, *Dynamometer Design for Traction Forces Measurement on Draught Horses.* AGRICULTURAL MECHANIZATION IN ASIA AFRICA AND LATIN AMERICA, 2004. **35**(2): p. 4.
58. Raheman, H. and R. Sahu, *Computer-Aided Design of Extended Octagonal Ring Transducer for Agricultural Implements.* AGRICULTURAL MECHANIZATION IN ASIA AFRICA AND LATIN AMERICA, 2006. **37**(2): p. 29.
59. SHISHVAN, S.H., et al., *The Evaluation and Comparison of Stress Node on Extended Octognal Ring Transducers by Strain Energy Theory and Finite Element Method.* Tarım Makinaları Bilimi Dergisi, 2011. **7**(3).
60. Nalavade, P.P., et al., *Performance of Free Rolling and Powered Tillage Discs.* Soil and Tillage Research, 2010. **109**(2): p. 87-93.
61. Nalavade, P.P., V.M. Salokhe, and T. Niyamapa, *Strain node identification by FEM and measurement of disc forces by double extended octagonal ring transducer.* Journal of Food, Agriculture & Environment, 2010. **8**(2 part 2): p. 730-735.
62. Abbaspour-Gilandeh, Y. and S. Haghighat-Shishvan, *Extended octagonal ring transducers for measurement of tractor-implement forces.* Instruments and Experimental Techniques, 2011. **54**(1): p. 136-140.
63. Abbaspour-Gilandeh, Y. and M. Khanramaki, *Design, Construction and Calibration of a Triaxial Dynamometer for Measuring Forces and Moments Applied on Tillage Implements in Field Conditions.* MAPAN, 2013. **28**(2): p. 119-127.
64. Godwin, R.J., *An extended octagonal ring transducer for use in tillage studies.* Journal of Agricultural Engineering Research, 1975. **20**(4): p. 347-352.
65. Godwin, R., et al., *A triaxial dynamometer for force and moment measurements on tillage implements.* Journal of agricultural engineering research, 1993. **55**(3): p. 189-205.
66. Prasad, M., et al., *Design studies of a square ring shaped force sensor.* International Journal of Applied Engineering Research, 2010. **1**(4): p. 727.
67. Mohit Kaushik, P., Syed Mazhar Ali, *Preliminary Investigation on Metrological Characterization of Elliptical Shaped Force Transducer* VSRD International Journal of Mechanical, Civil, Automobile and Production Engineering, 2013. **3**(6): p. 163-167.
68. Rahman, M.A., S. Rahman, and K.N.A. Noman, *Optimum Design of a Circular Proving Ring with Variable Cross Section.* HKIE Transactions, 2004. **11**(4): p. 53-55.
69. Rahman, M.A. and S. Rahman. *Design Parameters of a Circular Proving Ring of Uniform Strength*. in *Proceedings of the International Conference on Mechanical Engineering 2005 (ICME2005)*. 2005.
70. Rodríguez-Fuentes, H., et al., *DESIGN, MANUFACTURING AND CALIBRATION OF A CIRCULAR RING TYPE MONOLITHIC LOAD CELL ADDRESSED TO DRAWBAR PULL TESTING OF THE FARM TRACTOR.* Journal of Experimental Biology, 2014. **2**: p. 4.
71. Zhao, Y., et al., *Design and development of a cutting force sensor based on semi-conductive strain gauge.* Sensors and Actuators A: Physical, 2016. **237**: p. 119-127.
72. Zhao, Y., Y. Zhao, and X. Ge, *The Development of a Triaxial Cutting Force Sensor Based on a MEMS Strain Gauge.* Micromachines, 2018. **9**(1): p. 30.
73. Zhao, Y., et al., *A high performance sensor for triaxial cutting force measurement in turning.* Sensors, 2015. **15**(4): p. 7969-7984.

74. Liu, C.H., et al., *A three-component strain gage dynamometer for grinding and polishing force measurement.* Journal of Materials Engineering and Performance, 2005. **14**(2): p. 173-178.
75. Rao, J.N.M., A.C.K. Reddy, and P.R. Rao, *Design and fabrication of new type of dynamometer to measure radial component of cutting force and experimental investigation of optimum burnishing force in roller burnishing process.* Indian Journal of Science and Technology, 2010. **3**(7): p. 737-742.
76. Panzera, T.H., et al., *Development of a three-component dynamometer to measure turning force.* The International Journal of Advanced Manufacturing Technology, 2012. **62**(9): p. 913-922.
77. Qin, Y., et al., *A High Performance Torque Sensor for Milling Based on a Piezoresistive MEMS Strain Gauge.* Sensors, 2016. **16**(4): p. 513.
78. Qin, Y., et al., *A novel dynamometer for monitoring milling process.* The International Journal of Advanced Manufacturing Technology, 2017. **92**(5): p. 2535-2543.
79. Chen, Q., et al., *Nonlinear mechanics of a ring structure subjected to multi-pairs of evenly distributed equal radial forces.* Acta Mechanica Sinica, 2017. **33**(5): p. 942-953.
80. Brewer, R.M. and M.L. Hull, *The effect of interface plate compliance on dynamometers incorporating octagonal strain rings.* Experimental Mechanics, 1995. **35**(4): p. 337-344.
81. Godwin, R., et al., *Instrumentation to study the force systems and vertical dynamic behaviour of soil-engaging implements.* Journal of Agricultural Engineering Research, 1987. **36**(4): p. 301-310.
82. Andrew Pytel, F.L.S., *Strength of Materials 4th Edition.* 1987(4th Edition).
83. Lasdon, L.S., R.L. Fox, and M.W. Ratner, *Nonlinear optimization using the generalized reduced gradient method.* RAIRO-Operations Research-Recherche Opérationnelle, 1974. **8**(V3): p. 73-103.
84. Frank, M. and P. Wolfe, *An algorithm for quadratic programming.* Naval Research Logistics Quarterly, 1956. **3**(1-2): p. 95-110.
85. Huang, X. and M. Xie, *Evolutionary topology optimization of continuum structures: methods and applications*. 2010: John Wiley & Sons.
86. Huang, X. and Y.M. Xie, *Convergent and mesh-independent solutions for the bi-directional evolutionary structural optimization method.* Finite Elements in Analysis and Design, 2007. **43**(14): p. 1039-1049.